論文 / 著書情報
Article / Book Information

題目(和文)	
Title(English)	Phase dynamics approach to quantum synchronization
著者(和文)	加藤譲
Author(English)	Yuzuru Kato
出典(和文)	学位:博士(工学), 学位授与機関:東京工業大学, 報告番号:甲第11595号, 授与年月日:2020年9月25日, 学位の種別:課程博士, 審査員:中尾 裕也,井村 順一,倉林 大輔,早川 朋久,田中 正行,山本 直樹
Citation(English)	Degree:Doctor (Engineering), Conferring organization: Tokyo Institute of Technology, Report number:甲第11595号, Conferred date:2020/9/25, Degree Type:Course doctor, Examiner:,,,,,
学位種別(和文)	博士論文
Type(English)	Doctoral Thesis

Phase dynamics approach to quantum synchronization

Yuzuru Kato

A thesis presented for the degree of
Doctor of Engineering

Department of Systems and Control Engineering
School of Engineering
Tokyo Institute of Technology
Japan

Abstract

Synchronization of nonlinear oscillators is widely observed in the real world. Recently, experimental studies of synchronization phenomena have entered the quantum regime with the development of nanotechnology, and the need for theoretical studies of quantum synchronization is rapidly growing in order to unravel its novel features. In this thesis, we present several theoretical results using phase dynamics for the analysis of quantum synchronization. First, we formulate a phase reduction theory for quantum nonlinear oscillators in the semiclassical regime. Second, we apply the formulation to design optimal periodic waveforms for quantum entrainment. Third, we go beyond the semiclassical regime and propose a fully quantum-mechanical definition of the asymptotic phase for quantum nonlinear oscillators and use it for analyzing synchronization in the deep quantum regime. Finally, based on phase dynamics, we apply continuous measurement and feedback control for enhancement of quantum synchronization. These results help us understand novel features in quantum synchronization and will pave the way for future applications of quantum synchronization phenomena in the evolving field of quantum technologies.

Acknowledgements

First and foremost, I deeply thank my advisor Prof. Hiroya Nakao, who is giving me the opportunity to research as a member of his group. Thanks to his wealth of knowledge in various fields of science and technology, I have enjoyed conducting research in a interdisciplinary field between nonlinear dynamics, quantum physics, and control theory. I also would like to thank Prof. Naoki Yamamoto, who have been taking care of me after I graduated from his group. I also would like to thank Prof. Jr-shin Li for hosting my visit to his group. It was a very nice experience for me to discussion with him and his group members. I also would thank Dr. Anatoly Zlotnik for the fruitful discussion about my research at the international conference in Nice. Many thanks to the pioneering researchers in the fields of quantum synchronization, namely, Dr. Tony E Lee, Prof. Christoph Bruder, Dr. Niels Lörch, Prof. Rosario Fazio. I also would like to give my gratitude to the faculty; Prof. Jun-ichi Imura, Prof. Kenji Amaya, Prof. Daisuke Kurabayashi, Prof. Tomohisa Hayakawa, Prof. Masayuki Tanaka, who have supported my graduate education. I also thank the other group members for the stimulating discussion in the group meeting. Last but not least, I deeply thank my family who have always been taking care of me.

Contents

1 Introduction **1**
- 1.1 Synchronization of classical nonlinear oscillators 1
- 1.2 A brief historical perspective 2
- 1.3 Quantum synchronization 2
- 1.4 Overview of the thesis 3

2 Semiclassical Phase Reduction Theory for Quantum Synchronization **5**
- 2.1 Introduction 5
- 2.2 Theory 8
  - 2.2.1 Stochastic differential equation for phase-space variables 8
  - 2.2.2 Derivation of the phase equation 10
  - 2.2.3 Reconstruction of the density matrix 13
- 2.3 Examples 14
  - 2.3.1 Quantum van der Pol oscillator with harmonic driving and squeezing 14
  - 2.3.2 Weak squeezing 15
  - 2.3.3 Strong squeezing 16
  - 2.3.4 Reconstruction of density matrices 17
  - 2.3.5 Reconstruction of spectra and observed frequencies . . 18
- 2.4 Concluding remarks 22

3 Semiclassical optimization of entrainment stability and phase coherence in weakly forced quantum limit-cycle oscillators **25**
- 3.1 Introduction 26
- 3.2 Theory 28
  - 3.2.1 Master equation 28
  - 3.2.2 Phase equation and averaging 29
  - 3.2.3 Improvement of entrainment stability 31

3.2.4 Enhancement of phase coherence 32
3.3 Results 33
3.3.1 Quantum van der Pol oscillator 33
3.3.2 Improvement of entrainment stability 35
3.3.3 Enhancement of phase coherence 37
3.3.4 Comparison of two optimization problems 38
3.4 Discussion 40

4 Quantum asymptotic phase reveals signatures of quantum synchronization 43
4.1 Introduction 43
4.2 Asymptotic phase for quantum nonlinear oscillators 44
4.3 Quantum van der Pol oscillator with Kerr effect 47
4.4 Revealing multiple phase-locking structure 52
4.5 Conclusion 54

5 Continuous measurement and feedback control for enhancement of quantum synchronization 55
5.1 Introduction 55
5.2 Model 57
5.3 Results 59
5.3.1 Without a feedback control 59
5.3.2 With a feedback control 62
5.3.3 Dependence on the quadrature of the measurement . . 64
5.4 Conclusion 66

6 Conclusions 67
6.1 Summary 67
6.2 Outlook 68

A Explicit form of $\boldsymbol{\beta}(\boldsymbol{\alpha})$ 70

B Derivation of the phase equation 72

C Averaged phase equation 75

D Phase-space representation of a quantum vdP oscillator with harmonic driving and squeezing 78
D.1 Weak squeezing 78
D.2 Strong squeezing 80

E Derivation of the optimal waveforms **82**

F Asymptotic phase of classical nonlinear oscillators **84**
F.1 Background 84
F.2 Deterministic case 85
F.3 Stochastic case 86

G Quantum van der Pol oscillator with Kerr effect in the semi-classical regime **90**

H Classical limit of the Quantum asymptotic phase function **92**

I Asymptotic phase functions in the strong quantum regime **93**

J Asymptotic phase function for a damped harmonic oscillator **95**

K Feedback policy **97**

L Relation between the phase diffusion and purity **99**

Chapter 1

Introduction

1.1 Synchronization of classical nonlinear oscillators

Synchronization of rhythmic dynamical systems, or nonlinear self-sustained oscillators, is a ubiquitous phenomenon that can be seen in various fields of science and technology, for example, in electrical oscillations, chemical oscillations, biological rhythms, and mechanical vibrations [1, 2, 3, 4, 5, 6].

In analyzing the rhythmic dynamics of classical limit-cycle oscillators, the phase-reduction theory has played a central role [1, 2, 3, 7, 8, 9]. This theory enables us to quantitatively approximate the dynamics of a nonlinear multi-dimensional limit-cycle oscillator by a simple one-dimensional phase equation, which has greatly facilitated systematic analysis of universal properties of limit-cycle oscillators, such as synchronization of oscillators with external periodic forcing and mutual synchronization between coupled oscillators. The collective synchronization transition in a system of globally coupled phase oscillators (the Kuramoto model [2]) is one of the most prominent results predicted by the phase equation; the wobbling of Millennium footbridge in London caused by synchronization of many pedestrians is a well-known real-world example [10].

The phase equation has also been used in control and optimization of nonlinear oscillators [11], for example, minimization of control power for an oscillator [12, 13], maximization of the phase-locking range of an oscillator entrained to a periodic forcing [14], maximization of linear stability of an oscillator entrained to a periodic forcing [15] and of mutual synchronization between two coupled oscillators [16, 17], maximization of phase coherence of noisy oscillators [18], phase-selective entrainment of oscillators [19], and

phase distribution control for a population of oscillators [11].

Moreover, the phase equation has also been helpful for the analysis of engineering applications of synchronization such as the injection locking [20, 21], ring laser gyroscope [22, 23, 24, 25], Josephson voltage standard [26, 27, 4], phase lock loops in electrical circuits [28, 4], and deep brain stimulation for the treatment of Parkinson's disease [29].

1.2 A brief historical perspective

From a historical perspective, synchronization phenomena was first documented by Christiaan Huygens in the 17th century when there was an urgent need to invent accurate pendulum clocks for the determination of longitude in ocean navigation. In his attempt to invent such a clock, he coincidentally noticed that two clocks hanging on a wall synchronize with each other as a result of weak interaction through the wall. Several centuries had passed, with the development of electrical and radio engineering, W. H. Eccles and J. H. Vincent [30] experimentally studied the synchronization property of a triode generator that produces a periodically alternating electrical current. This discovery was followed by the theoretical investigation of the synchronization property of coupled oscillators performed by Edward Appleton [31] and Balthasar van der Pol [32, 33], who first found the entrainment of an oscillator to a weak external signal having a slightly different frequency and applied it to stabilize the frequency of the triode generators in radio communication systems. After World War II, with the development of computer-based numerical simulation, Arthur Winfree first used a reduced phase equation for the analysis of biological oscillators in 1967 [34]. Inspired by his work, Yoshiki Kuramoto proposed the well-known Kuramoto model, an analytically solvable model for a population of oscillators exhibiting collective synchronization, in 1975 [35]. After these historically significant discoveries, synchronization has been studied in various fields of science and engineering such as network theory, control theory, physics, chemistry, biology, and so on [1, 2, 3, 4, 5, 6]. With the recent development of nanotechnology in the 21th century, studies on synchronization of rhythmic dynamical systems have now entered the quantum regimes.

1.3 Quantum synchronization

Experimental realization of synchronization in nonlinear oscillators have recently reached micro and nano scales [36, 37, 38, 39, 40, 41] and the de-

mand for theoretical studies of synchronization in the quantum regime is rapidly increasing in order to unravel its novel features. Many research papers about quantum synchronization have been published in the last several years [42, 43, 44, 45, 46, 47, 48, 49, 50, 51, 52, 53, 54, 55, 56, 57, 58, 59, 60, 61, 62, 63, 64, 65, 66, 67, 68, 69, 70], and future potential applications of quantum synchronization in the fields of quantum methodology, quantum standard, and quantum information have also been discussed in the literature [46, 62, 63]. In order to systematically analyze quantum synchronization dynamics, analysis using phase dynamics of quantum limit-cycle oscillators is significantly important.

1.4 Overview of the thesis

In this thesis, we present several theoretical results on the phase-dynamics approach to the analysis of quantum synchronization.

In Chapter 2, we generalize the conventional phase-reduction theory to quantum limit-cycle oscillators in the semiclassial regime where the quantum dynamics can be approximately described by a stochastic differential equation representing a system state in the phase space fluctuating along a deterministic classical trajectory due to small quantum noise. The developed semiclassical phase-reduction theory enables us to quantitatively approximate a quantum oscillator exhibiting stable limit-cycle oscillations by a simple one-dimensional phase equation, facilitating a systematic analysis of quantum synchronization in this regime. As a simple example, we analyze synchronization properties of a typical model of quantum limit-cycle oscillators, known as the quantum van der Pol oscillator, subjected to a harmonic driving and squeezing, including the case that the squeezing is strong and the oscillation is asymmetric. In comparison with the previous studies that derived a phase equation for quantum oscillator having a symmetric limit-cycle in the classical limit, the proposed semiclassical phase-reduction theory provides a systematic analysis tool for quantum synchronization in a general class of asymmetric limit-cycle oscillators.

In Chapter 3, using the semiclassical phase-reduction theory formulated in Chapter 2, we consider optimal entrainment of a quantum nonlinear oscillator to a periodically modulated weak harmonic drive in the semiclassical regime. We analyze two types of optimization problems, one for the stability and the other for the phase coherence of the oscillator, and derive optimal waveforms for the periodic modulation by applying the optimization methods originally developed for classical nonlinear oscillators to a quantum

nonlinear oscillator in the semiclassical regime. Using the van der Pol model with squeezing and Kerr effects, we numerically analyze the performance of the optimization schemes and discuss their differences.

In Chapter 4, we go beyond the semiclassical regime and introduce an asymptotic phase, a fundamental quantity characterizing the limit-cycle oscillation, of quantum nonlinear oscillators in a fully quantum-mechanical way. This extends the applicability of the asymptotic phase to the strong quantum regime and enabling analysis of nontrivial quantum synchronization phenomena. We analyze a quantum van der Pol oscillator with Kerr effect and show that our quantum asymptotic phase yields appropriate results in the strong quantum regime while reproducing the conventional asymptotic phase in the semiclassical regime. We then use the quantum asymptotic phase for analyzing the multiple phase locking of the system with a harmonic drive at several different frequencies, an explicit quantum effect observed only in the strong quantum regime, and clarify that it can be understood as synchronization of the system on a torus rather than on a simple limit cycle.

In Chapter 5, we analyze synchronization of a quantum van der Pol oscillator with a harmonic driving signal based on phase dynamics and demonstrate that performing continuous homodyne measurement and applying a feedback control can enhance quantum synchronization. We argue that the phase coherence of the oscillator is increased by the reduction of quantum fluctuations due to the continuous measurement and that a simple feedback policy can suppress the measurement-induced fluctuations by adjusting the frequency detuning between the oscillator and the driving signal. We further demonstrate that the maximum enhancement of synchronization is achieved by performing the measurement on the quadrature angle at which the phase diffusion of the oscillator is maximal and the maximum information about the phase of the oscillator is extracted.

Finally, Chapter 6 gives the conclusions and the appendices give details of the calculations.

We note that the mathematical symbols are introduced independently in each chapter.

Chapter 2

Semiclassical Phase Reduction Theory for Quantum Synchronization

In this chapter, we develop a general theoretical framework of semiclassical phase reduction for analyzing synchronization of quantum limit-cycle oscillators. The dynamics of quantum dissipative systems exhibiting limit-cycle oscillations are reduced to a simple, one-dimensional classical stochastic differential equation approximately describing the phase dynamics of the system under the semiclassical approximation. The density matrix and power spectrum of the original quantum system can be approximately reconstructed from the reduced phase equation. The developed framework enables us to analyze synchronization dynamics of quantum limit-cycle oscillators using the standard methods for classical limit-cycle oscillators in a quantitative way. As an example, we analyze synchronization of a quantum van der Pol oscillator under harmonic driving and squeezing, including the case that the squeezing is strong and the oscillation is asymmetric. The developed framework provides insights into the relation between quantum and classical synchronization and will facilitate systematic analysis and control of quantum nonlinear oscillators.

2.1 Introduction

Spontaneous rhythmic oscillations and synchronization arise in various science and technology fields, such as laser oscillations, electronic oscillators, and spiking neurons [1, 2, 3, 4, 5, 6]. Various nonlinear dissipative systems

exhibiting rhythmic dynamics can be modeled as limit-cycle oscillators. A standard theoretical framework for analyzing limit-cycle oscillators in classical dissipative systems is the *phase reduction theory* [1, 2, 7, 3, 8, 9]. By using this framework, we can systematically reduce multi-dimensional nonlinear dynamical equations describing weakly-perturbed limit-cycle oscillators to a one-dimensional phase equation that approximately describes the oscillator dynamics. The simple semi-linear form of the phase equation, characterized only by the *natural frequency* and *phase sensitivity function* (PSF) of the oscillator, facilitates detailed theoretical analysis of the oscillator dynamics.

The phase reduction theory has been successfully used to analyze universal properties of limit-cycle oscillators in a systematic way, such as synchronization of oscillators with periodic forcing and mutual synchronization of coupled oscillators [1, 2, 3, 4, 5, 6]. It has been essential in the understanding of synchronization phenomena in classical rhythmic systems, for example, the collective synchronization transition of a population of oscillators and oscillatory pattern dynamics in spatially extended chemical or biological systems [1, 2]. Recently, generalizations of the phase reduction theory to non-conventional physical systems, such as time-delayed oscillators [71, 72], piecewise-smooth oscillators [73], collectively oscillating networks [74], and rhythmic spatiotemporal patterns [75, 76], have also been discussed.

Recent progress in experimental studies has revealed that synchronization can take place in coupled nonlinear oscillators with intrinsically quantum-mechanical origins, such as micro and nanomechanical oscillators [36, 37, 38, 39, 40, 41], spin torque oscillators [77], and cooled atomic ensembles [78, 79]. Moreover, theoretical studies have been performed on the synchronization of nonlinear oscillators which explicitly show quantum signatures [42, 43, 44, 45, 46, 47, 48, 49, 50, 51, 52, 53, 54, 55, 56, 57, 58, 59, 60, 61, 62, 63, 64, 65, 66, 67, 68, 69, 70], such as optomechanical oscillators [42, 43, 44], cooled atomic ensembles [45, 46], trapped ions [47, 48, 49], spins [50, 51], and superconducting circuits [53]. In particular, a number of studies have analyzed the quantum van der Pol (vdP) oscillator [47], which is a typical model of quantum self-sustained oscillators, for example, synchronization of a quantum vdP oscillator by harmonic driving [54, 44] or squeezing [55], mutual synchronization of coupled quantum vdP oscillators [48, 56], and quantum fluctuations around oscillating and locked states of a quantum vdP oscillator [60, 61].

In addition to its fundamental importance as a novel physical phenomenon where nonlinear and quantum phenomena have combined effect, quantum synchronization may also be useful in developing metrological applications, such as the improvement of the measurement accuracy in the Ramsey spec-

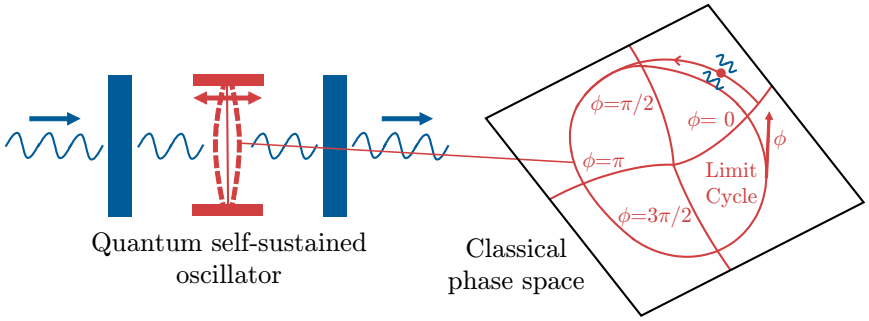

Figure 2.1: A schematic diagram of the semiclassical phase reduction for quantum synchronization. A quantum self-sustained oscillator, which has a stable limit-cycle solution in the classical limit, can be described by an approximate one-dimensional stochastic differential equation for a phase variable ϕ that characterizes the system state. The system state can be approximately reconstructed from the reduced phase equation.

troscopy for atomic clocks [46] and the precise measurement of the resistance standard with a superconducting device [62]; an application of the limit-cycle oscillation to analog memory in a quantum optical device [63] has also been considered.

Considering the importance of phase reduction for analyzing synchronization of classical nonlinear oscillators, we aim to develop a phase reduction theory also for quantum nonlinear oscillators. In the analysis of quantum synchronization, phase-space approaches using the quasiprobability distributions of quantum systems are commonly employed. In a pioneering study, Hamerly and Mabuchi [63] derived a phase equation from the stochastic differential equation (SDE) describing a truncated Wigner function of a quantum limit-cycling system in a free-carrier cavity. However, it is not fully consistent with the classical phase reduction theory, because the notions of the asymptotic phase and PSF, which are essential in the classical theory, are not introduced. Consequently, the limit cycle needs to be approximately symmetric for the analysis of synchronization with periodic forcing [63]. Similar phenomenological phase equations, where the phase simply represents the geometric angle of a circular limit cycle, have also been used in several studies on quantum synchronization [42, 46, 67, 44]; however, a systematic phase reduction theory has not been established so far.

In this study, we formulate a general framework of the phase reduction

theory for quantum synchronization under the semiclassical approximation, where the quantum dynamics can be approximately described by a SDE representing a system state in the phase space fluctuating along a deterministic classical trajectory due to small quantum noise. We derive a linearized multi-dimensional semiclassical SDE from a general master equation that describes weakly-perturbed quantum dissipative systems with a single degree of freedom exhibiting stable nonlinear oscillations, and subsequently reduce it to an approximate one-dimensional classical SDE for the phase variable of the system (see Fig. 2.1). The derived phase equation has a simple form, characterized by the natural frequency, PSF, and Hessian matrix of the limit cycle in the classical limit, and a noise term arising from quantum fluctuations around the limit cycle. The quantum-mechanical density matrix and power spectrum of the original system can be approximately reconstructed from the reduced phase equation.

On the basis of the reduced phase equation, synchronization dynamics of quantum nonlinear oscillators can be analyzed in detail by using standard techniques for classical nonlinear oscillators [1, 2, 7, 3, 8, 9]. As an example, we analyze synchronization of a quantum vdP oscillator under harmonic driving and squeezing. In particular, we consider the case with strong squeezing, where the oscillation is asymmetric and the analytical solution is not available. It is shown that, even in such cases, we can numerically calculate the necessary quantities in the classical limit and use them to analyze the synchronization dynamics of the original quantum system, provided that the quantum noise and the perturbations given to the oscillator are sufficiently weak.

The rest of this chapter is organized as follows; In Sec. II, the derivation of the approximate phase equation for a quantum limit-cycle oscillator subjected to weak perturbations is given. In Sec. III, we analyze a quantum vdP oscillator with harmonic driving and squeezing using the derived phase equation. Section IV gives concluding remarks, and Appendices provide detailed derivations of the equations and discussions.

2.2 Theory

2.2.1 Stochastic differential equation for phase-space variables

We consider quantum dissipative systems with a single degree of freedom interacting with linear and nonlinear reservoirs, which has a stable limit-cycle solution in the classical limit and is driven by weak perturbations. Under the

assumption that correlation times of the reservoirs are significantly shorter than the time scale of the main system, a Markovian approximation of the reservoirs can be employed and the evolution of the system can be described by a quantum master equation [80, 81],

$$\dot{\rho} = -i[H + \epsilon\tilde{H}(t), \rho] + \sum_{m=1}^{n} \mathcal{D}[L_m]\rho, \tag{2.1}$$

where ρ is a density matrix representing the system state, H is a system Hamiltonian, $\epsilon\tilde{H}(t)$ is a time-dependent Hamiltonian representing weak external perturbations applied to the system ($0 < \epsilon \ll 1$), n is the number of reservoirs, L_m is the coupling operator between the system and the mth reservoir ($m = 1, \ldots, n$), $\mathcal{D}[L]\rho = L\rho L^\dagger - (\rho L^\dagger L + L^\dagger L\rho)/2$ denotes the Lindblad form, and the reduced Planck constant is set as $\hbar = 1$. We consider a physical condition where the effects of the quantum noise and external perturbations are sufficiently weak and of the same order, and perturbatively analyze their effect on the semiclassical dynamics of the system.

First, we transform Eq. (2.1) into a multi-dimensional SDE by introducing a phase-space quasiprobability distribution, such as the P, Q, or Wigner representation [80, 81]. We use the P representation, because the density matrix and spectrum can be reconstructed using a simple and natural approximation. In the P representation, the density matrix ρ is represented as $\rho = \int P(\boldsymbol{\alpha})|\alpha\rangle\langle\alpha|d\boldsymbol{\alpha}$, where $|\alpha\rangle$ is a coherent state specified by a complex value $\alpha \in \mathbb{C}$, or equivalently by a two-dimensional complex vector $\boldsymbol{\alpha} = (\alpha, \alpha^*)^T \in \mathbb{C}^{2\times 1}$, $P(\boldsymbol{\alpha})$ is a quasiprobability distribution of $\boldsymbol{\alpha}$, $d\boldsymbol{\alpha} = d\alpha d\alpha^*$, the integral is taken over the entire space spanned by $\boldsymbol{\alpha}$, and * indicates complex conjugate.

The Fokker-Planck equation (FPE) equivalent to Eq. (2.1) can be written as

$$\frac{\partial P(\boldsymbol{\alpha}, t)}{\partial t} = \Big[-\sum_{j=1}^{2} \partial_j \{A_j(\boldsymbol{\alpha}) + \epsilon\tilde{A}_j(\boldsymbol{\alpha}, t)\} + \frac{1}{2}\sum_{j=1}^{2}\sum_{k=1}^{2} \partial_j\partial_k\{\epsilon D_{jk}(\boldsymbol{\alpha})\}\Big] P(\boldsymbol{\alpha}, t), \tag{2.2}$$

where $A_j(\boldsymbol{\alpha})$ and $\tilde{A}_j(\boldsymbol{\alpha}, t)$ are the jth components of complex vectors $\boldsymbol{A}(\boldsymbol{\alpha}) = (A_1(\boldsymbol{\alpha}),\ A_1^*(\boldsymbol{\alpha}))^T \in \mathbb{C}^{2\times 1}$ and $\tilde{\boldsymbol{A}}(\boldsymbol{\alpha}, t) = (\tilde{A}_1(\boldsymbol{\alpha}, t), \tilde{A}_1^*(\boldsymbol{\alpha}, t))^T \in \mathbb{C}^{2\times 1}$ representing the system dynamics and perturbations, respectively, $\epsilon D_{jk}(\boldsymbol{\alpha})$ is the (j, k)-th component of the symmetric diffusion matrix $\epsilon\boldsymbol{D}(\boldsymbol{\alpha}) \in \mathbb{C}^{2\times 2}$ representing quantum fluctuations, and the complex partial derivatives are defined as $\partial_1 = \partial/\partial\alpha$ and $\partial_2 = \partial/\partial\alpha^*$ (note that $A_2(\boldsymbol{\alpha}) = A_1^*(\boldsymbol{\alpha})$ and $\tilde{A}_2(\boldsymbol{\alpha}, t) = \tilde{A}_1^*(\boldsymbol{\alpha}, t)$).

The drift term $\boldsymbol{A}(\boldsymbol{\alpha})$ consists of terms arising from the system Hamiltonian H and the dissipation $\{L_m\}$, $\epsilon\tilde{\boldsymbol{A}}(\boldsymbol{\alpha},t)$ represents the small terms arising from the perturbation Hamiltonian $\epsilon\tilde{H}(t)$, and the diffusion matrix $\epsilon\boldsymbol{D}(\boldsymbol{\alpha})$ represents the intensity of the small quantum noise, generally arising from all terms of H, $\epsilon\tilde{H}(t)$, and $\{L_m\}$. These terms can be explicitly calculated from the master equation in Eq. (2.1) by using the standard calculus for phase-space representation when H, $\epsilon\tilde{H}(t)$, and $\{L_m\}$ are given [80, 81]. The external perturbation $\epsilon\tilde{\boldsymbol{A}}(\boldsymbol{\alpha},t)$ and the diffusion matrix $\epsilon\boldsymbol{D}(\boldsymbol{\alpha})$ are assumed to be of the same order, $\mathcal{O}(\epsilon)$.

By introducing an appropriate complex matrix $\sqrt{\epsilon}\boldsymbol{\beta}(\boldsymbol{\alpha}) \in \mathbb{C}^{2\times 2}$ (see Appendix for the explicit form), the diffusion matrix $\epsilon\boldsymbol{D}(\boldsymbol{\alpha})$ can be represented as $\epsilon\boldsymbol{D}(\boldsymbol{\alpha}) = \sqrt{\epsilon}\boldsymbol{\beta}(\boldsymbol{\alpha})(\sqrt{\epsilon}\boldsymbol{\beta}(\boldsymbol{\alpha}))^T$ and the Ito SDE corresponding to Eq. (2.2) for the phase-space variable $\boldsymbol{\alpha}(t)$ is given by

$$d\boldsymbol{\alpha} = \{\boldsymbol{A}(\boldsymbol{\alpha}) + \epsilon\tilde{\boldsymbol{A}}(\boldsymbol{\alpha},t)\}dt + \sqrt{\epsilon}\boldsymbol{\beta}(\boldsymbol{\alpha})d\boldsymbol{W}, \tag{2.3}$$

where $\boldsymbol{W}(t) = (W_1(t), W_2(t))^T \in \mathbb{R}^{2\times 1}$ represents a vector of independent Wiener processes $W_i(t)$ $(i = 1, \ldots, 2)$ satisfying $\langle dW_i dW_j\rangle = \delta_{ij}dt$.

It should be noted that diffusion matrix of certain quantum systems in the P representation becomes negative definite for certain $\boldsymbol{\alpha}$ [80, 81]. For such systems, we need to employ, for example, the positive P representation with two additional nonclassical variables in place of the P representation, as used by Navarrete-Benlloch *et al.* [60] in the Floquet analysis of quantum oscillations. In this study, to present the fundamental idea of the semiclassical phase reduction in its simplest form, we only consider the case for which the diffusion matrix is always positive semidefinite along the limit cycle and formulate the phase reduction theory in the two-dimensional phase space of classical variables.

2.2.2 Derivation of the phase equation

Our aim is to derive an approximate one-dimensional SDE for the phase variable of the system from the SDE in Eq. (2.3) in the P representation. To this end, we define a real vector $\boldsymbol{X} = (x,p)^T = (\mathrm{Re}\ \alpha, \mathrm{Im}\ \alpha)^T \in \mathbb{R}^{2\times 1}$ from the complex vector $\boldsymbol{\alpha}$. The real-valued expression of Eq. (2.3) for $\boldsymbol{X}(t)$ is then given by an Ito SDE,

$$d\boldsymbol{X} = \{\boldsymbol{F}(\boldsymbol{X}) + \epsilon\boldsymbol{q}(\boldsymbol{X},t)\}dt + \sqrt{\epsilon}\boldsymbol{G}(\boldsymbol{X})d\boldsymbol{W}, \tag{2.4}$$

where $\boldsymbol{F}(\boldsymbol{X}) \in \mathbb{R}^{2\times 1}$, $\boldsymbol{q}(\boldsymbol{X},t) \in \mathbb{R}^{2\times 1}$, and $\boldsymbol{G}(\boldsymbol{X}) \in \mathbb{R}^{2\times 2}$ are real-valued equivalent representations of the system dynamics $\boldsymbol{A}(\boldsymbol{\alpha}) \in \mathbb{C}^{2\times 1}$, perturba-

tion $\tilde{\boldsymbol{A}}(\boldsymbol{\alpha}, t) \in \mathbb{C}^{2\times 1}$, and noise intensity $\boldsymbol{\beta}(\boldsymbol{\alpha}) \in \mathbb{C}^{2\times 2}$ in Eq. (2.3), respectively.

We assume that the system in the classical limit without perturbation and quantum noise, $\dot{\boldsymbol{X}} = \boldsymbol{F}(\boldsymbol{X})$, has an exponentially stable limit-cycle solution $\boldsymbol{X}_0(t) = (x_0(t), p_0(t))^T = \boldsymbol{X}_0(t+T)$ with a natural period T and frequency $\omega = 2\pi/T$. In the same way as the phase reduction for classical limit cycles [1, 2, 7, 3, 8, 9], we can introduce an asymptotic phase function $\Phi(\boldsymbol{X}) : B \subset \mathbb{R}^{2\times 1} \to [0, 2\pi)$ such that $\nabla\Phi(\boldsymbol{X}) \cdot \boldsymbol{F}(\boldsymbol{X}) = \omega$ is satisfied for all system states $\boldsymbol{X}$ in the basin B of the limit cycle in the classical limit, where $\nabla\Phi(\boldsymbol{X}) \in \mathbb{R}^{2\times 1}$ is the gradient of $\Phi(\boldsymbol{X})$. Using this phase function, we define the phase of a system state $\boldsymbol{X} \in B$ as $\phi = \Phi(\boldsymbol{X})$. It then follows that $\dot{\phi} = \dot{\Phi}(\boldsymbol{X}) = \boldsymbol{F}(\boldsymbol{X}) \cdot \nabla\Phi(\boldsymbol{X}) = \omega$, i.e., ϕ always increases at a constant frequency ω with the evolution of $\boldsymbol{X}$. Here, the inner product between two vectors $\boldsymbol{a} = (a_0, a_2, \cdots, a_{N-1})^T \in \mathbb{R}^{N\times 1}$ and $\boldsymbol{b} = (b_0, b_2, \cdots, b_{N-1})^T \in \mathbb{R}^{N\times 1}$ is defined as $\boldsymbol{a} \cdot \boldsymbol{b} = \sum_{i=0}^{N-1} a_i b_i$. In the following formulation, we represent the system state $\boldsymbol{X}$ on the limit cycle as $\boldsymbol{X}_0(\phi) = (x_0(\phi), p_0(\phi))^T$ as a function of the phase ϕ rather than the time t. In this representation, $\boldsymbol{X}_0(\phi)$ is a 2π-periodic function of ϕ, $\boldsymbol{X}_0(\phi) = \boldsymbol{X}_0(\phi + 2\pi)$. Note that an identity $\Phi(\boldsymbol{X}_0(\phi)) = \phi$ is satisfied by the definition of $\Phi(\boldsymbol{X})$.

When the noise and perturbations are sufficiently weak and the deviation of the state $\boldsymbol{X}$ from the limit cycle is small, we can approximate $\boldsymbol{X}(t)$ by a state $\boldsymbol{X}_0(\phi(t))$ on the limit cycle as $\boldsymbol{X}(t) \approx \boldsymbol{X}_0(\phi(t))$ and derive a SDE for the phase in the lowest order approximation by using the Ito formula as (see Appendix for details)

$$d\phi = \{\omega + \epsilon \boldsymbol{Z}(\phi) \cdot \boldsymbol{q}(\phi, t) + \epsilon g(\phi)\}\, dt + \sqrt{\epsilon}\{\boldsymbol{G}(\phi)^T \boldsymbol{Z}(\phi)\} \cdot d\boldsymbol{W}, \qquad (2.5)$$

where the drift term is correct up to $\mathcal{O}(\epsilon)$ and the noise intensity is correct up to $\mathcal{O}(\sqrt{\epsilon})$.

In the above phase equation, the gradient $\nabla\Phi$ of $\Phi(\boldsymbol{X})$ at $\boldsymbol{X}$ is approximately evaluated at $\boldsymbol{X}(\phi)$ on the limit cycle and is denoted as $\boldsymbol{Z}(\phi) = \nabla\Phi|_{\boldsymbol{X}=\boldsymbol{X}_0(\phi)} \in \mathbb{R}^{2\times 1}$. We call this $\boldsymbol{Z}(\phi)$ the *phase sensitivity function* (PSF) of the limit cycle, which characterizes the linear response property of the oscillator phase to given perturbations [2, 7]. Similarly, the perturbation and noise intensity can also be evaluated approximately at $\boldsymbol{X} = \boldsymbol{X}_0(\phi)$ on the limit cycle and they are denoted as $\boldsymbol{q}(\phi, t) = \boldsymbol{q}(\boldsymbol{X}_0(\phi), t)$ and $\boldsymbol{G}(\phi) = \boldsymbol{G}(\boldsymbol{X}_0(\phi))$, respectively. The additional function $g(\phi)$ in the drift term in Eq. (2.5) arises from the change of the variables and is given by

$$g(\phi) = \frac{1}{2}\mathrm{Tr}\left\{\boldsymbol{G}(\phi)^T \boldsymbol{Y}(\phi) \boldsymbol{G}(\phi)\right\}, \qquad (2.6)$$

where $\boldsymbol{Y}(\phi) = \nabla^T \nabla \Phi|_{\boldsymbol{X}=\boldsymbol{X}_0(\phi)}$ is a Hessian matrix of the phase function $\Phi(\boldsymbol{X})$ also evaluated at $\boldsymbol{X} = \boldsymbol{X}_0(\phi)$ on the limit cycle. All these functions are 2π-periodic, as they are functions of $\boldsymbol{X}_0(\phi)$.

It is well known in the classical phase reduction theory that the PSF can be obtained as a 2π-periodic solution to the following adjoint equation and an additional normalization condition [8, 9, 7]:

$$\omega \frac{d}{d\phi} \boldsymbol{Z}(\phi) = -\boldsymbol{J}^T(\phi) \boldsymbol{Z}(\phi), \quad \boldsymbol{Z}(\phi) \cdot \frac{d\boldsymbol{X}_0(\phi)}{d\phi} = 1, \tag{2.7}$$

respectively, where $\boldsymbol{J}(\phi) = \boldsymbol{J}(\boldsymbol{X}_0(\phi)) \in \mathbb{R}^{2\times 2}$ is a Jacobian matrix of $\boldsymbol{F}(\boldsymbol{X})$ at $\boldsymbol{X} = \boldsymbol{X}_0(\phi)$ on the limit cycle. It is also known that the Hessian matrix $\boldsymbol{Y}(\phi)$ on the limit cycle can be calculated as a 2π-periodic solution of an adjoint-type equation [82, 83] with an appropriate constraint. These equations for $\boldsymbol{Y}(\phi)$ are detailed in the Appendix. In the numerical calculations, $\boldsymbol{Z}(\phi)$ can easily be obtained by the backward integration of the adjoint equation with occasional normalization as proposed by Ermentrout [3], and then the Hessian $\boldsymbol{Y}(\phi)$ can be obtained by a shooting method [82].

Because of the additional term $g(\phi)$ in Eq. (2.10), the *effective* frequency $\tilde{\omega} = \langle d\phi \rangle / dt$ of the oscillator in the absence of the perturbation $\boldsymbol{q}(\phi, t)$ is given by

$$\tilde{\omega} = \omega + \frac{\epsilon}{2\pi} \int_0^{2\pi} g(\psi') d\psi', \tag{2.8}$$

which is slightly different from the natural frequency of the oscillator ω in the classical limit. Though not used in the present study, we can further introduce a new phase variable ψ that is only slightly different from ϕ by a near-identity transform as $\phi = \psi + \epsilon n(\psi)$, where $n(\psi)$ is a 2π-periodic function with $n(0) = 0$, and eliminate the additional function $g(\phi)$ in Eq. (2.5) by renormalizing it into the frequency term. The new phase ψ then obeys a simpler SDE of the form

$$d\psi = \{\tilde{\omega} + \epsilon \boldsymbol{Z}(\psi) \cdot \boldsymbol{q}(\psi, t)\} dt + \sqrt{\epsilon} h(\psi) dW, \tag{2.9}$$

where $h(\psi) = \sqrt{\sum_{i=1}^{2} \{\boldsymbol{G}(\psi)^T \boldsymbol{Z}(\psi)\}_i^2}$ and $W(t)$ is a one-dimensional Wiener process. As before, the drift term is correct up to $\mathcal{O}(\epsilon)$ and the noise intensity is correct up to $\mathcal{O}(\sqrt{\epsilon})$. See Appendix for the details. In this study, we use the original phase equation in Eq. (2.5) for numerical simulations and verify its validity. We also note here that the phase equation derived in Ref. [63] does not contain a term with the Hessian matrix, because the order of the noise intensity is implicitly assumed to be $\mathcal{O}(\epsilon)$ in [63].

From the reduced SDE in Eq. (2.5), we can derive a corresponding FPE describing the probability density function $P(\phi, t)$ of the phase variable ϕ as

$$\frac{\partial}{\partial t}P(\phi,t) = -\frac{\partial}{\partial \phi}\left\{\omega + \epsilon \boldsymbol{Z}(\phi)\cdot\boldsymbol{q}(\phi,t) + \epsilon g(\phi)\right\}P(\phi,t) + \frac{\epsilon}{2}\frac{\partial^2}{\partial\phi^2}h(\phi)^2 P(\phi,t). \tag{2.10}$$

Using this FPE, we can obtain the stationary distribution and transition probability of the phase variable ϕ and use them to reconstruct the density matrix and power spectrum.

2.2.3 Reconstruction of the density matrix

From the reduced phase equation, we can approximately reconstruct the quantum state as follows. Using the phase variable ϕ, the oscillator state in the classical limit can be approximated as $\boldsymbol{X} \approx \boldsymbol{X}_0(\phi) = (x_0(\phi), p_0(\phi))^T$, or $\boldsymbol{\alpha} \approx \boldsymbol{\alpha}_0(\phi) = (\alpha_0(\phi), \alpha_0(\phi)^*)^T = (x_0(\phi) + ip(\phi), x_0(\phi) - ip(\phi))^T$ in the original complex representation. Therefore, the quantum state at phase ϕ is approximately described as $|\alpha_0(\phi)\rangle$ and the density matrix ρ is approximately represented by using the probability density function $P(\phi)$ of the phase variable ϕ, obtained from the SDE in Eq. (2.5) or FPE in Eq. (2.10), as

$$\rho \approx \int_0^{2\pi} d\phi P(\phi)\left|\alpha_0(\phi)\right\rangle\left\langle\alpha_0(\phi)\right|, \tag{2.11}$$

which is simply a mixture of coherent states weighted by the distribution of the phase on the classical limit cycle. Thus, we can approximately reconstruct the density matrix of the original quantum oscillator from the classical SDE for the phase variable ϕ, which is characterized by the natural frequency ω, PSF $\boldsymbol{Z}(\phi)$, Hessian matrix $\boldsymbol{Y}(\phi)$, and noise intensity $\boldsymbol{G}(\phi)$ that represents quantum fluctuations around the limit cycle.

The derivation of the phase equation in Eq. (2.5) from the original quantum-mechanical master equation in Eq. (2.1) and reconstruction of the quantum-mechanical density matrix from the approximate phase equation, Eq. (2.11), are the main result of the present work. A schematic diagram of the proposed method is illustrated in Fig. 2.1. The reduced phase equation is essentially the same as that for the classical limit-cycle oscillator driven by noise, and synchronization dynamics of the weakly perturbed quantum nonlinear oscillator in the semiclassical regime can be analyzed on the basis of the reduced phase equation by using the standard methods for the classical limit-cycle oscillator.

2.3 Examples

2.3.1 Quantum van der Pol oscillator with harmonic driving and squeezing

As an example, we consider a quantum vdP oscillator subjected to harmonic driving and squeezing. We assume that the harmonic driving is sufficiently weak and treat it as a perturbation. As for the squeezing, we consider two cases; (i) the squeezing is sufficiently weak and can also be treated as a perturbation, and (ii) the squeezing is relatively strong and cannot be treated as a perturbation.

We denote by ω_0, ω_d, and ω_{sq} the frequencies of the oscillator, harmonic driving, and pump beam of squeezing, respectively. We consider the case where the squeezing is generated by a degenerate parametric amplifier and assume $\omega_{sq} = 2\omega_d$ [81]. In the rotating coordinate frame of frequency ω_d, the master equation is given by [54, 55]

$$\dot{\rho} = -i\left[-\Delta a^\dagger a + iE(a - a^\dagger) + i\eta(a^2 e^{-i\theta} - a^{\dagger 2} e^{i\theta}), \rho\right] + \gamma_1 \mathcal{D}[a^\dagger]\rho + \gamma_2 \mathcal{D}[a^2]\rho, \tag{2.12}$$

where $\Delta = \omega_d - \omega_0$ is the frequency detuning of the harmonic driving from the oscillator, E is the intensity of the harmonic driving, $\eta e^{i\theta}$ is the squeezing parameter and γ_1 and γ_2 are the decay rates for negative damping and nonlinear damping, respectively. The harmonic driving is represented by a constant E, because a coordinate frame rotating with the driving frequency ω_d is used. Note that the Lindblad term with the quadratic annihilation operator, $\mathcal{D}[a^2]$, is essentially important in giving rise to the limit-cycle oscillations.

We assume that γ_2 is sufficiently small and of $\mathcal{O}(\epsilon)$, for which the semiclassical approximation is valid, and represent γ_2 as $\gamma_2 = \epsilon\gamma_1{\gamma_2}'$ using a dimensionless parameter ${\gamma_2}'$ of $\mathcal{O}(1)$. In this setting, the size of the stable limit-cycle solution in Eq. (2.12) in the classical limit is $\mathcal{O}(1/\sqrt{\epsilon})$, while we have implicitly assumed it to be $\mathcal{O}(1)$ in the derivation of Eq. (2.5). Therefore, we introduce a rescaled annihilation operator a' and the corresponding classical variable α' ($\boldsymbol{\alpha}' = (\alpha', \alpha'^*)$ in the vector representation) as $a'|\alpha'\rangle = \sqrt{\epsilon}a|\sqrt{\epsilon}\alpha\rangle$, and represent the parameters as $\Delta = \gamma_1\Delta', E = \sqrt{\epsilon}\gamma_1 E', \eta = \delta\gamma_1\eta'$, where Δ', E', and η' are dimensionless parameters of $\mathcal{O}(1)$. By this rescaling, the size of the limit cycle becomes $\mathcal{O}(1)$ and the parameter δ determines the relative intensity of the squeezing.

The real-valued representation $\boldsymbol{X} = (x', p')^T = (\mathrm{Re}\,\alpha', \mathrm{Im}\,\alpha')^T$ of Eq. (2.4)

after rescaling is then obtained as

$$d\boldsymbol{X} = \begin{pmatrix} \frac{1}{2}x' - \Delta' p' - \gamma_2' x'(x'^2 + p'^2) - \epsilon E' - 2\delta\eta'(x'\cos\theta + p'\sin\theta) \\ \frac{1}{2}p' + \Delta' x' - \gamma_2' p'(x'^2 + p'^2) + 2\delta\eta'(p'\cos\theta - x'\sin\theta) \end{pmatrix} dt' \\ + \sqrt{\epsilon}\boldsymbol{G}(\boldsymbol{X})d\boldsymbol{W}', \tag{2.13}$$

where $dt' = \gamma_1 dt$ and $d\boldsymbol{W}' = \sqrt{\gamma_1}d\boldsymbol{W}$. The noise intensity matrix is explicitly given by

$$\boldsymbol{G}(\boldsymbol{X}) = \begin{pmatrix} \sqrt{\frac{(1+R_1')}{2}}\cos\frac{\chi_1'}{2} & \sqrt{\frac{(1-R_1')}{2}}\sin\frac{\chi_1'}{2} \\ \sqrt{\frac{(1+R_1')}{2}}\sin\frac{\chi_1'}{2} & -\sqrt{\frac{(1-R_1')}{2}}\cos\frac{\chi_1'}{2} \end{pmatrix}, \tag{2.14}$$

with $R_1' e^{i\chi_1'} = -(\gamma_2'(x' + ip')^2 + 2\delta\eta' e^{i\theta})$. Further details of the derivation can be found in the Appendix.

2.3.2 Weak squeezing

First, we consider the case of weak squeezing with $\delta = \epsilon$. The rescaled system and perturbation Hamiltonians are given by

$$H = -\Delta' a'^{\dagger} a', \quad \epsilon\tilde{H} = \epsilon\{iE'(a' - a'^{\dagger}) + i\eta'(a'^2 e^{-i\theta} - a'^{\dagger 2} e^{i\theta})\}. \tag{2.15}$$

For this system, we obtain $\boldsymbol{F}(\boldsymbol{X}) = (x'/2 - \Delta' p' - \gamma_2' x'(x'^2 + p'^2),\ p'/2 + \Delta' x' - \gamma_2' p'(x'^2 + p'^2))^T$. The perturbation is represented by $\boldsymbol{q}(\boldsymbol{X}, t) = (-E' - 2\eta'(x'\cos\theta + p'\sin\theta),\ 2\eta'(p'\cos\theta - x'\sin\theta))^T$. Note that the vector field $\boldsymbol{F}(\boldsymbol{X})$ in this case is simply a normal form of the supercritical Hopf bifurcation. A classical nonlinear oscillator described by this $\boldsymbol{F}(\boldsymbol{X})$ is known as the *Stuart-Landau* (SL) oscillator [2] (which is different from the classical vdP oscillator) and it is analytically solvable.

The stable limit cycle of the SL oscillator is given by

$$\boldsymbol{X}_0(\phi) = \sqrt{\frac{1}{2\gamma_2'}}\begin{pmatrix} \cos\phi \\ \sin\phi \end{pmatrix} \tag{2.16}$$

as a function of phase $\phi = \omega t$, where the frequency is given by $\omega = \Delta'$. The basin B of this limit cycle is the whole (x', p')-plane except $(0, 0)$. The phase function $\Phi(\boldsymbol{X})$ of this limit cycle can be expressed as $\Phi(x', p') =$

$\tan^{-1}(p'/x')$ [7], which gives $\dot{\phi} = \dot{\Phi}(x', p') = \omega$. The PSF $\boldsymbol{Z}(\phi)$ and Hessian matrix $\boldsymbol{Y}(\phi)$ can be obtained by calculating the gradients of the phase function $\Phi(\boldsymbol{X})$ at $\boldsymbol{X} = \boldsymbol{X}_0(\phi)$ on the limit cycle as

$$\boldsymbol{Z}(\phi) = \sqrt{2\gamma_2'}\begin{pmatrix} -\sin\phi \\ \cos\phi \end{pmatrix}, \quad \boldsymbol{Y}(\phi) = 2\gamma_2'\begin{pmatrix} \sin 2\phi & -\cos 2\phi \\ -\cos 2\phi & -\sin 2\phi \end{pmatrix}. \tag{2.17}$$

In this case, the additional term $g(\phi)$ in Eq. (2.5) and therefore the frequency shift in Eq. (2.8) vanishes, i.e., $\tilde{\omega} = \omega$. The $\mathcal{O}(\epsilon\sqrt{\epsilon})$ terms in the noise intensity $\boldsymbol{G}(\phi)$ given by Eq. (2.14) are neglected.

From these results, the phase equation in Eq. (2.5) for the quantum vdP oscillator driven by weak harmonic driving and squeezing is explicitly given by

$$d\phi = \left\{\Delta' + \sqrt{2}\epsilon\sqrt{\gamma_2'}E'\sin\phi + 2\epsilon\eta'\sin(2\phi - \theta)\right\}dt' + \sqrt{\epsilon}\sqrt{\frac{3\gamma_2'}{2}}dW' \tag{2.18}$$

in the lowest-order approximation, where $dW' = \sqrt{\gamma_1}dW$. Using the probability density function $P(\phi)$ of the phase ϕ described by the FPE (2.10) corresponding to Eq. (2.18), the approximate density matrix, Eq. (2.11), is explicitly given by

$$\rho \approx \int_0^{2\pi} d\phi P(\phi)\left|\sqrt{\frac{\gamma_1}{2\gamma_2}}e^{i\phi}\right\rangle\left\langle\sqrt{\frac{\gamma_1}{2\gamma_2}}e^{i\phi}\right|. \tag{2.19}$$

2.3.3 Strong squeezing

Next, we consider the case of strong squeezing with $\delta = 1$ and incorporate it into the system Hamiltonian. The rescaled system and perturbation Hamiltonians are given by

$$H = -\Delta' a'^{\dagger}a' + i\eta'(a'^2 e^{-i\theta} - a'^{\dagger 2}e^{i\theta}), \quad \epsilon\tilde{H} = \epsilon i E'(a' - a'^{\dagger}). \tag{2.20}$$

We obtain $\boldsymbol{F}(\boldsymbol{X}) = (x'/2 - \Delta' p' - \gamma_2' x'(x'^2 + p'^2) - 2\eta'(x'\cos\theta + p'\sin\theta),\ p'/2 + \Delta' x' - \gamma_2' p'(x'^2 + p'^2) + 2\eta'(p'\cos\theta - x'\sin\theta))^T$ with extra terms due to squeezing, characterized by the parameter η'. When $\Delta' > 2\eta'$ (i.e., $\Delta > 2\eta$), this vector field $\boldsymbol{F}(\boldsymbol{X})$ possesses a stable limit-cycle solution $\boldsymbol{X}_0(t)$ in the classical limit. Due to the strong squeezing, this limit cycle is asymmetric and the angular velocity of the oscillator state is non-uniform. At $\Delta' = 2\eta'$, this limit cycle disappears via a saddle-node bifurcation on invariant circle. The perturbation is given by $\boldsymbol{q}(\boldsymbol{X}, t) = (-E', 0)$.

In this case, the system is not analytically solvable, but we can numerically obtain the limit-cycle solution $\boldsymbol{X}_0(\phi) = (x_0(\phi), p_0(\phi))^T$, natural frequency ω, PSF $\boldsymbol{Z}(\phi)$, and Hessian matrix $\boldsymbol{Y}(\phi)$, and use them in the phase equation in Eq. (2.5). The density matrix can be approximately reconstructed from Eq. (2.11), where $\alpha_0(\phi) = x_0(\phi) + ip_0(\phi)$. In this case, the frequency shift does not vanish generally and the effective frequency $\tilde{\omega}$ is slightly different from ω in the classical limit without noise.

An example of the limit cycle in the classical limit is shown in Fig. 2.3(c), and the PSF is shown in Fig. 2.3(d) and (e). The effective frequency is evaluated as $\tilde{\omega} = 0.7743$ at the parameter values given in Fig. 2.3, which is slightly different from the natural frequency $\omega = 0.7746$ of the system in the classical limit without noise. From the phase equation, we can obtain the stationary phase distribution $P(\phi)$ by solving the corresponding FPE and reconstruct the density matrix as a mixture of the coherent states on the limit cycle.

2.3.4 Reconstruction of density matrices

To test the validity of the reduced phase equation, we compare the density matrix ρ_{sc}, which is reconstructed from Eq. (2.11) by using $P(\phi)$ obtained from the FPE in Eq. (2.10) associated with the reduced phase equation in Eq. (2.5), with the true density matrix ρ_{qm}, which is obtained by direct numerical simulation of master equation in Eq. (2.12), in the steady state of the system. We use the fidelity $F = \mathrm{Tr}\left[\sqrt{\sqrt{\rho_{sc}}\rho_{qm}\sqrt{\rho_{sc}}}\right]$ [84] to quantify the similarity between ρ_{sc} and ρ_{qm}. Numerical simulations of the master equation have been performed by using QuTiP [85, 86] numerical toolbox.

Figure 2.2(a)-(d) show the steady-state Wigner distributions corresponding to ρ_{sc} and ρ_{qm} under the weak harmonic driving or the squeezing. In both cases, the distribution is localized along the limit cycle in the classical limit, where the width of the distribution is determined by the intensity of the quantum noise. In Fig. 2.2(a) and (b), only the harmonic driving is given as the perturbation ($\eta = 0$), while in Fig. 2.2(c) and (d), only the squeezing is given as the perturbation ($E = 0$). It can be seen that the true density matrix ρ_{qm} is accurately approximated by the density matrix ρ_{sc} reconstructed from the phase equation in both cases. The fidelity is $F = 0.963$ in the former case and $F = 0.982$ in the latter case.

It is notable that the Wigner distribution is localized around one phase point on the limit cycle in Fig. 2.2(a) and (b), which indicates that there is a 1:1 phase locking [4] between the oscillator and the harmonic driving; In the classical limit, the phase is locked to the point where the deterministic

part of Eq. (2.18) vanishes, and thus the Wigner distribution takes large values around such a point. Similarly, the Wigner distribution is localized around two phase points on the cycle shown in Fig. 2.2(c) and (d), because the frequency of the squeezing is twice that of the harmonic driving and 1:2 phase locking occurs, as can be expected from the third term in the deterministic part of Eq. (2.18) representing the effect of the squeezing. Note that Fig. 2.2 is depicted in the rotating coordinate frame of frequency ω_d and the locked phase rotates with frequency ω_d in the original coordinate.

Figure 2.3(a) and (b) show the Wigner distributions in the case of strong squeezing and weak harmonic driving, where all quantities are calculated numerically. In this case, the system exhibits a stable limit cycle in the rotating coordinate frame of frequency ω_d, and constant driving is applied on the the system as in Eq. (2.13). The limit cycle in the classical limit is shown in Fig. 2.3(c), the x and p components of the PSF obtained from Eq. (2.7) are shown in Figs. 2.3(d) and (e), the xx, pp, xp components of the Hessian matrix are shown in Fig. 2.3(f),(g), and (h) (the px component is equal to the xp component), and the additional term $g(\phi)$ is shown in Fig. 2.3(i). The origin of the phase $\phi = 0$ is chosen as the intersection of the limit cycle and the x' axis with $x' > 0$.

It can be seen that the limit cycle in the classical limit is asymmetric due to the effect of the strong squeezing. The density matrix ρ_{sc} can be reconstructed from the phase distribution $P(\phi)$ obtained numerically. As shown in Fig. 2.3(a) and (b), the true density matrix ρ_{qm} is well approximated by ρ_{sc} with fidelity $F = 0.976$. In Fig. 2.3(a) and (b), the Wigner distribution is concentrated around the stable phase point where the deterministic part of the phase equation vanishes. Thus, the reduced phase equation well reproduces the density matrix of the original quantum system also in this case. Note that the reconstructed density matrix ρ_{sc} is slightly more concentrated than the original density matrix ρ_{qm} in Figs. 2.2 and 2.3. This is because ρ_{sc} is approximated as a weighted mixture of coherent states with minimum uncertainty along the limit cycle.

2.3.5 Reconstruction of spectra and observed frequencies

The power spectrum S_{qm} of the original quantum system in the steady state is defined as

$$\begin{aligned} S_{qm}(\omega) &= \int_{-\infty}^{\infty} d\tau e^{i\omega\tau} R_{qm}(\tau), \\ R_{qm}(\tau) &= \langle a^\dagger(\tau) a(0) \rangle_{qm} - \langle a^\dagger(\tau) \rangle_{qm} \langle a(0) \rangle_{qm}, \end{aligned} \tag{2.21}$$

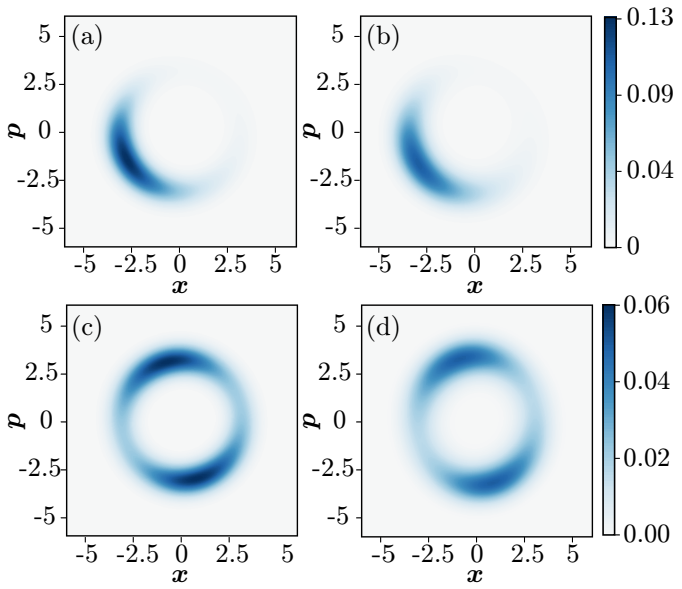

Figure 2.2: Results for the quantum van der Pol oscillator under harmonic driving (a, b) and under weak squeezing (c,d). (a,c): Wigner distributions of ρ_{sc} reconstructed from the reduced phase equation, and (b,d): Wigner distributions of ρ_{qm} obtained by direct numerical simulation of the original master equation. In (a,b), weak harmonic driving with $(\Delta, \gamma_2, \eta e^{i\theta}, E)/\gamma_1 = (0.05, 0.05, 0, \sqrt{0.1})$ is applied, and in (c,d), weak squeezing with $(\Delta, \gamma_2, \eta e^{i\theta}, E)/\gamma_1 = (0.05, 0.05, 0.025, 0)$ is applied. The fidelities between ρ_{sc} and ρ_{qm} are $F = 0.963$ in (a,b) and $F = 0.982$ in (c,d), respectively. Note that the figures are drawn using x and p before rescaling.

where R_{qm} is the autocovariance and $\langle A \rangle_{qm} = \mathrm{Tr}\,[A\rho_{qm}]$ represents the expectation value of an operator A with respect to the steady state density matrix ρ_{qm} obtained from the master equation in Eq. (2.12). From the reduced phase equation, using the correspondence between the operators and c-numbers in the P representation, the power spectrum in Eq. (2.21) under the semiclassical approximation can be reconstructed as

$$\begin{aligned} S_{sc}(\omega) &= \int_{-\infty}^{\infty} d\tau e^{i\omega\tau} R_{sc}(\tau), \\ R_{sc}(\tau) &= \langle \alpha_0^*(\phi_2(\tau))\alpha_0(\phi_1(0))\rangle_{sc} - \langle \alpha_0^*(\phi_2(\tau))\rangle_{sc}\langle \alpha_0(\phi_1(0))\rangle_{sc}. \end{aligned} \tag{2.22}$$

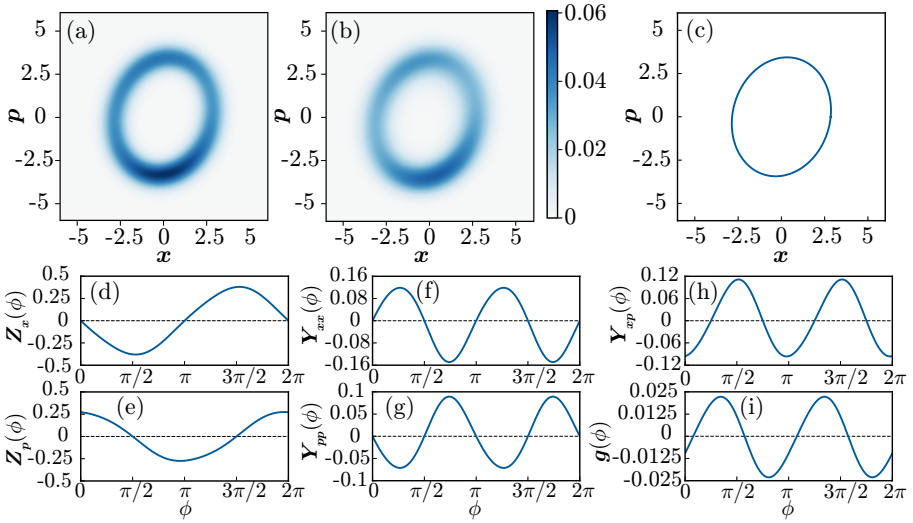

Figure 2.3: Results for the quantum van der Pol oscillator under strong squeezing and weak harmonic driving with parameters $(\Delta, \gamma_2, \eta e^{i\theta}, E)/\gamma_1 = (0.8, 0.05, -0.1i, \sqrt{0.1})$. (a): Wigner distribution of ρ_{sc} reconstructed from the reduced phase equation. (b): Wigner distribution of ρ_{qm} obtained by direct numerical simulation of the original master equation. (c): Limit cycle $\boldsymbol{X}_0(\phi) = (x_0(\phi), p_0(\phi))^T$ in the classical limit. (d, e): The $x = \mathrm{Re}\ \alpha$ and $p = \mathrm{Im}\ \alpha$ components of the PSF $\boldsymbol{Z}(\phi)$. (f, g, h): The xx, pp, xp component of the Hessian matrix $\boldsymbol{Y}(\phi)$. (i): Additional term $g(\phi)$ arising form the change of variables. In (a,b), the fidelity between ρ_{sc} and ρ_{qm} is $F = 0.976$.

Here, R_{sc} is the autocovariance reconstructed from the phase equation, the mean of a 2π-periodic function $B(\phi)$ is given by $\langle B(\phi)\rangle_{sc} = \int_0^{2\pi} d\phi B(\phi) P_{sc}(\phi)$, and the autocorrelation is given by $\langle B(\phi_2(\tau))B(\phi_1(0))\rangle_{sc} = \int_0^{2\pi} d\phi_1 \int_0^{2\pi} d\phi_2 (B(\phi_2(\tau))B(\phi_1(0)))P(\phi_2, \tau|\phi_1, 0)P_{sc}(\phi_1)$, where $P_{sc}(\phi)$ is a steady phase distribution and $P(\phi_2, t_2|\phi_1, t_1)$ is a transition probability. Both of these probability distributions can be calculated from Eq. (2.10). The observed frequency ω_{qm} of the original system and its approximation ω_{sc} by the phase reduction can be evaluated from the maxima of the spectra as $\omega_{qm,sc} = \arg\max_{\omega} S_{qm,sc}(\omega)$, respectively.

First, we consider the cases with weak squeezing. Figure 2.4(a) shows the two power spectra S_{qm} and S_{sc} for the case where only the harmonic driving is given, and Fig. 2.4(b) shows the spectra for the case with squeezing only.

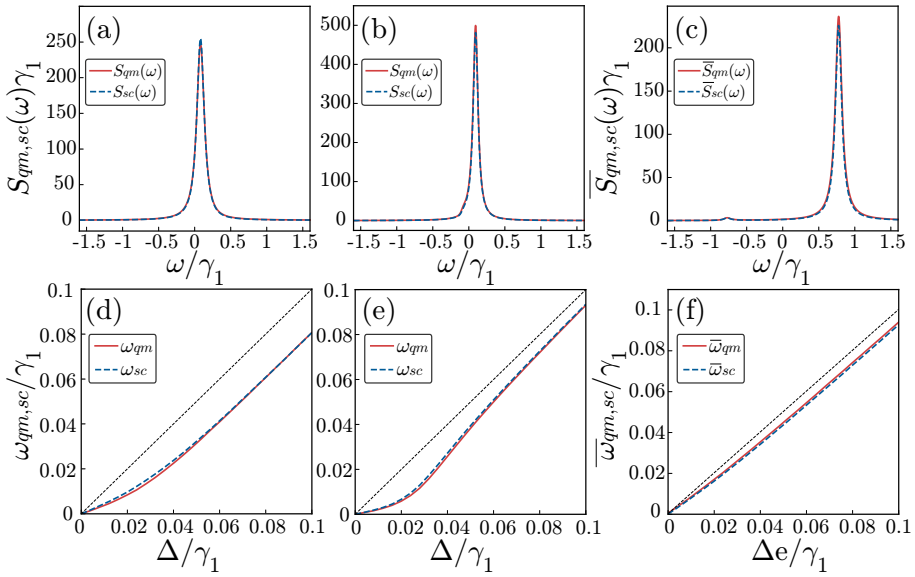

Figure 2.4: Power spectra (a-c) and observed frequencies (d-f) obtained by direct numerical simulations of the master equation (red solid lines) and obtained from the reduced phase equation (blue dotted lines). (a,d): Weak harmonic driving without squeezing, $(\gamma_2, \eta e^{i\theta}, E)/\gamma_1 = (0.05, 0, \sqrt{0.1})$. $\Delta = 0.1$ in (a). (b,e): Weak squeezing without harmonic driving, $(\gamma_2, \eta e^{i\theta}, E)/\gamma_1 = (0.05, 0.025, 0)$. $\Delta = 0.1$ in (b). (c,f): Strong squeezing and weak harmonic driving, $(\Delta, \gamma_2, \eta e^{i\theta}, E)/\gamma_1 = (0.8, 0.05, -0.1i, \sqrt{0.1})$. $\Delta_e = 0.1$ in (c). In (d-f), the black-dotted lines correspond to the unperturbed cases.

In both cases, the true spectrum S_{qm} can be accurately approximated by the reconstructed spectrum S_{sc}. The dependence of the observed frequencies $\omega_{qm,sc}$ on the parameter Δ, where Δ determines the natural frequency of the limit cycle in the classical limit, is shown in Fig. 2.4(d) and (e). It can be confirmed that ω_{qm} is accurately approximated by ω_{sc} in both cases. The oscillator strictly synchronizes to the external driving when the frequency of the oscillator vanishes in the classical limit, because the harmonic driving acts as a constant force in the rotating frame. Here, strict synchronization is prevented by the quantum noise and the observed frequencies $\omega_{qm,sc}$ do not vanish completely; however, the tendency toward synchronization can be clearly seen from the decrease in the observed frequency compared to that of the unperturbed case.

Next, we consider the case with strong squeezing, where the system exhibits asymmetric limit cycle in the classical limit when $\Delta > 2\eta$. We cannot analyze synchronization with the harmonic driving as a stationary problem by using a rotating coordinate frame of frequency ω_d, because the limit cycle is asymmetric and the variation in Δ does not correspond directly to the variation in ω_d. We thus explicitly apply harmonic driving with periodic amplitude modulation $E\cos\omega_e t$ of frequency ω_e and measure ω_{qm} and ω_{sc} as functions of $\Delta_e = \omega - \omega_e$ for $0 \leq \Delta_e \leq 0.1$ ($\omega - 0.1 \leq \omega_e \leq \omega$), where $\omega = 0.7746$.

In this case, we obtain a periodic (cyclo-stationary) solution of period $T_e = 2\pi/\omega_e$ instead of a stationary solution. As shown in Fig. 2.5(a), the quantum-mechanical averages $\langle x\rangle$ and $\langle p\rangle$ of the position and momentum operators $x = (a + a^\dagger)/2$ and $p = -i(a - a^\dagger)/2$ exhibit steady periodic dynamics after the initial transient. Here, the initial condition is a coherent state $|\alpha_0(\phi = 0)\rangle$, where $\boldsymbol{\alpha}_0(\phi = 0)$ is a point on the limit cycle with $\phi = 0$. Figure 2.5(b)-(e) show snapshots of the Wigner distributions in the periodic state, where the system evolves as (b) $\to$ (c) $\to$ (d) $\to$ (e) $\to$ (b). The tendency toward synchronization can be clearly observed from the existence of the dense region co-rotating with the external forcing.

We denote the quantum and approximated autocovariance functions at a given time t_e ($0 \leq t_e < T_e$) of the steady state oscillation as $R^{t_e}_{qm,sc}(\tau)$, where $R^{t_e}_{qm}(\tau)$ is calculated by using a density matrix $\rho_{qm}(t_e)$ at time t_e and $R^{t_e}_{sc}(\tau)$ is calculated by using a phase distribution $P_{sc}(\phi, t_e)$ at time t_e, respectively, in the steadily oscillating state. Then we use the averaged power spectra $\bar{S}_{qm,sc}(\omega) = \int_{-\infty}^{\infty} d\tau e^{i\omega\tau} \int_0^{T_e} dt_e R^{t_e}_{qm,sc}(\tau)/T_e$ to evaluate the observed frequencies relative to the frequency of the amplitude modulation as $\bar{\omega}_{qm,sc} = \arg\max \bar{S}_{qm,sc}(\omega) - \omega_e$. Figure 2.4(c) and (f) compare the averaged spectra $\bar{S}_{qm,sc}(\omega)$ and observed frequencies $\bar{\omega}_{qm,sc}$ obtained by direct numerical simulation of the original master equation and by the approximate phase equation, respectively. It can be seen that the spectrum and observed frequency obtained from the original master equation are accurately reproduced by those obtained from the approximate phase equation. Thus, by using the reduced phase equation, we can approximately reconstruct the spectrum and observed frequency of the original system also in this case.

2.4 Concluding remarks

We have developed a general framework of the phase reduction theory for quantum limit-cycle oscillators under the semiclassical approximation and

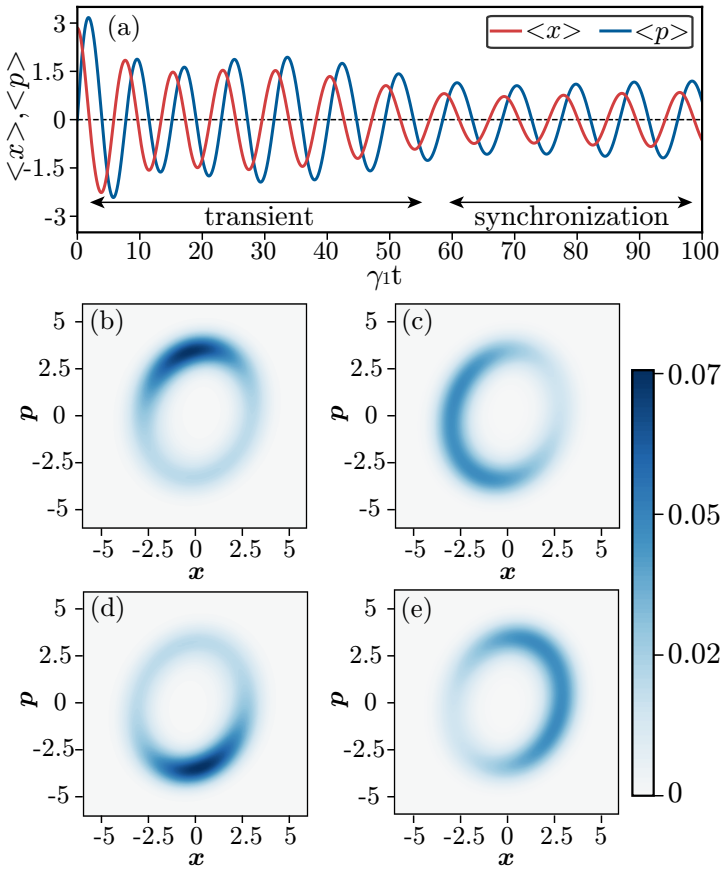

Figure 2.5: Synchronization of a quantum vdP oscillator subjected to harmonic driving with periodic amplitude modulation. (a): Evolution of the averages $\langle x \rangle$ and $\langle p \rangle$ from a coherent-state initial condition. (b-e): Snapshots of the Wigner distributions in the periodic steady (cyclo-stationary) state at time $t = 89.5$ (b), 91.8 (c), 94.1 (d), and 96.4 (e), respectively. The parameters are given by $(\Delta, \gamma_2, \eta e^{i\theta}, E,)/\gamma_1 = (0.8, 0.05, -0.1i, \sqrt{0.1})$ and $\Delta_e = 0.1$.

confirmed its validity by analyzing synchronization dynamics of the quantum vdP model. The proposed framework can approximately characterize the dynamics of a quantum nonlinear oscillator by using a simple classical phase equation, which would serve as a starting point for analyzing synchronization of quantum nonlinear oscillators under the semiclassical approxi-

mation. Although we have only analyzed a single-oscillator problem with a single degree of freedom in this study, the developed framework can be directly extended to two or more quantum oscillators with weak coupling by using standard methods from the classical phase reduction theory. Analysis of large many-body systems and the study of their collective dynamics are of particular interest [48, 67, 42, 47, 68].

In this study, we have employed the P-representation for formulating the semiclassical phase reduction theory; however, other quasiprobability distributions can also be used for the formulation. Detailed comparisons of the results between different representations, including the positive-P representation which is necessary to treat negative-definite diffusion matrices [80], will be discussed in our forthcoming studies. Also, analysis on the genuine quantum signature of a quantum limit-cycle oscillator, which, for instance, can be measured by the negativity of Wigner quasiprobability distributions [61, 57] as observed in the steady state of a quantum vdP oscillator with a strong Kerr drive and external drive [57], could be performed via an extended version of the developed phase reduction theory.

Recently, the phase reduction theory has been applied to control and optimization of synchronization dynamics in classical nonlinear oscillators [14, 13, 15, 18, 17, 87]. In classical dissipative systems, the phase reduction theory has already been used in technical applications of synchronization such as in the ring laser gyroscope [22, 23, 24, 25], phase-locked loop [28, 4], and Josephson voltage standard [26, 27, 4]. The quantum version of these applications, as well as the recent demonstrations [46, 63], could be systematically investigated via the semiclassical phase reduction theory developed in the present study. These subjects will also be discussed in our forthcoming studies.

Chapter 3

Semiclassical optimization of entrainment stability and phase coherence in weakly forced quantum limit-cycle oscillators

In this chapter, optimal entrainment of a quantum nonlinear oscillator to a periodically modulated weak harmonic drive is studied in the semiclassical regime. By using the semiclassical phase reduction theory recently developed for quantum nonlinear oscillators [88], two types of optimization problems, one for the stability and the other for the phase coherence of the entrained state, are considered. The optimal waveforms of the periodic amplitude modulation can be derived by applying the classical optimization methods to the semiclassical phase equation that approximately describes the quantum limit-cycle dynamics. Using a quantum van der Pol oscillator with squeezing and Kerr effects as an example, the performance of optimization is numerically analyzed. It is shown that the optimized waveform for the entrainment stability yields faster entrainment to the driving signal than the case with a simple sinusoidal waveform, while that for the phase coherence yields little improvement from the sinusoidal case. These results are explained from the properties of the phase sensitivity function.

3.1 Introduction

Synchronization of rhythmic nonlinear systems are widely observed all over the real world, including laser oscillations, mechanical vibrations, and calling frogs [89, 1, 2, 4, 3, 7]. It often plays important functional roles in biological or artificial systems, such as cardiac resynchronization [90], phase locked loops in electrical circuits [28], and synchronous power generators [91, 92].

Recently, experimental studies of synchronization have been performed in micro- and nano-scale nonlinear oscillators [36, 37, 39, 77, 78, 79] and theoretical studies of synchronization in the quantum regime have predicted novel features of quantum synchronization [44, 42, 43, 45, 46, 47, 54, 55, 48, 56, 61, 49, 50, 51, 53, 57, 67, 69]. In particular, experimental realization of quantum synchronization is expected in optomechanical oscillators [39, 42, 43, 44], oscillators consisting of cooled atomic ensembles [78, 79, 45, 46], and superconducting devices [53]. Once realized, quantum synchronization may be applicable in quantum metrology, e.g., improvement of the accuracy of measurements in Ramsey spectroscopy for atomic clocks [46].

Nonlinear oscillators possessing a stable limit cycle can be analyzed by using the *phase reduction theory* [2, 4, 7] when the forcing given to the oscillator is sufficiently weak. In the phase reduction theory, multi-dimensional nonlinear dynamical equations describing a limit-cycle oscillator under weak forcing are approximately reduced to a simple one-dimensional phase equation, characterized only by the *natural frequency* and *phase sensitivity function* (PSF) of the oscillator. The reduced phase equation enables us to systematically analyze universal dynamical properties of limit-cycle oscillators, such as the entrainment of an oscillator to a weak periodic forcing or mutual synchronization of weakly coupled oscillators.

The phase reduction theory has also been used in control and optimization of nonlinear oscillators [11]. For example, using the reduced phase equations, minimization of control power for an oscillator [12, 13], maximization of the phase-locking range of an oscillator [14], maximization of linear stability of an oscillator entrained to a periodic forcing [15] and of mutual synchronization between two coupled oscillators [16, 17], maximization of phase coherence of noisy oscillators [18], and phase-selective entrainment of oscillators [19] have been studied.

Similar to classical nonlinear oscillators, quantum nonlinear oscillators in the semiclassical regime can also be analyzed by using the phase equation. In Ref. [63], Hamerly and Mabuchi derived a phase equation from the stochastic differential equation (SDE) describing a truncated Wigner function of a quantum limit-cycle oscillator in a free-carrier cavity. In Ref. [88], we further

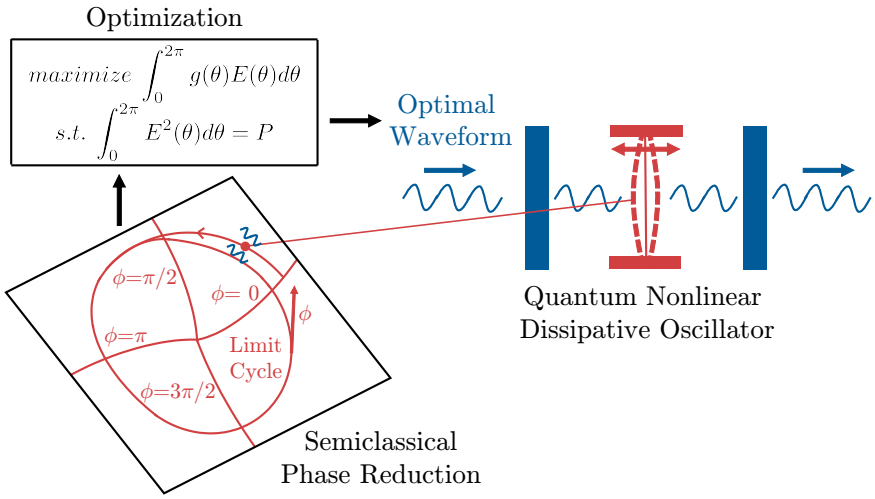

Figure 3.1: A schematic diagram showing optimization of entrainment of a quantum limit-cycle oscillator subjected to a periodically modulated harmonic drive. In the semiclassical regime, the oscillator can be described by a one-dimensional phase equation. Using the reduced phase equation, we can formulate optimization problems and solve them to derive the optimal waveforms of the periodic amplitude modulation of the harmonic drive.

developed a phase reduction framework that is applicable to general single-mode quantum nonlinear oscillators.

In this chapter, using the semiclassical phase reduction theory [88], we optimize entrainment of a quantum nonlinear oscillator to a weak harmonic drive with periodic modulation in the semiclassical regime by employing the optimization methods originally developed for classical oscillators (see Fig. 3.1 for a schematic diagram). Specifically, we consider two types of optimization problems, i.e., (i) improving entrainment stability [15] and (ii) enhancing phase coherence [18] of the oscillator. By using the quantum van der Pol (vdP) oscillator with squeezing and Kerr effects as an example, we illustrate the results of optimization by numerical simulations.

We show that, for the vdP oscillator used in the example, the optimal waveform for the problem (i) leads to larger stability and faster entrainment than the case with the simple sinusoidal waveform, while the optimal waveform for the problem (ii) provides only tiny enhancement of phase coherence from the sinusoidal case. We discuss the difference between the two

optimization problems from the properties of the PSF.

This chapter is organized as follows. In Sec. II, we derive a semiclassical phase equation for a weakly perturbed quantum nonlinear oscillator and derive the optimal waveforms for entrainment. In Sec. III, we illustrate the results of the two optimization methods by numerical simulations and discuss their difference. Sec. IV gives discussion and Appendix gives details of calculations.

3.2 Theory

3.2.1 Master equation

We consider a quantum dissipative system with a single degree of freedom, which is interacting with linear and nonlinear reservoirs and has a stable limit-cycle solution in the classical limit. The system is subjected to a weak harmonic drive with a periodic amplitude modulation of an arbitrary waveform. Under the Markovian approximation of the reservoirs, the system obeys a quantum master equation [81, 80]

$$\dot{\rho} = -i[H - i\epsilon E(\omega_e t)(a - a^\dagger), \rho] + \sum_{m=1}^{n} \mathcal{D}[L_m]\rho, \tag{3.1}$$

in the rotating coordinate frame of the harmonic drive, where ρ is a density matrix representing the system state, H is a system Hamiltonian, a and $a^\dagger$ denote annihilation and creation operators ($\dagger$ represents Hermitian conjugate), respectively, $E(\omega_e t)$ is a 2π-periodic scalar function representing the periodic amplitude modulation with frequency ω_e, ϵ is a tiny parameter ($0 < \epsilon \ll 1$) characterizing weakness of the harmonic drive, n is the number of reservoirs, L_m is the coupling operator between the system and mth reservoir ($m = 1, \ldots, n$), $\mathcal{D}[L]\rho = L\rho L^\dagger - (\rho L^\dagger L + L^\dagger L\rho)/2$ denotes the Lindblad form, and the reduced Planck constant is set as $\hbar = 1$. It is assumed that the modulation frequency ω_e is sufficiently close to the natural frequency ω of the limit cycle in the classical limit.

Using the P representation [81, 80], a Fokker-Planck equation (FPE) equivalent to Eq. (3.1) can be derived as

$$\frac{\partial P(\boldsymbol{\alpha},t)}{\partial t} = \Big[-\sum_{j=1}^{2} \partial_j \{A_j(\boldsymbol{\alpha}) + \epsilon E(\omega_e t)\} + \frac{1}{2}\sum_{j=1}^{2}\sum_{k=1}^{2} \partial_j\partial_k \{\epsilon D_{jk}(\boldsymbol{\alpha})\} \Big] P(\boldsymbol{\alpha}, t), \tag{3.2}$$

where $\boldsymbol{\alpha} = (\alpha, \alpha^*)^\mathsf{T} \in \mathbb{C}^{2\times 1}$ is a two-dimensional complex vector with $\alpha \in \mathbb{C}$ ($*$ represents complex conjugate and T represents transpose), $P(\boldsymbol{\alpha})$ is

the P distribution of $\boldsymbol{\alpha}$, $A_j(\boldsymbol{\alpha})$ is the jth components of a complex vector $\boldsymbol{A}(\boldsymbol{\alpha}) = (A_1(\boldsymbol{\alpha}),\, A_1^*(\boldsymbol{\alpha}))^{\mathsf{T}} \in \mathbb{C}^{2\times 1}(A_2(\boldsymbol{\alpha}) = A_1^*(\boldsymbol{\alpha}))$ representing the system dynamics, $\epsilon D_{jk}(\boldsymbol{\alpha})$ is a (j,k)-component of a symmetric diffusion matrix $\epsilon \boldsymbol{D}(\boldsymbol{\alpha}) \in \mathbb{C}^{2\times 2}$ representing quantum fluctuations, and the complex partial derivatives are defined as $\partial_1 = \partial/\partial\alpha$ and $\partial_2 = \partial/\partial\alpha^*$. The drift term $\boldsymbol{A}(\boldsymbol{\alpha})$ and the diffusion matrix $\epsilon \boldsymbol{D}(\boldsymbol{\alpha})$ can be calculated from the master equation (3.1) by using the standard operator correspondence for the P-representation [81, 80]. The weak harmonic drive with a periodic modulation $\epsilon E(\omega_e t)$ and the diffusion matrix $\epsilon \boldsymbol{D}(\boldsymbol{\alpha})$ are assumed to be of the same order, $\mathcal{O}(\epsilon)$.

Introducing a complex matrix $\sqrt{\epsilon}\boldsymbol{\beta}(\boldsymbol{\alpha}) \in \mathbb{C}^{2\times 2}$ satisfying $\epsilon \boldsymbol{D}(\boldsymbol{\alpha}) = \sqrt{\epsilon}\boldsymbol{\beta}(\boldsymbol{\alpha})(\sqrt{\epsilon}\boldsymbol{\beta}(\boldsymbol{\alpha}))^T$, the Ito SDE corresponding to Eq. (3.2) for the phase-space variable $\boldsymbol{\alpha}(t)$ is obtained as

$$d\boldsymbol{\alpha}(t) = \{\boldsymbol{A}(\boldsymbol{\alpha}(t)) + \epsilon E(\omega_e t)(1,1)^{\mathsf{T}}\}dt + \sqrt{\epsilon}\boldsymbol{\beta}(\boldsymbol{\alpha}(t))d\boldsymbol{W}(t), \tag{3.3}$$

where $\boldsymbol{W} = (W_1, W_2)^{\mathsf{T}} \in \mathbb{R}^{2\times 1}$ is a vector of independent Wiener processes $W_i (i = 1, 2)$ satisfying $\mathbb{E}[dW_i dW_j] = \delta_{ij} dt$ and the explicit form of $\boldsymbol{\beta}(\boldsymbol{\alpha})$ is given by

$$\boldsymbol{\beta}(\boldsymbol{\alpha}) = \begin{pmatrix} \sqrt{\frac{(R_{12}(\boldsymbol{\alpha})+R_{11}(\boldsymbol{\alpha}))}{2}}e^{i\chi(\boldsymbol{\alpha})/2} & -i\sqrt{\frac{(R_{12}(\boldsymbol{\alpha})-R_{11}(\boldsymbol{\alpha}))}{2}}e^{i\chi(\boldsymbol{\alpha})/2} \\ \sqrt{\frac{(R_{12}(\boldsymbol{\alpha})+R_{11}(\boldsymbol{\alpha}))}{2}}e^{-i\chi(\boldsymbol{\alpha})/2} & i\sqrt{\frac{(R_{12}(\boldsymbol{\alpha})-R_{11}(\boldsymbol{\alpha}))}{2}}e^{-i\chi(\boldsymbol{\alpha})/2} \end{pmatrix} \tag{3.4}$$

where $R_{11}(\boldsymbol{\alpha})e^{i\chi(\boldsymbol{\alpha})} = D_{11}(\boldsymbol{\alpha})$ and $R_{12}(\boldsymbol{\alpha}) = D_{12}(\boldsymbol{\alpha})$ [88]. In what follows, we only consider the case in which the diffusion matrix is always positive semidefinite along the limit cycle in the classical limit and derive the phase equation in the two-dimensional phase space of the classical variables [88].

3.2.2 Phase equation and averaging

As discussed in our previous study [88], we can derive an approximate SDE for the phase variable of the system from the SDE (3.3) in the P representation. We define a real vector $\boldsymbol{X} = (x, p)^{\mathsf{T}} = (\mathrm{Re}\ \alpha, \mathrm{Im}\ \alpha)^{\mathsf{T}} \in \mathbb{R}^{2\times 1}$ from the complex vector $\boldsymbol{\alpha}$. Then, the real-valued expression of Eq. (3.3) for $\boldsymbol{X}$ is given by an Ito SDE,

$$d\boldsymbol{X}(t) = \{\boldsymbol{F}(\boldsymbol{X}(t)) + \epsilon E(\omega_e t)(1,0)^{\mathsf{T}}\}dt + \sqrt{\epsilon}\boldsymbol{G}(\boldsymbol{X}(t))d\boldsymbol{W}(t), \tag{3.5}$$

where $\boldsymbol{F}(\boldsymbol{X}) \in \mathbb{R}^{2\times 1}$ and $\boldsymbol{G}(\boldsymbol{X}) \in \mathbb{R}^{2\times 2}$ are real-valued representations of the system dynamics $\boldsymbol{A}(\boldsymbol{\alpha}) \in \mathbb{C}^{2\times 1}$ and noise intensity $\boldsymbol{\beta}(\boldsymbol{\alpha}) \in \mathbb{C}^{2\times 2}$ of Eq. (3.3), respectively.

We assume that the system in the classical limit without perturbation and quantum noise, i.e., $\dot{\boldsymbol{X}} = \boldsymbol{F}(\boldsymbol{X})$, has an exponentially stable limit-cycle solution $\boldsymbol{X}_0(t) = \boldsymbol{X}_0(t+T)$ with a natural period T and frequency $\omega = 2\pi/T$. Following the standard method in the classical phase reduction theory [1, 2, 4, 3, 7], we can introduce an asymptotic phase function $\Phi(\boldsymbol{X}) : \mathbb{R}^{2\times 1} \to [0, 2\pi)$ such that $\nabla\Phi(\boldsymbol{X}) \cdot \boldsymbol{F}(\boldsymbol{X}) = \omega$ is satisfied in the basin of the limit cycle, where $\nabla\Phi(\boldsymbol{X}) \in \mathbb{R}^{2\times 1}$ is the gradient of $\Phi(\boldsymbol{X})$ [2, 7]. The phase of a system state $\boldsymbol{X}$ is defined as $\phi = \Phi(\boldsymbol{X})$, which satisfies $\dot{\phi} = \dot{\Phi}(\boldsymbol{X}) = \boldsymbol{F}(\boldsymbol{X}) \cdot \nabla\Phi(\boldsymbol{X}) = \omega$ ($\cdot$ represents a scalar product between two vectors). We represent the system state $\boldsymbol{X}$ on the limit cycle as $\boldsymbol{X}_0(\phi)$ as a function of the phase ϕ. Note that an identity $\Phi(\boldsymbol{X}_0(\phi)) = \phi$ is satisfied by the definition of $\Phi(\boldsymbol{X})$.

Since we assume that the quantum noise and perturbations are sufficiently weak and the deviation of the state $\boldsymbol{X}(t)$ from the limit cycle is small, at the lowest-order approximation, we can approximate $\boldsymbol{X}(t)$ by $\boldsymbol{X}_0(\phi(t))$ and derive a Ito SDE for the phase ϕ as

$$d\phi = \left\{\omega + \epsilon \boldsymbol{Z}(\phi) \cdot E(\omega_e t)(1,0)^{\mathsf{T}} + \epsilon g(\phi)\right\} dt + \sqrt{\epsilon}\{\boldsymbol{G}(\phi)^{\mathsf{T}} \boldsymbol{Z}(\phi)\} \cdot d\boldsymbol{W}. \tag{3.6}$$

Here, we introduced the PSF $\boldsymbol{Z}(\phi) = \nabla\Phi|_{\boldsymbol{X}=\boldsymbol{X}_0(\phi)} \in \mathbb{R}^{2\times 1}$ characterizing linear response of the oscillator phase to weak perturbations, a noise intensity matrix $\boldsymbol{G}(\phi) = \boldsymbol{G}(\boldsymbol{X}_0(\phi))$, and a function $g(\phi) = \frac{1}{2}\mathrm{Tr}\left\{\boldsymbol{G}(\phi)^{\mathsf{T}} \boldsymbol{Y}(\phi) \boldsymbol{G}(\phi)\right\}$ where $\boldsymbol{Y}(\phi) = \nabla^{\mathsf{T}}\nabla\Phi|_{\boldsymbol{X}=\boldsymbol{X}_0(\phi)} \in \mathbb{R}^{2\times 2}$ is a Hessian matrix of the phase function $\Phi(\boldsymbol{X})$ at $\boldsymbol{X} = \boldsymbol{X}_0(\phi)$ on the limit cycle. The PSF [3] and Hessian [82] can be numerically obtained as 2π-periodic solutions to adjoint-type equations with appropriate constraints. See Ref. [88] for details.

To formulate the optimization problem, we further derive an averaged phase equation from the semiclassical phase equation (3.6). We introduce a phase difference $\psi = \phi - \omega_e t$ between the oscillator and periodic modulation, which is a slow variable obeying

$$\begin{aligned} d\psi = {} & \epsilon \left\{\Delta_e + Z_x(\psi + \omega_e t) E(\omega_e t) + g(\psi + \omega_e t)\right\} dt \\ & + \sqrt{\epsilon}\{\boldsymbol{G}(\psi + \omega_e t)^{\mathsf{T}} \boldsymbol{Z}(\psi + \omega_e t)\} \cdot d\boldsymbol{W}, \end{aligned} \tag{3.7}$$

where $\epsilon\Delta_e = \omega - \omega_e$ and Z_x is the x components of the PSF. Following the standard averaging procedure [2], the small right-hand side of this equation can be averaged over one-period of oscillation via the corresponding FPE [88], yielding an averaged phase equation

$$d\psi = \epsilon \left\{\tilde{\Delta}_e + \Gamma(\psi)\right\} dt + \sqrt{\epsilon}\boldsymbol{D}_0 \cdot d\boldsymbol{W} \tag{3.8}$$

which is correct up to $O(\epsilon)$. Here, $\Gamma(\psi)$ is the phase coupling function defined as

$$\Gamma(\psi) = \langle Z_x(\psi + \theta)E(\theta)\rangle_\theta \,, \tag{3.9}$$

$\tilde{\Delta}_e = \Delta_e + \langle g(\theta)\rangle_\theta = \omega + \langle g(\theta)\rangle_\theta - \omega_e = \tilde{\omega} - \omega_e$ is the effective detuning of the oscillator frequency from the periodic modulation ($\tilde{\omega} := \omega + \langle g(\theta)\rangle_\theta$ is the effective frequency of the oscillator), $\boldsymbol{D}_0 = \left\langle \boldsymbol{G}(\theta)^\mathsf{T}\boldsymbol{Z}(\theta)\right\rangle_\theta$, and the one-period average is denoted as $\langle\cdot\rangle_\theta = \frac{1}{2\pi}\int_0^{2\pi}(\cdot)d\theta$.

If the deterministic part of Eq. (3.8) has a stable fixed point at ψ^*, the phase of the oscillator can be locked to the periodic amplitude modulation, namely, the phase difference ψ between the oscillator and periodic modulation stays around ψ^* as long as the quantum noise is sufficiently weak. We consider optimization of the waveform E of the periodic amplitude modulation for (i) improving entrainment stability and (ii) enhancing phase coherence of the oscillator. For the simplicity of the problem, we assume $\tilde{\Delta} = 0$, that is, the frequency of the periodic amplitude modulation is identical with the effective frequency of the system, $\omega_e = \tilde{\omega}$.

3.2.3 Improvement of entrainment stability

First, we apply the optimization method of the waveform for stable entrainment, formulated by Zlotnik *et al.* [15] for classical limit-cycle oscillators, to the semiclassical phase equation describing a quantum oscillator. The entrainment stability is characterized by the linear stability of the phase-locking point ψ^* in the classical limit without noise, which is given by the slope $-\Gamma'(\psi^*)$. The optimization problem is defined as follows:

$$\text{maximize } -\Gamma^{'}(0), \text{ s.t. } \left\langle E^2(\theta)\right\rangle_\theta = P. \tag{3.10}$$

Here, we assume that the phase locking to the periodic modulation occurs at the phase difference $\psi^* = 0$ without losing generality by shifting the origin of the phase.

The solution to this problem maximizes the linear stability $-\Gamma'(0)$ of the fixed point $\psi^* = 0$ of the deterministic part of Eq. (3.8). Maximization of the linear stability minimizes the convergence time to the fixed point, resulting in faster entrainment of the oscillator to the driving signal when the noise is absent. This problem is solved under the condition that the control power $\langle E^2(\theta)\rangle_\theta$ is fixed to P, where P is assumed to be sufficiently small. As derived in Appendix, the optimal waveform for Eq. (3.10) is explicitly given

by

$$E(\theta) = -\sqrt{\frac{P}{\langle Z_x'(\theta)^2 \rangle_\theta}} Z_x'(\theta), \tag{3.11}$$

which is proportional to the differential of the x component $Z_x(\theta)$ of the PSF.

3.2.4 Enhancement of phase coherence

Next, we apply the optimization method of the waveform for enhancement of phase coherence in the weak noise limit, which was formulated by Pikovsky [18] for classical noisy limit-cycle oscillators, to the semiclassical phase equation describing a quantum oscillator. In the weak noise limit, the phase coherence is characterized by the depth $v(\psi_{max}) - v(\psi^*)$ of the potential $v(\psi) = \int^{\psi} \{-\Gamma(\theta)\} d\theta$ of the deterministic part of Eq. (3.8), where ψ_{max} and ψ^* give the maximum and minimum of the potential $v(\psi)$, respectively (we assume that ψ^* corresponds to the potential minimum, i.e., we focus on the most stable fixed point if there are multiple stable fixed points). In this case, the optimization problem is defined as follows:

$$\text{maximize} \int_{\psi^*}^{\psi_{max}} \{-\Gamma(\psi)\} d\psi, \text{ s.t. } \left\langle E^2(\theta) \right\rangle_\theta = P. \tag{3.12}$$

The solution to this optimization problem maximizes the depth of the potential $v(\psi)$ at the phase-locked point, thereby minimizing the escape rate of noise-induced phase slipping and maximizing the phase coherence of the oscillator under sufficiently weak noise, as discussed in Ref. [18] for the classical case. As in the previous problem, this optimization problem is solved under the condition that the control power $\left\langle E^2(\theta) \right\rangle_\theta$ is fixed to P.

In what follows, we introduce $\Delta_\psi = \psi_{max} - \psi^*$ and assume $\psi^* = 0$ without loss of generality. Then, the optimal waveform is obtained as (see Appendix for the derivation)

$$E(\theta) = -\sqrt{\frac{P}{\left\langle \left(\int_\theta^{\theta+\Delta_\psi} Z_x(\bar{\theta}) d\bar{\theta} \right)^2 \right\rangle_\theta}} \int_\theta^{\theta+\Delta_\psi} Z_x(\bar{\theta}) d\bar{\theta}, \tag{3.13}$$

which is proportional to the integral of the x component $Z_x(\phi)$ of the PSF, in contrast to the previous case in which the optimal waveform is proportional to the differential of $Z_x(\phi)$.

3.3 Results

3.3.1 Quantum van der Pol oscillator

As an example, we consider a quantum vdP oscillator with squeezing and Kerr effects subjected to a periodically modulated harmonic drive. In our previous study [88], we have analyzed entrainment of a vdP oscillator with only a squeezing effect to a purely sinusoidal periodic modulation; in this study, we seek optimal waveforms of the periodic modulation for a vdP oscillator with both squeezing and Kerr effects. We use QuTiP numerical toolbox for direct numerical simulations of the master equation [85, 86].

We assume that the harmonic drive is sufficiently weak and treat it as a perturbation, while the squeezing and Kerr effects are both relatively strong and cannot be treated as perturbations. The frequencies of the oscillator, harmonic drive, and pump beam of squeezing are denoted by ω_0, ω_d, and ω_{sq}, respectively. We consider the case in which the squeezing is generated by a degenerate parametric amplifier and we set $\omega_{sq} = 2\omega_d$.

In the rotating coordinate frame of frequency ω_d, the master equation for the quantum vdP oscillator is given by [88, 57]

$$\begin{aligned}\dot{\rho} = &-i[-\Delta a^\dagger a + K a^{\dagger 2} a^2 - iE(\omega_e t)(a - a^\dagger) + i\eta(a^2 e^{-i\theta} - a^{\dagger 2} e^{i\theta}), \rho] \\ &+ \gamma_1 \mathcal{D}[a^\dagger]\rho + \gamma_2 \mathcal{D}[a^2]\rho, \end{aligned} \tag{3.14}$$

where $\Delta = \omega_d - \omega_0$ is the frequency detuning of the harmonic drive from the oscillator, K is the Kerr parameter, $E(\omega_e t)$ is the periodic amplitude modulation of the harmonic drive, $\eta e^{i\theta}$ is the squeezing parameter, γ_1 and γ_2 are the decay rates for negative damping and nonlinear damping, respectively.

We assume γ_2 to be sufficiently small, for which the semiclassical approximation is valid, and represent γ_2 as $\gamma_2 = \epsilon\gamma_1\gamma_2^{'}$ with a dimensionless parameter $\gamma_2^{'}$ of $\mathcal{O}(1)$. As discussed in Ref. [88], to rescale the size of the limit cycle to be $O(1)$, we introduce a rescaled annihilation operator a', classical variable α', and rescaled parameters $\Delta = \gamma_1\Delta', K = \epsilon\gamma_1 K^{'}, E(\omega_e t) = \sqrt{\epsilon}\gamma_1 E'(\omega_e t), \eta = \gamma_1\eta'$, where Δ', K', E', η' are dimensionless parameters of $\mathcal{O}(1)$. We also rescale the time and frequency of the periodic modulation as $t' = \gamma_1 t$ and $\omega_e = \gamma_1\omega_e'$, respectively. The FPE for the P distribution

corresponding to Eq. (3.14) is then given by

$$\frac{\partial P(\boldsymbol{\alpha'},t')}{\partial t'} = \Big[-\sum_{j=1}^{2} \partial'_j \{A_j(\boldsymbol{\alpha'}) + \epsilon E'(\omega'_e t')\} + \frac{1}{2}\sum_{j=1}^{2}\sum_{k=1}^{2} \partial'_j \partial'_k \{\epsilon D_{jk}(\boldsymbol{\alpha'})\}\Big] P(\boldsymbol{\alpha'},t'), \tag{3.15}$$

where $\boldsymbol{\alpha'} = (\alpha', \alpha'^*) = \sqrt{\epsilon}(\alpha, \alpha^*)$, $\partial'_1 = \partial/\partial\alpha'$, $\partial'_2 = \partial/\partial\alpha'^*$,

$$\boldsymbol{A}(\boldsymbol{\alpha'}) = \begin{pmatrix} \left(\frac{1}{2} + i\Delta'\right)\alpha' - (\gamma'_2 + 2K'i)\alpha'^*\alpha'^2 - 2\eta' e^{i\theta}\alpha'^* \\ \left(\frac{1}{2} - i\Delta'\right)\alpha'^* - (\gamma'_2 - 2K'i)\alpha'\alpha'^{*2} - 2\eta' e^{-i\theta}\alpha' \end{pmatrix}, \tag{3.16}$$

and

$$\boldsymbol{D}(\boldsymbol{\alpha'}) = \begin{pmatrix} -((\gamma'_2 + 2K'i)\alpha'^2 + 2\eta' e^{i\theta}) & 1 \\ 1 & -((\gamma'_2 - 2K'i)\alpha'^{*2} + 2\eta' e^{-i\theta}) \end{pmatrix}. \tag{3.17}$$

The real-valued vector $\boldsymbol{X} = (x', p')^{\mathsf{T}} = (\mathrm{Re}\ \alpha', \mathrm{Im}\ \alpha')^{\mathsf{T}}$ of Eq. (3.5) after rescaling is

$$d\boldsymbol{X} = \begin{pmatrix} \frac{1}{2}x' - \Delta' p' - (\gamma'_2 x' - 2K' p')(x'^2 + p'^2) + \epsilon E'(\omega'_e t') - 2\eta'(x'\cos\theta + p'\sin\theta) \\ \frac{1}{2}p' + \Delta' x' - (\gamma'_2 p' + 2K' x')(x'^2 + p'^2) + 2\eta'(p'\cos\theta - x'\sin\theta) \end{pmatrix} dt + \sqrt{\epsilon}\boldsymbol{G}(\boldsymbol{X}) d\boldsymbol{W}', \tag{3.18}$$

where $d\boldsymbol{W'} = \sqrt{\gamma_1} d\boldsymbol{W}$ and the noise intensity matrix is explicitly given by

$$\boldsymbol{G}(\boldsymbol{X}) = \begin{pmatrix} \sqrt{\frac{(1+R'_1)}{2}}\cos\frac{\chi'_1}{2} & \sqrt{\frac{(1-R'_1)}{2}}\sin\frac{\chi'_1}{2} \\ \sqrt{\frac{(1+R'_1)}{2}}\sin\frac{\chi'_1}{2} & -\sqrt{\frac{(1-R'_1)}{2}}\cos\frac{\chi'_1}{2} \end{pmatrix} \tag{3.19}$$

with $R'_1 e^{i\chi'_1} = -((\gamma'_2 + 2K'i)\alpha'^2 + 2\eta' e^{i\theta})$. The deterministic part of Eq. (3.18) without the harmonic drive ($E' = 0$) gives an asymmetric limit cycle when $\eta' > 0$ and cannot be solved analytically. Hence, we numerically obtain the limit cycle $\boldsymbol{X}_0(\phi)$ and evaluate the PSF $\boldsymbol{Z}(\phi)$, Hessian matrix $\boldsymbol{Y}(\phi)$, and noise intensity $\boldsymbol{G}(\phi)$. We then use these quantities to derive the optimal waveforms.

We consider two parameter sets, which correspond to (i) a limit cycle with asymmetry due to the effect of squeezing, $(\Delta, \gamma_2, \eta e^{i\theta}, K)/\gamma_1 =$

$(0.575, 0.05, 0.2, 0)$, and (ii) a limit cycle with asymmetry due to squeezing and Kerr effects, $(\Delta, \gamma_2, \eta e^{i\theta}, K)/\gamma_1 = (0, 0.05, 0.15, 0.03)$. Note that we use parameter sets for which the limit cycles in the classical limits are asymmetric for the evaluation of the optimization methods. This is because the optimal waveform is given by a trivial sinusoidal function when the limit cycle is symmetric and the x component of the PSF has a sinusoidal form (see Appendix). We set the control power as $P = \sqrt{0.2}$ and compare the results for optimal waveforms with those for the simple sinusoidal waveform.

Figures 3.2 (1a-1c) and (2a-2c) show the limit cycles and PSFs in the classical limit for the cases (i) and (ii), respectively. The natural and effective frequencies of the oscillator are $(\omega, \tilde{\omega}) = (0.413, 0.407)$ in the case (i) and $(\omega, \tilde{\omega}) = (0.510, 0.451)$ in the case (ii), respectively. In the case (i), the drift coefficient of the phase variable is positive when the oscillator rotates counterclockwise and the origin of the phase $\phi = 0$ is chosen as the intersection of the limit cycle and the x' axis with $x' > 0$. In the case (ii), the drift coefficient of the phase variable is positive when the oscillator rotates clockwise and the origin of the phase $\phi = 0$ is chosen as the intersection of the limit cycle and the x' axis with $x' < 0$.

3.3.2 Improvement of entrainment stability

To evaluate the performance of the optimal waveform for the entrainment stability, we use half the square of the Bures distance $F_q(\rho_1, \rho_2) = 1 - \mathrm{Tr}\left[\sqrt{\sqrt{\rho_2}\rho_1\sqrt{\rho_2}}\right]$ obtained by direct numerical simulations of the master equation (3.14) and the corresponding classical distance $F_c(P_1(\psi), P_2(\psi)) = 1 - \left\langle \sqrt{P_1(\psi)P_2(\psi)} \right\rangle_\psi$ for the probability distributions of the phase variable [93] obtained from the reduced phase equation (3.6). We consider the distance between the system states at t and $t + T_e$ with $T_e = 2\pi/\omega_e$ (i.e., one period later), and use $F_q(\rho_t, \rho_{t+T_e})$ and $F_c(P_t(\psi), P_{t+T_e}(\psi))$ to measure the performance, since $F_q(\rho_t, \rho_{t+T_e})$ and $F_c(P_t(\psi), P_{t+T_e}(\psi))$ converge to zero when the system converges to a periodic steady (cyclo-stationary) state with period T_e.

To eliminate the dependence on the initial phase θ_0 of the input, we calculate $F_{c,q}^{\theta_0}$ by using an input signal $E(\omega_e t + \theta_0)$, average it over $0 \leq \theta_0 < 2\pi$ to obtain $\left\langle F_{c,q}^{\theta_0} \right\rangle_{\theta_0}$, and use this as the measure for evaluating the entrainment of the oscillator. We set the initial state of the density matrix as the steady state of Eq. (3.14) without the periodically modulated harmonic drive (E = 0), and the initial state of the corresponding phase distribution as a uniform distribution $P(\psi) = 1/(2\pi)$. Figures 3.3(1a-1d) and 3.3(2a-2d)

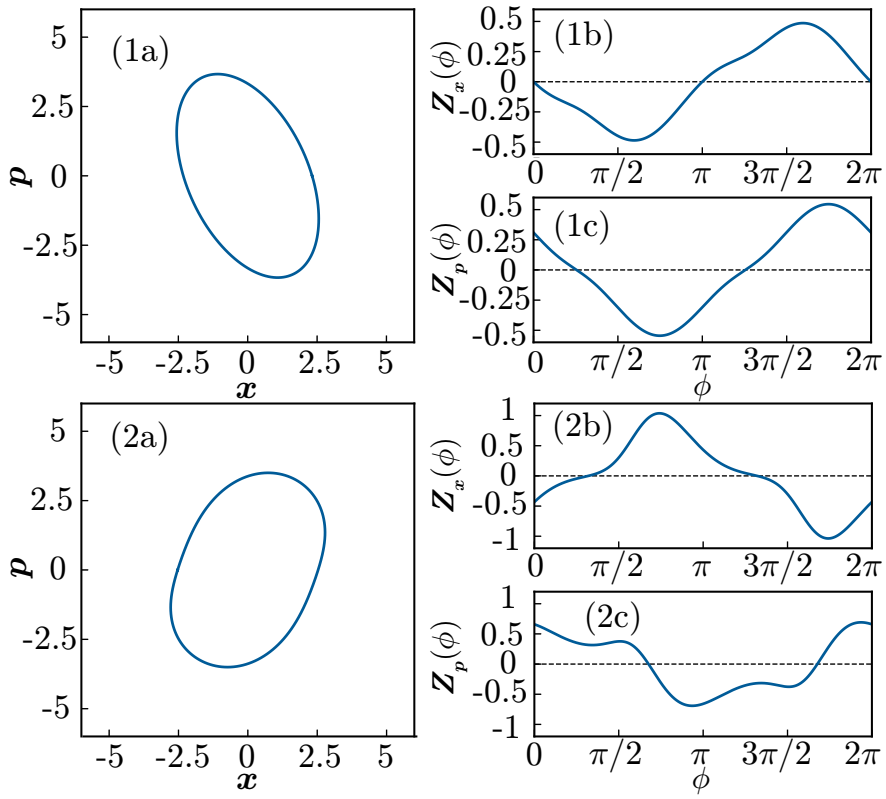

Figure 3.2: Limit cycles and phase sensitivity functions of a quantum van der Pol oscillator with only the squeezing effect (1a, 1b, 1c) and with both squeezing and Kerr effects (2a, 2b, 2c). (1a,2a): Limit cycle $\boldsymbol{X}_0(\phi)$ in the classical limit. (1b,2b): x component $Z_x(\phi)$ of the PSF $\boldsymbol{Z}(\phi)$. (1c,2c): p component $Z_p(\phi)$ of the PSF $\boldsymbol{Z}(\phi)$. Note that the figures are drawn using x and p before rescaling.

show the results for the cases (i) and (ii), respectively, where the optimal waveforms of E are plotted in Figs. 3.3(1a, 2a), the phase-coupling functions Γ are plotted in Figs. 3.3(1b, 2b), the classical distances F_c are plotted in Figs. 3.3(1c, 2c), and the quantum distance F_q are plotted in Figs. 3.3(1d, 2d).

In the case (i), the linear stability of the entrained state is given by $-\Gamma'_{opt}(0) = 0.226$ in the optimized case, which is higher than $-\Gamma'_{sin}(0) = 0.208$ in the sinusoidal case by a factor $\Gamma'_{opt}(0)/\Gamma'_{sin}(0) = 1.083$. As a

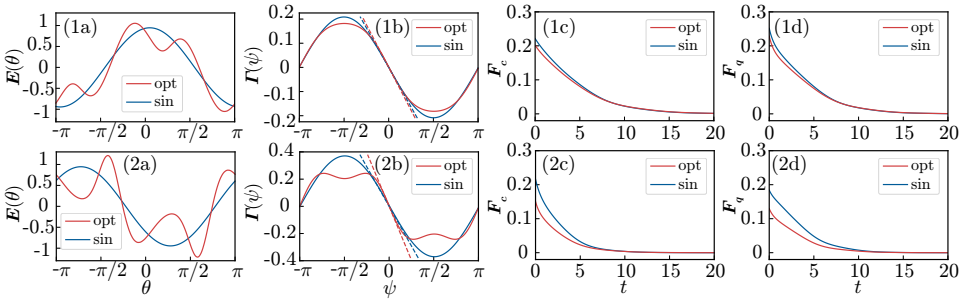

Figure 3.3: Results of optimization for the entrainment stability in the case (i) (1a-1d) and case (ii) (2a-2d). Red lines show the results for the optimal waveform, and blue lines show the results for the sinusoidal waveform. (1a,2a): Optimal waveform E of the periodic amplitude modulation. (1b,2b): Interaction function Γ. (1c,2c): Classical distance F_c. (1d,2d): Quantum distance F_q.

result, faster entrainment to the entrained state can be observed in both Figs. 3.3(1c) and 3.3(1d) in the optimized cases. In the case (ii), the linear stability is given by $-\Gamma'_{opt}(0) = 0.503$ in the optimized case, which is higher than $-\Gamma'_{sin}(0) = 0.371$ in the sinusoidal case by a factor $\Gamma'_{opt}(0)/\Gamma'_{sin}(0) = 1.358$. Faster entrainment to the entrained state can also be confirmed from Figs. 3.3(2c) and 3.3(2d), where both F_c and F_q converge faster in the optimized cases.

Note that larger improvement factor is attained in the case (ii) than in the case (i), which results from stronger anharmonicity of the PSF in the case (ii) than in the case (i). This point will be discussed in Sec. III D.

3.3.3 Enhancement of phase coherence

To evaluate the performance of the optimal waveform for the phase coherence, we use the averaged maximum value of the Wigner function $\langle \max W^{\psi} \rangle_{\psi}$, where W^{ψ} is the Wigner distribution of the density matrix ρ at phase ψ of the periodic steady state obtained by direct numerical simulations of the master equation (3.14). We also use the averaged maximum value for the corresponding probability distribution of the phase variable $\langle \max P^{\psi} \rangle_{\psi}$, where P^{ψ} is the probability distribution at phase ψ of the periodic steady state obtained from the reduced phase equation (3.6).

Figure 3.4(1a) and 3.4(2a) show the optimal waveforms of E, and

Fig. 3.4(1b) and 3.4(2b) show the potential v of the phase difference. In the case (i), the maximum value of the potential v is given by $v_{opt}(\Delta_\psi) = 0.4172$ in the optimized case, which is slightly higher than $v_{sin}(\Delta_\psi) = 0.4167$ in the sinusoidal case by a factor $v_{opt}(\Delta_\psi)/v_{sin}(\Delta_\psi) = 1.001$. Accordingly, we obtain a tiny enhancement of phase coherence from the averaged maximum values of both the Wigner distribution of the quantum system $\left\langle \max W^{\psi}_{opt} \right\rangle_{\psi} / \left\langle \max W^{\psi}_{sin} \right\rangle_{\psi} = 1.0028$ and the corresponding probability distribution of the classical phase variable $\left\langle \max P^{\psi}_{opt} \right\rangle_{\psi} / \left\langle \max P^{\psi}_{sin} \right\rangle_{\psi} = 1.0076$, although it is difficult to see the difference from Fig. 3.4(1b) itself.

In the case (ii), the maximum value of the potential v is given by $v_{opt}(\Delta_\psi) = 0.7447$ in the optimized case, which is also slightly higher than $v_{sin}(\Delta_\psi) = 0.7411$ in the sinusoidal case by $v_{opt}(\Delta_\psi)/v_{sin}(\Delta_\psi) = 1.005$. We obtain a tiny enhancement of phase coherence from both the averaged maximum values of the Wigner function of the quantum system $\left\langle \max W^{\psi}_{opt} \right\rangle_{\psi} / \left\langle \max W^{\psi}_{sin} \right\rangle_{\psi} = 1.0063$ and the corresponding probability distribution of the classical phase variable $\left\langle \max P^{\psi}_{opt} \right\rangle_{\psi} / \left\langle \max P^{\psi}_{sin} \right\rangle_{\psi} = 1.0143$.

For the vdP oscillator used here, only tiny enhancements in the phase coherence can be observed in both case (i) and case (ii). This is because the PSF does not have strong high-harmonic components in both cases (see Fig. 3.5). It should also be noted that the improvement factor in the case (ii) is larger than in case (i), which results from stronger anharmonicity of the PSF in the case (ii) than in the case (i). We discuss these points in Sec. III D.

3.3.4 Comparison of two optimization problems

In Sec. III B, we could observe that the optimized waveforms yield clearly faster convergence to the entrained state than the sinusoidal waveform, indicating improvements in the stability of the entrained state, while in Sec. III C, we could observe only tiny enhancements in the phase coherence from the sinusoidal case. This difference between the two optimization problems can be explained from the general expressions for the optimized waveforms.

The optimal waveform for the entrainment stability is proportional to the differential of the x component Z_x of the PSF as can be seen from Eq. (3.11), while that for the phase coherence is proportional to the integral of Z_x as in Eq. (3.13). Because the PSF is a 2π-periodic function, Z_x can

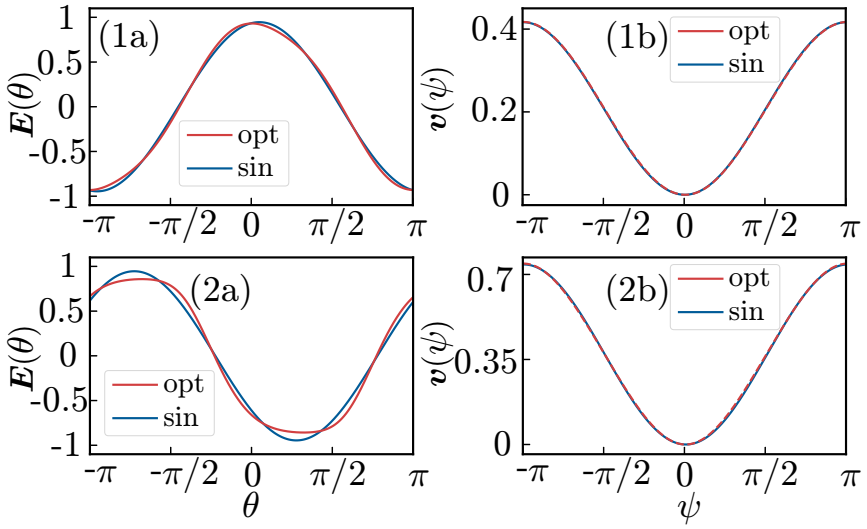

Figure 3.4: Results for enhancement of phase coherence in the case (i) (1a, 1b) and case (ii) (2a, 2b). Red lines show the results for the optimal waveform, and blue lines show the results for the sinusoidal waveform, respectively. (1a,1b): Optimal waveform E of the periodic amplitude modulation. (2a,2b): Potential v of the phase difference.

be expanded in a Fourier series as

$$Z_x(\theta) = \sum_{n=-\infty}^{\infty} Z_n \exp[in\theta], \tag{3.20}$$

where Z_n $(n = 0, \pm 1, \pm 2, \cdots)$ are the Fourier coefficients. The differential of $Z_x(\theta)$ can then be expressed as

$$Z'_x(\theta) = \sum_{n=-\infty}^{\infty} inZ_n \exp[in\theta], \tag{3.21}$$

and the integral of $Z_x(\theta)$ can be expressed as

$$\int_{\theta}^{\theta+\Delta_\psi} Z_x(\bar{\theta})d\bar{\theta} = \sum_{n=-\infty(n\neq 0)}^{\infty} \frac{Z_n(\exp[in(\theta+\Delta_\psi)] - \exp[in\theta])}{in}, \tag{3.22}$$

where $n = 0$ is omitted from the sum to avoid vanishing denominator without changing the result. Thus, the deviation of the differential $Z'_x(\theta)$ from

the sinusoidal function is larger because the nth Fourier component is multiplied by n, while the deviation of the integral $\int_\theta^{\theta+\Delta_\psi} Z_x(\psi)d\psi$ from the sinusoidal function is smaller because the nth Fourier component is divided by n. This explains the difference in the performance of the two optimization problems, namely, why we observed considerable improvement in the entrainment stability while only tiny improvement in the phase coherence from the simple sinusoidal waveform.

From the above expressions, we also find that the deviations of $Z_x'(\theta)$ and $\int_\theta^{\theta+\Delta_\psi} Z_x(\theta)d\psi$ from the sinusoidal function are more pronounced when the PSF possesses stronger high-frequency components. Figures 3.5(1a,1b) and 3.5(2a,2b) show the absolute values of the normalized Fourier components $\bar{Z}_n = |Z_n|/\sum_{n=0}^{\infty}|Z_n|$ in the cases (i) and (ii), respectively. It can be seen that the PSF $\bar{Z}_n$ in the case (ii) has larger values of the normalized high-frequency Fourier components than in the case (i), which leads to the larger improvement factor by the optimization in the case (ii) than in the case (i).

3.4 Discussion

We considered two types of optimization problems for the entrainment of a quantum nonlinear oscillator to a harmonic drive with a periodic amplitude modulation in the semiclassical regime. We derived the optimal waveforms of the periodic amplitude modulation by applying the optimization methods originally formulated for classical limit-cycle oscillators to the semiclassical phase equation describing a quantum nonlinear oscillator. Numerical simulations for the quantum vdP oscillator with squeezing and Kerr effects showed that the optimization of the entrainment stability leads to visibly faster convergence to the entrained state than the simple sinusoidal waveform, while the optimization for the phase coherence provides only tiny enhancement of the phase coherence from the sinusoidal case. These results were explained from the Fourier-spectral properties of the PSF. The squeezing and Kerr effects induced asymmetry of the limit-cycle orbit in the classical limit and yielded PSFs with stronger high-harmonic components, resulting in larger optimization performance. It was also shown that optimization provides better performance when the PSF of the limit cycle has stronger high-frequency Fourier components in both problems.

The optimal waveforms for three typical optimization problems, i.e., improvement of entrainment stability [15], phase coherence [18], and locking range [14] (not considered in this study), which have been discussed for classical nonlinear oscillators in the literature, are proportional to the differential

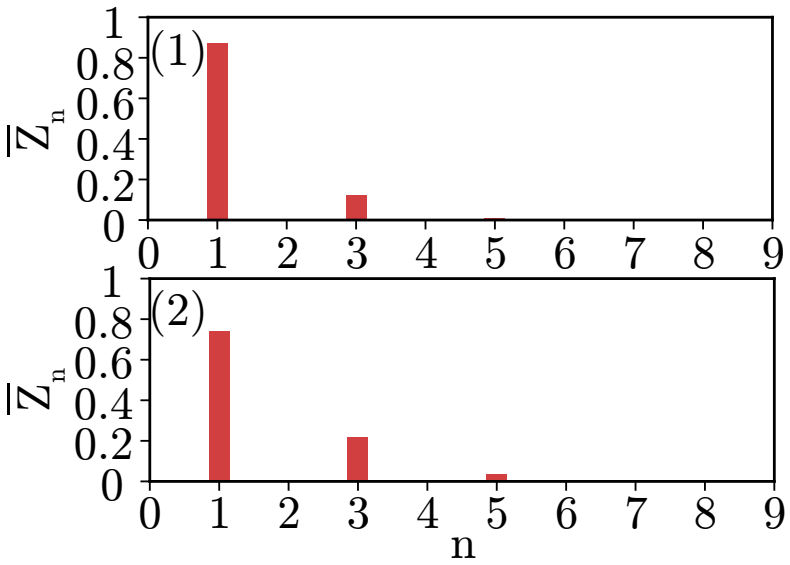

Figure 3.5: Normalized absolute value of Fourier components $\bar{Z}_n = |Z_n|/\sum_{n=0}^{\infty}|Z_n|$ in the cases (i) (top) and (ii) (bottom). In case (i) $(\bar{Z}_0, \bar{Z}_1, \bar{Z}_2, \bar{Z}_3, \bar{Z}_4, \bar{Z}_5, \bar{Z}_6, \bar{Z}_7, \bar{Z}_8, \bar{Z}_9) = (0, 0.87, 0, 0.12, 0, 0.009, 0, 0.001, 0, 0)$, and in case (ii) $(\bar{Z}_0, \bar{Z}_1, \bar{Z}_2, \bar{Z}_3, \bar{Z}_4, \bar{Z}_5, \bar{Z}_6, \bar{Z}_7, \bar{Z}_8, \bar{Z}_9) = (0, 0.741, 0, 0.219, 0, 0.034, 0, 0.005, 0, 0.001)$, respectively.

of the PSF, integral of PSF, and PSF itself, respectively. All these waveforms yield negative feedback to the phase difference between the oscillator and the periodic forcing. It is interesting to note that these relations between the optimal waveforms and PSFs bear some similarity to the proportional-integral-differential (PID) controller in the feedback control theory; in the framework of the PID control for linear time invariant systems [94], the differential control is often used for improving convergence, the integral control is used for improving the steady-state property, and the proportional control is used for improving the stability of the system. Thus, similar to the PID controller, combined use of the three types of optimization methods for nonlinear oscillators could yield even better performance for achieving specific control goals of entrainment.

Though we have considered only the optimization problems for the stability and phase coherence of the entrained state in the present study, we would also be able to apply other optimization and control methods devel-

oped for classical limit-cycle oscillators, e.g. the phase-selective entrainment of oscillators [19] and maximization of the linear stability of mutual synchronization between two oscillators [16, 17], to quantum nonlinear oscillators by using the phase equation for a quantum nonlinear dissipative oscillator under the semiclassical approximation. Such methods of optimal entrainment could be physically implemented with semiconductor optical cavities [63] or optomechanical systems consisting of optical cavities and mechanical devices [44] exhibiting limit-cycle behaviors, and useful in future applications of quantum synchronization phenomena in quantum technologies.

Chapter 4

Quantum asymptotic phase reveals signatures of quantum synchronization

In this chapter, we propose a fully quantum-mechanical definition of the asymptotic phase for quantum nonlinear oscillators. The asymptotic phase function of the system is introduced in terms of the eigenoperator of the adjoint Liouville superoperator associated with the fundamental frequency. This *quantum asymptotic phase* yields appropriate phase values of the system even in the strong quantum regime, while reproducing the conventional asymptotic phase in the semiclassical regime. We analyze a quantum van der Pol oscillator with Kerr effect and show that several dominant eigenoperators with different fundamental frequencies exist in the strong quantum regime. Using the quantum asymptotic phase functions with respective fundamental frequencies, we reveal that the multiple phase locking of the system with a harmonic drive at several different frequencies, an explicit quantum signature observed only in the strong quantum regime, can be interpreted as synchronization on a torus rather than a simple limit cycle.

4.1 Introduction

Synchronization of spontaneous rhythmic oscillations are widely observed in nature [1, 2, 4, 7, 3, 6]. Recently, rapid progress has been made in the experimental realization of synchronization in micro- and nanoscale devices [41, 95, 96, 97] and theoretical investigations have been performed to reveal quantum signatures in synchronization [57, 69, 43, 49, 61, 65, 88, 98, 47,

54, 55, 45, 50, 48]. In the strong quantum regime where only a small number of energy states participate in the system dynamics, the discrete nature of the energy spectrum can give rise to explicit quantum signatures, such as multiple phase locking at different frequencies [57] and synchronization blockade [69]. Several measures of the system's phase values for characterizing quantum synchronization have also been proposed [57, 43, 49, 61, 65].

In the classical case, rhythmic oscillations are typically modeled by nonlinear dynamical systems possessing a stable limit-cycle solution. In analyzing synchronization properties of such nonlinear oscillators, the *asymptotic phase* [1, 2, 4, 7, 3], defined by the oscillator's vector field and increasing with a constant frequency in the basin of the limit-cycle attractor, plays a central role. It provides the basis for *phase reduction* [1, 2, 4, 7, 3, 6], a standard method for deriving phase equations of weakly-coupled oscillators by dimensionality reduction. Derivation of phase equations for quantum nonlinear oscillators in the semiclassical regime has also been performed, where the system is described by a stochastic differential equation for the phase-space state fluctuating along a deterministic classical trajectory due to small quantum noise [63, 88, 98]. However, this method is not applicable in the strong quantum regime where such a description is not allowed. In particular, we cannot define the asymptotic phase of the system by using the classical deterministic trajectory.

In this study, we propose a fully quantum-mechanical definition of the asymptotic phase for quantum nonlinear oscillators. Our idea is inspired by the definition of the asymptotic phase for classical stochastic oscillators in terms of the eigenfunction of the backward Kolmogorov operator by Thomas and Lindner [99], which is natural from the Koopman-operator viewpoint (see Appendix). We introduce asymptotic phase functions in terms of the eigenoperators of the system's adjoint Liouville superoperator and show that they can reveal the structure of multiple phase locking of the quantum van der Pol oscillator with a harmonic drive at several different frequencies [57], which is observed only in the strong quantum regime.

4.2 Asymptotic phase for quantum nonlinear oscillators

We consider quantum dissipative oscillatory systems with a single degree of freedom. Assuming that interactions of the system with the reservoirs are instantaneous and Markovian approximation can be employed, the evolution

of the system's density matrix ρ is described by a quantum Master equation

$$\dot{\rho} = \mathcal{L}\rho = -i[H, \rho] + \sum_{j=1}^{n} \mathcal{D}[C_j]\rho \tag{4.1}$$

in the Schrödinger picture, where $\mathcal{L}$ is a Liouville superoperator representing the evolution of ρ, H is a system Hamiltonian, C_j is a coupling operator between the system and jth reservoir ($j = 1, \ldots, n$), $\mathcal{D}[C]\rho = C\rho C^\dagger - (\rho C^\dagger C + C^\dagger C\rho)/2$ is the Lindblad form ($\dagger$ denotes Hermitian conjugate), and the reduced Planck constant is set as $\hbar = 1$.

We introduce an inner product $\langle X, Y\rangle_{tr} = \mathrm{Tr}\,(X^\dagger Y)$ of linear operators X and Y and define the adjoint superoperator $\mathcal{L}^*$ of $\mathcal{L}$ satisfying $\langle \mathcal{L}^* X, Y\rangle_{tr} = \langle X, \mathcal{L}Y\rangle_{tr}$,

$$\mathcal{L}^* X = i[H, X] + \sum_{j=1}^{n} \mathcal{D}^*[C_j]X, \tag{4.2}$$

where $\mathcal{D}^*[C]X = C^\dagger X C - (XC^\dagger C + C^\dagger C X)/2$. This $\mathcal{L}^*$ describes the evolution of an observable F as $\dot{F} = \mathcal{L}^* F$ in the Heisenberg picture, in which the density matrix ρ does not vary with time while the expectation value $\langle F\rangle = \mathrm{Tr}(\rho F) = \langle \rho, F\rangle_{tr}$ of F with respect to ρ is kept the same as in the Schrödinger picture (note that ρ and F are self-adjoint).

We assume that the superoperators $\mathcal{L}$ has a set of eigensystem (an eigenvalue and right and left eigenoperators) $\{\lambda_k, U_k, V_k\}$ satisfying

$$\mathcal{L}U_k = \lambda_k U_k, \quad \mathcal{L}^* V_k = \overline{\lambda_k} V_k, \quad \langle V_k, U_l\rangle_{tr} = \delta_{kl}, \tag{4.3}$$

for $k, l = 0, 1, 2, \ldots$, where the overline indicates complex conjugate [100]. Among $\{\lambda_k\}_{k\geq 0}$, one eigenvalue is always 0, which is associated with the stationary state ρ_0 of the system satisfying $\mathcal{L}\rho_0 = 0$, and all other eigenvalues have negative real parts. We assume that the eigenvalues with the largest non-vanishing real part (the slowest decay rate) are given by a complex-conjugate pair, reflecting the system's oscillatory dynamics, and denote them as Λ_1 and $\overline{\Lambda_1}$, where $\Omega_1 = \mathrm{Im}\ \overline{\Lambda_1}$ (with the sign to be determined later) gives the fundamental frequency [1]. There may also exist other complex eigenvalues with different fundamental frequencies that are dominant in the sense explained later; we denote such eigenvalues by $\Lambda_2, \Lambda_3, \ldots$ and their imaginary parts by $\Omega_j = \mathrm{Im}\ \overline{\Lambda_j}$ ($j \geq 2$), and call $\{\Lambda_j\}_{j\geq 1}$ the *principal eigenvalues*.

[1] One may also choose $\Omega_1 = \mathrm{Im}\ \Lambda_1$, which reverses the direction of the asymptotic phase.

The density matrix ρ can also be described by a quasiprobability distribution in the phase space [80, 81, 101]. We use the P-representation and write ρ as

$$\rho = \int p(\boldsymbol{\alpha})|\alpha\rangle\langle\alpha| d\boldsymbol{\alpha}, \tag{4.4}$$

where $|\alpha\rangle$ is a coherent state specified by a complex value $\alpha \in \mathbb{C}$, or equivalently by a complex vector $\boldsymbol{\alpha} = (\alpha, \overline{\alpha})^T \in \mathbb{C}^2$, $p(\boldsymbol{\alpha})$ is a quasiprobability distribution of $\boldsymbol{\alpha}$, $d\boldsymbol{\alpha} = d\alpha d\overline{\alpha}$, and the integral is taken over $\mathbb{C}$. Defining the P-representation of an observable F as

$$f(\boldsymbol{\alpha}) = \langle\alpha|F|\alpha\rangle, \tag{4.5}$$

where the operator F is in the normal order [80, 81, 101], the expectation value of F is expressed as $\langle F\rangle = \mathrm{Tr}(\rho F) = \int d\boldsymbol{\alpha} p(\boldsymbol{\alpha}) f(\boldsymbol{\alpha}) = \langle p(\boldsymbol{\alpha}), f(\boldsymbol{\alpha})\rangle_{\boldsymbol{\alpha}}$, where we defined the L^2 inner product $\langle g(\boldsymbol{\alpha}), h(\boldsymbol{\alpha})\rangle_{\boldsymbol{\alpha}} = \int \overline{g(\boldsymbol{\alpha})} h(\boldsymbol{\alpha}) d\boldsymbol{\alpha}$ of two functions $g(\boldsymbol{\alpha})$ and $h(\boldsymbol{\alpha})$.

The time evolution of $p(\boldsymbol{\alpha})$ corresponding to Eq. (4.1) obeys a partial differential equation

$$\partial_t p(\boldsymbol{\alpha}) = L p(\boldsymbol{\alpha}), \tag{4.6}$$

where the differential operator L satisfies $\mathcal{L}\rho = \int Lp(\boldsymbol{\alpha})|\alpha\rangle\langle\alpha| d\boldsymbol{\alpha}$ and can be explicitly calculated from Eq. (4.1) by using the standard calculus for the phase-space representation [80, 81, 101]. The corresponding evolution of $f(\boldsymbol{\alpha})$ in the Heisenberg picture is given by

$$\partial_t f(\boldsymbol{\alpha}) = L^+ f(\boldsymbol{\alpha}), \tag{4.7}$$

where the differential operator L^+ is the adjoint of L with respect to the L^2 inner product, i.e., $\langle L^+ g(\boldsymbol{\alpha}), h(\boldsymbol{\alpha})\rangle_{\boldsymbol{\alpha}} = \langle g(\boldsymbol{\alpha}), Lh(\boldsymbol{\alpha})\rangle_{\boldsymbol{\alpha}}$, satisfying $L^+ f(\boldsymbol{\alpha}) = \langle\alpha|\mathcal{L}^* F|\alpha\rangle$.

The differential operator L also has a set of eigensystem (an eigenvalue and right and left eigenfunctions) $\{\lambda_k, u_k(\boldsymbol{\alpha}), v_k(\boldsymbol{\alpha})\}$ satisfying

$$L u_k = \lambda_k u_k, \quad L^+ v_k = \overline{\lambda_k} v_k, \quad \langle v_k, u_l\rangle_{\boldsymbol{\alpha}} = \delta_{kl}, \tag{4.8}$$

which has one-to-one correspondence with Eq. (4.3); the eigenvalues $\{\lambda_k\}_{k\geq 0}$ are the same as those of $\mathcal{L}$, and the eigenfunctions u_k, v_k of L are related to the eigenoperators U_k, V_k of $\mathcal{L}$ as

$$U_k = \int u_k(\boldsymbol{\alpha})|\alpha\rangle\langle\alpha| d\boldsymbol{\alpha}, \quad v_k(\boldsymbol{\alpha}) = \langle\alpha|V_k|\alpha\rangle, \tag{4.9}$$

which follow from $\mathcal{L}U_k = \int u_k(\boldsymbol{\alpha}) \{\mathcal{L}|\alpha\rangle\langle\alpha|\} d\boldsymbol{\alpha} = \int \{Lu_k(\boldsymbol{\alpha})\} |\alpha\rangle\langle\alpha| d\boldsymbol{\alpha} = \lambda_k U_k$ and $L^+ v_k = L^+ \langle\alpha|V_k|\alpha\rangle = \langle\alpha|\mathcal{L}^* V_k|\alpha\rangle = \overline{\lambda_k}\langle\alpha|V_k|\alpha\rangle = \overline{\lambda_k} v_k$.

Now we introduce the quantum asymptotic phase function Φ_j ($j = 1, 2, \ldots$) of $\boldsymbol{\alpha}$ as the argument (polar angle) of the P-representation of the eigenoperator V_j associated with the principal eigenvalue Λ_j satisfying $\mathcal{L}^* V_j = \overline{\Lambda_j} V_j$, namely,

$$\Phi_j(\boldsymbol{\alpha}) = \arg v_j(\boldsymbol{\alpha}) = \arg\langle\alpha|V_j|\alpha\rangle. \tag{4.10}$$

In particular, the phase function Φ_1 associated with Λ_1 corresponds to the asymptotic phase in the classical limit (see Appendix). In the classical limit, Φ_j ($j \geq 2$) is not independent from Φ_1 and does not provide additional information, because Ω_j ($j \neq 1$) is equal to Ω_1. However, as we will see, this relation breaks down in the strong quantum regime and the phase function Φ_j yields independent information of the system from Φ_1.

4.3 Quantum van der Pol oscillator with Kerr effect

As an example, we consider a quantum van der Pol oscillator with Kerr effect. The master equation is given by [98, 57]

$$\dot{\rho} = \mathcal{L}_0\rho, \quad \mathcal{L}_0\rho = -i\,[H, \rho] + \gamma_1 \mathcal{D}[a^\dagger]\rho + \gamma_2 \mathcal{D}[a^2]\rho, \tag{4.11}$$

where $H = \omega_0 a^\dagger a + K a^{\dagger 2} a^2$, ω_0 is the natural frequency of the oscillator, K is the Kerr parameter, and γ_1 and γ_2 are the decay rates for negative damping and nonlinear damping, respectively.

We first consider the semiclassical regime where γ_2 and K are small. In this case, we can approximate Eq. (4.6) by a Fokker-Planck equation for $p(\boldsymbol{\alpha})$ (see Appendix), whose drift term gives the following deterministic equation:

$$\dot{\alpha} = \left(\frac{\gamma_1}{2} - i\omega_0\right)\alpha - (\gamma_2 + 2Ki)\overline{\alpha}\alpha^2. \tag{4.12}$$

This equation describes the Stuart-Landau oscillator (Hopf normal form) [2] and possesses a stable limit cycle

$$\boldsymbol{\alpha}_0(\phi) = R\left(e^{i\phi},\ e^{-i\phi}\right)^T, \tag{4.13}$$

which is represented as a function of the phase $\phi = \Omega_C t$ with natural frequency $\Omega_C = -\omega_0 - K\gamma_1/\gamma_2$ and radius $R = \sqrt{\frac{\gamma_1}{2\gamma_2}}$. The basin B of this

limit cycle is the whole complex plane except the origin. Introducing a real representation $(x, p) = (\mathrm{Re}\ \alpha, \mathrm{Im}\ \alpha)$, the classical asymptotic phase function Φ_C of this deterministic system is expressed as

$$\Phi_C(\boldsymbol{\alpha}) = \tan^{-1}\left(\frac{p}{x}\right) - \frac{2K}{\gamma_2} \ln \frac{\sqrt{x^2+p^2}}{R} + const., \tag{4.14}$$

where the constant determines the phase origin [7]. This phase function satisfies $\dot{\Phi}_C(\boldsymbol{\alpha}) = \Omega_c$ for all $\boldsymbol{\alpha}$ in B. In Ref. [88], we used this Φ_C for the phase reduction analysis of quantum synchronization in the semiclassical regime with weak quantum noise.

Figure 4.1(a) shows the eigenvalues of $\mathcal{L}_0$ near the imaginary axis obtained numerically, where the principal eigenvalue $\Lambda_1 = -\mu_1 + i\Omega_1$ is shown by a red dot ($\mu_1 > 0$). Here, we adopt a positive value for Ω_1 so that the resulting phase function Φ_1 increases in the counterclockwise direction from 0 to 2π, i.e., Φ_1 satisfies $\oint_C \nabla\Phi_1(\boldsymbol{x}) \cdot d\boldsymbol{x} = 2\pi$ where $\boldsymbol{x} = (x, p)$ and C is a circle around 0. The rightmost branch of the eigenvalues, approximately given by a parabola $\hat{\lambda}_n = i\Omega_1 n - \mu_1 n^2$ ($n = 0, \pm1, \pm2, \ldots$) passing through $\overline{\Lambda_1}$, is isolated from other branches of eigenvalues with faster deca y rates. Also, the fundamental frequencies of the other branches, defined as the smallest absolute imaginary part of the eigenvalues, are approximately equal to Ω_1. Thus, it is sufficient to consider only Λ_1 and introduce a single phase function Φ_1 in this case.

Figures 4.1(b) and 4.1(c) compare the quantum-mechanical phase function Φ_1 with the corresponding classical phase function Φ_C. As the quantum noise is small, the two phase functions closely resemble each other and their frequencies Ω_1 and Ω_C are also close to each other. Indeed, in the limit of vanishing quantum noise, the eigenfunction v_1 of L coincides with the Koopman eigenfunction of Eq. (4.12) with eigenvalue $i\Omega_C$ and therefore Φ_1 reproduces the classical phase function Φ_C (see Appendix). Thus, in the semiclassical regime, we can use Φ_C for analyzing the system [88].

Next, we consider a strong quantum regime with large γ_2 and K, where only a small number of energy states participates in the system dynamics and the semiclassical description is not valid. The eigenvalues of $\mathcal{L}_0$ are shown in Fig. 4.1(d). In contrast to Fig. 4.1(a), we can identify several branches of eigenvalues near the imaginary axis characterized by the principal eigenvalues $\Lambda_1, \Lambda_2, \Lambda_3, \ldots$ whose fundamental frequencies $\Omega_1 = \mathrm{Im}\ \overline{\Lambda_1}, \Omega_2 = \mathrm{Im}\ \overline{\Lambda_2}, \Omega_3 = \mathrm{Im}\ \overline{\Lambda_3}, \ldots$ are different from each other. It is discussed in Ref. [57] that $|m+1\rangle\langle m|$ is an approximate eigenoperator of

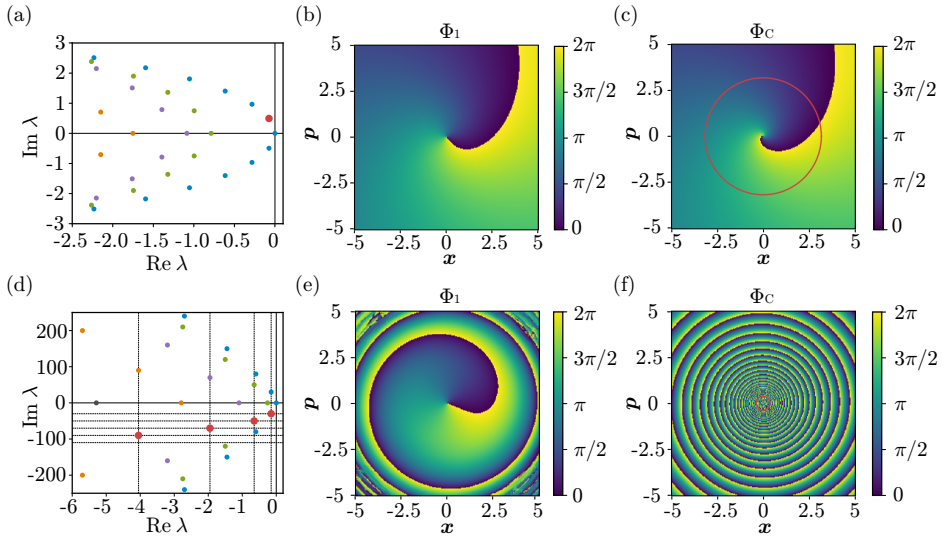

Figure 4.1: Eigenvalues of the Liouville superoperator and the quantum and classical asymptotic phase functions. (a-c): Semiclassical regime. The parameters are $\gamma_1 = 1$ and $(\omega_0, \gamma_2, K)/\gamma_1 = (-1, 0.05, 0.025)$. (a): Eigenvalues of $\mathcal{L}_0$ near the imaginary axis. The red dot represents the principal eigenvalue Λ_1 with the the slowest decay rate. (b): Quantum asymptotic phase function Φ_1 with $\Omega_1 = 0.495$. (c): Classical asymptotic phase function Φ_C with $\Omega_C = 0.5$. (d-f): Strong quantum regime. The parameters are $\gamma_1 = 0.1$ and $(\omega_0, \gamma_2, K)/\gamma_1 = (300, 4, 100)$. (d): Eigenvalues of $\mathcal{L}_0$. The red dots represent the principal eigenvalues Λ_j ($j = 1, 2, 3, 4$ from the right) with the fundamental frequencies in individual branches, and the dotted lines indicate $\widetilde{\lambda}_m$ ($m = 0, 1, 2, 3$) in Eq. (4.15). (e): Φ_1 with $\Omega_1 = -30$. (f): Φ_C with $\Omega_C = -32.5$. In (a) and (d), individual branches of eigenvalues are shown with different colors. In (b), (c), (e) and (f), $(x, p) = (2.5, 0)$ is chosen as the phase origin. In (c) and (f), the red-thin lines represent limit cycles in the classical limit given by Eq. (4.13).

$\mathcal{L}_0$ with eigenvalue

$$\widetilde{\lambda}_m = i[\Delta - 2mK] - \frac{1}{2}\{\gamma_1(2m+3) + 2\gamma_2 m^2\} \tag{4.15}$$

for $m = 0, 1, 2, \ldots$. As shown in Fig. 4.1(d), these eigenvalues correspond to the principal eigenvalues, i.e., $\Lambda_j \approx \widetilde{\lambda}_{j-1}$ and thus $V_j \approx |j\rangle\langle j-1|$ ($j =$

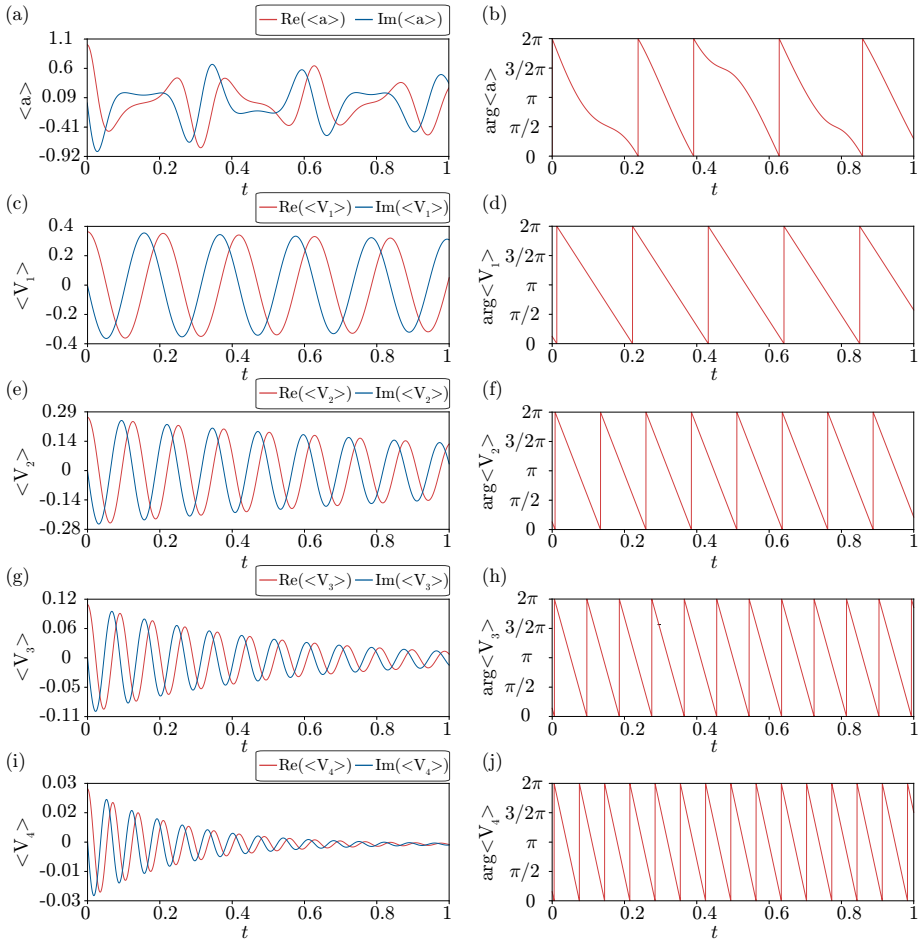

Figure 4.2: Evolution of the expectation values of a and V_j ($j = 1, 2, 3, 4$) and their arguments from a pure coherent state in the strong quantum regime. The parameters are $\gamma_1 = 0.1$ and $(\omega_0, \gamma_2, K)/\gamma_1 = (300, 4, 100)$. (a): $\langle a \rangle$, (c,e,g,i): $\langle V_j \rangle$, (b): $\arg\langle a \rangle$, (d,f,h,j): $\arg\langle V_j \rangle$.

$1, 2, 3, 4$). The existence of several different fundamental frequencies suggests that the system behaves like a torus rather than a limit cycle with a single fundamental frequency and that we need to consider phase functions $\Phi_2, \Phi_3, \ldots$ associated with $\Lambda_2, \Lambda_3, \ldots$ in addition to Φ_1 and Λ_1. Here, we take negative value for each Ω_j so that the corresponding Φ_j increases from

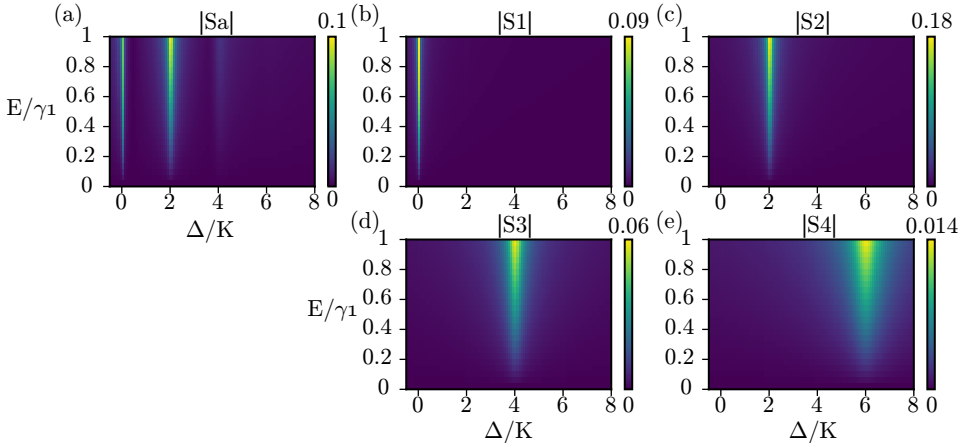

Figure 4.3: Dependence of the order parameters on the frequency detuning Δ (divided by K) and driving strength E (divided by γ_1). (a): $|S_a|$. (b-e): $|S_j|$ $(j = 1, 2, 3, 4)$. The parameters are $\gamma_1 = 0.1$ and $(\gamma_2, K)/\gamma_1 = (4, 100)$.

0 to 2π in the counterclockwise direction.

Figures 4.1(e) and 4.1(f) show the quantum-mechanical phase function Φ_1 and the corresponding classical phase function Φ_C. Because the system is in the strong quantum regime, Φ_C is distinctly different from Φ_1 and the classical frequency Ω_C also differs from the true quantum frequency Ω_1. The other asymptotic phase functions Φ_j $(j = 2, 3, 4)$ are shown in Appendix. Though these phase functions look similar to each other, they characterize oscillatory dynamics of the system at different frequencies.

To demonstrate that the quantum asymptotic phase functions yield appropriate phase values even in this strong quantum regime, we consider free oscillatory relaxation of ρ from a coherent initial state $\rho = |\alpha_0\rangle\langle\alpha_0|$ with $\alpha_0 = 1$ at $t = 0$ and measured the evolution of the expectation values of V_j and their arguments $\arg\langle V_j\rangle$ $(j = 1, 2, 3, 4)$, as well as those of the annihilation operator a for comparison. Note that $\langle V_j\rangle$ at t can be expressed as $\mathrm{Tr}\,[V_j\rho(t)] = \langle\alpha_0|V_j(t)|\alpha_0\rangle = \langle\delta(\boldsymbol{\alpha} - \boldsymbol{\alpha}_0)v_j(\boldsymbol{\alpha}, t)\rangle_{\boldsymbol{\alpha}} = v_j(\boldsymbol{\alpha}_0, t) = e^{\overline{\Lambda_j}t}v_j(\boldsymbol{\alpha}_0, 0)$ with $\boldsymbol{\alpha}_0 = (\alpha_0, \alpha_0^*)$, so its argument should give the asymptotic phase of the system, i.e., $\arg\langle V_j\rangle(t) = \Phi_j(\boldsymbol{\alpha_0}) + \Omega_j t$, where we explicitly denoted the time dependence. It is remarkable that each $\arg\langle V_j\rangle$ appropriately gives constantly varying phase values with frequency Ω_j as shown in Fig. 4.2, verifying the validity of the quantum asymptotic phase Φ_j. In contrast, $\arg\langle a\rangle$ does not vary constantly with time.

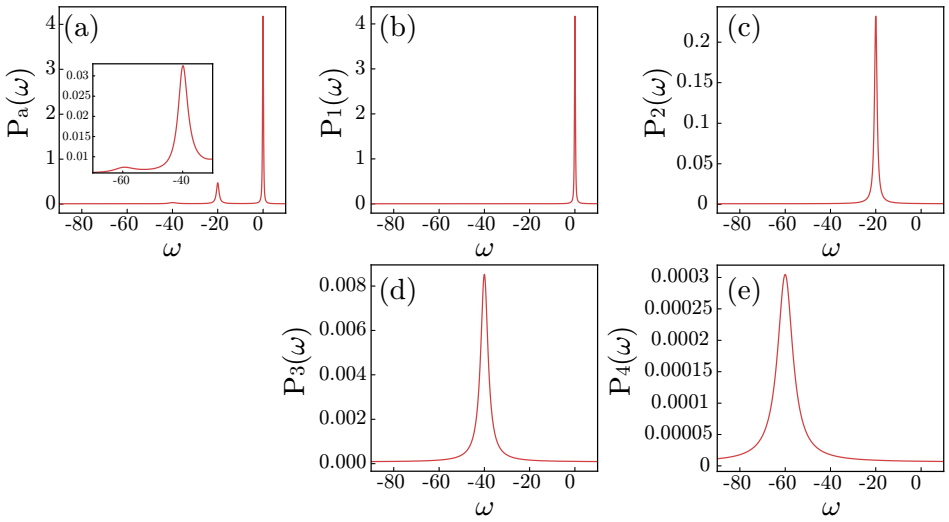

Figure 4.4: Power spectra. The parameters are $\gamma_1 = 0.1$ and $(\Delta, \gamma_2, K, E)/\gamma_1 = (0, 4, 100, 1)$. (a): P_a. (b-e): P_j $(j = 1, 2, 3, 4)$.

4.4 Revealing multiple phase-locking structure

We now consider quantum synchronization of the oscillator with a harmonic drive. The master equation in the rotating frame of the frequency ω_d of the harmonic drive is

$$\dot{\rho} = (\mathcal{L}_0 + \mathcal{L}_1)\rho, \tag{4.16}$$

where the $\mathcal{L}_0$ is now given by Eq. (4.11) with $H = -\Delta a^\dagger a + K a^{\dagger 2} a^2$, $\mathcal{L}_1 \rho = -i\left[iE(a - a^\dagger), \rho\right]$, $\Delta = \omega_d - \omega_0$ is the frequency detuning of the harmonic drive from the oscillator, and E is the strength of the harmonic drive [98, 57]. We use the same parameters as in Fig. 4.2(d)-4.2(f) and vary the detuning parameter Δ by varying ω_d while keeping the natural frequency ω_0 fixed. Lörch *et al.* [57] showed that this system under strong Kerr effect exhibits phase locking to the harmonic drive at several detuning frequencies $\Delta = 2mK$ $(m = 0, 1, 2, \ldots)$ observed as multiple sharp Arnold tongues, while the corresponding classical system exhibits only a single broad Arnold tongue. In Ref. [57], the following order parameter S_a and power spectrum P_a defined

using the annihilation operator a are used to analyze the system:

$$S_a = |S_a| e^{i\theta_a} = \frac{\langle a \rangle}{\sqrt{\langle a^\dagger a \rangle}}, \tag{4.17}$$

$$P_a(\omega) = \int_{-\infty}^{\infty} d\tau e^{i\omega\tau} \langle a^\dagger(\tau) a(0) \rangle - \langle a^\dagger(\tau) \rangle \langle a(0) \rangle, \tag{4.18}$$

where the expectation is taken with respect to the steady-state density matrix obtained from the master equation (4.16). Here, instead of these quantities, we use the order parameters and the power spectra based on the quantum asymptotic phase, which are defined in terms of the eigenoperators V_j of $\mathcal{L}_0$ as

$$S_j = |S_j| e^{i\theta_j} = \frac{\langle V_j \rangle}{\sqrt{\langle V_j^\dagger V_j \rangle}}, \tag{4.19}$$

$$P_j(\omega) = \int_{-\infty}^{\infty} d\tau e^{i\omega\tau} \left(\langle V_j^\dagger(\tau) V_j(0) \rangle - \langle V_j^\dagger(\tau) \rangle \langle V_j(0) \rangle \right), \tag{4.20}$$

where $V_j^\dagger(\tau) = e^{\Lambda_j \tau} V_j(0)$ and $j = 1, 2, 3, 4$. Note that $|S_a|$ and $|S_j|$ quantify the phase coherence of the system, while θ_a and θ_j characterize the averaged phase of the system relative to the harmonic drive.

Figure 4.3 shows the dependence of the order parameters $|S_a|$ and $|S_j|$ on the detuning Δ and strength E of the harmonic drive. In Fig. 4.3(a) for $|S_a|$, several Arnold tongues representing phase locking of the oscillator at different frequencies are observed [57]. Remarkably, these Arnold tongues are clearly decomposed into individual Arnold tongues around $\Delta = 2(j-1)K$ in Figs. 4.3(b)-4.3(e) for $|S_j|$ ($j = 1, 2, 3, 4$). Similarly, Fig. 4.4 shows the power spectra P_a and P_j. Multiple peaks of P_a in Fig. 4.4(a), which indicate phase-locking frequencies of the oscillator, are clearly decomposed into individual peaks around $\omega = \Delta - 2(j-1)K$ in Figs. 4.4(b)-4.4(e) for P_j ($j = 1, 2, 3, 4$). The Arnold tongue and power spectrum are sharper when the decay rate characterized by Re Λ_j is smaller. Though not shown, we can also detect even smaller tongues and peaks with $j \geq 5$.

The above results reveal that, in the strong quantum regime, the system behaves like a torus with several fundamental frequencies and each of the associated oscillating mode individually exhibits phase locking to the harmonic drive at the respective frequency [102], resulting in the multiple Arnold tongues and spectral peaks. The quantum asymptotic phase proposed in this study reveals the structure of such mode-wise dynamics of the system in the strong quantum regime.

4.5 Conclusion

We proposed a definition of the asymptotic phase for quantum nonlinear oscillators in terms of the eigenoperator of the adjoint Liouville superoperator, which is fully quantum-mechanical and valid in the strong quantum regime. By using the order parameters and power spectra based on the quantum asymptotic phase, the structure of the multiple phase locking, an explicit quantum signature in synchronization, was successfully characterized. The proposed quantum asymptotic phase will serve as a fundamental quantity for analyzing quantum effects in synchronization [57, 69] and be useful for future applications of quantum synchronization in the growing fields of quantum technologies.

Chapter 5

Continuous measurement and feedback control for enhancement of quantum synchronization

In this chapter, we analyze synchronization of a quantum van der Pol (vdP) oscillator with a harmonic driving signal and demonstrate that performing continuous homodyne measurement on a linear additional bath and applying a feedback control can enhance quantum synchronization. We argue that the phase coherence of the oscillator is increased by the reduction of quantum fluctuations due to the continuous measurement, but also that the measurement backaction inevitably induces fluctuations around the phase-locking point. We propose a simple feedback policy that can suppress the measurement-induced fluctuations by adjusting the frequency detuning between the oscillator and the driving signal, which leads to enhancement of quantum synchronization. We further demonstrate that the maximum phase coherence can be achieved by performing the quantum measurement on the quadrature angle at which the phase diffusion of the oscillator is the largest and the maximal information of the oscillator phase is attained.

5.1 Introduction

Studies on synchronization of nonlinear oscillators date back to Huygens' well-known discovery of mutual synchronization between two pendulum clocks

in the 17th century. Since then, synchronization phenomena have widely been analyzed in various fields of science and technology, such as chemical oscillations, spiking neurons, chorusing crickets, and mechanical vibrations [1, 2, 4, 7, 6]. Engineering applications of synchronization have also been developed, such as injection locking [20] and phase lock loops in electrical circuits [28] and deep brain stimulation for the treatment of Parkinson's disease [29].

Recently, experimental studies of synchronizing nonlinear oscillators are reaching the micrometer and nanometer scales [36, 78, 41] and there has been increasing attention on the theoretical analysis of quantum synchronization [47, 54, 48, 55, 88, 98, 43, 50, 57]. It has been revealed that quantum fluctuations generally induce phase diffusion of quantum limit-cycle oscillators and disturb strict synchronization [47, 54, 48, 55, 88]. To overcome this drawback of quantum effects in synchronization, for example, Sonar [55] utilized the squeezing effect and demonstrated that entrainment of quantum van der Pol (vdP) oscillator to the squeezing signal can suppress quantum fluctuations and consequently enhance quantum synchronization.

In quantum systems, one of the peculiar features is the measurement, which can change the quantum state of the system depending on its probabilistic outcomes [103, 84]. Specifically, when the output of the field environment interacting with an open quantum system is continuously monitored and knowledge about the system is indirectly obtained, the dynamics of the system under the measurement can be described by a continuous quantum trajectory, i.e. a conditional stochastic evolution of the system [104, 105]. This continuous measurement framework enables us to investigate novel dynamical features of the quantum measurement, such as state preparation [106, 107], dynamical creation of entanglement [108], and unveiling [109, 110] and controlling [111] chaotic behavior of quantum systems. It is also notable that experimental aspects of continuous measurement have been intensively studied [112, 113].

Recently, several investigations on the continuous measurement performed on quantum limit-cycle oscillators have been carried out, such as measurement-induced transition between in-phase and anti-phase quantum synchronization [43], unraveling nonclassicality in optomechanical oscillators via measurement [114], and improvement of the accuracy of Ramsey spectroscopy through measurement of synchronized atoms [46]. However, as far as our knowledge is concerned, the effect of continuous measurement on the enhancement of quantum synchronization has never been discussed.

In this chapter, we consider synchronization of a quantum vdP oscillator with a harmonic driving signal and demonstrate that performing continuous

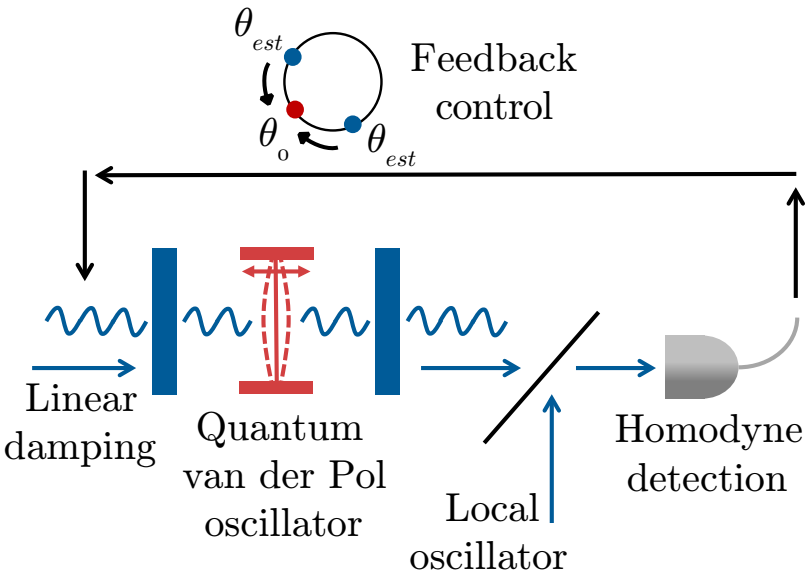

Figure 5.1: Enhancement of synchronization of a quantum vdP oscillator with a harmonic driving signal by continuous homodyne measurement and a feedback control.

homodyne measurement on a linear additional bath and applying a feedback control can enhance quantum synchronization. We show that quantum fluctuations disturbing the phase coherence can be reduced by the continuous homodyne measurement, while fluctuations around the phase-locking point are inevitably induced by the measurement backaction. We propose a simple feedback policy for suppressing the fluctuations by adjusting the frequency detuning of the quantum vdP oscillator from the harmonic driving signal. We further demonstrate that the maximum increase in phase coherence is achieved by performing the measurement on the quadrature angle at which the phase diffusion of the oscillator is the largest and the maximum information on the phase of the oscillator can be extracted via the measurement.

5.2 Model

We consider a quantum vdP oscillator subjected to a harmonic driving signal. A schematic diagram of the physical setup is shown in Fig. 5.1. We introduce an additional bath linearly coupled to the oscillator, perform con-

tinuous homodyne measurement of the outgoing field from the oscillator to the bath, and apply a feedback control to adjust the frequency detuning of the driving signal from the oscillator (Fig.5.1).

We denote by ω_0 and ω_d the frequencies of the vdP oscillator and the harmonic driving, respectively. The stochastic master equation of this quantum system in the coordinate frame rotating with the frequency ω_d is given by

$$\begin{aligned} d\rho =& \Big\{ -i \Big[-(\Delta + \Delta_{fb}) a^\dagger a + iE(a - a^\dagger), \rho \Big] \\ &+ \gamma_1 \mathcal{D}[a^\dagger]\rho + \gamma_2 \mathcal{D}[a^2]\rho \\ &+ \gamma_3 \mathcal{D}[a]\rho \Big\} dt + \sqrt{\eta\gamma_3}\mathcal{H}[ae^{-i\theta}]\rho dW, \\ dY =& \sqrt{\eta\gamma_3}\,\mathrm{Tr}[(ae^{-i\theta} + a^\dagger e^{i\theta})\rho]dt + dW, \end{aligned} \tag{5.1}$$

with $\mathcal{D}[L]\rho = L\rho L^\dagger - \frac{1}{2}(L^\dagger L\rho + \rho L^\dagger L), \mathcal{H}[L]\rho = L\rho + \rho L^\dagger - \mathrm{Tr}\left[(L + L^\dagger)\rho\right]\rho$, where $\mathcal{D}$ is the Lindblad form and $\mathcal{H}[ae^{-i\theta}]$ characterizes the measurement on the quadrature $ae^{-i\theta} + a^\dagger e^{i\theta}$. In the equations above, ρ is a density matrix representing the system state, a and $a^\dagger$ denote annihilation and creation operators ($\dagger$ represents Hermitian conjugate), respectively, $\Delta = \omega_d - \omega_0$ is the frequency detuning of the harmonic driving signal from the oscillator, Δ_{fb} is the feedback control to adjust the frequency detuning, E is the intensity of the driving signal, γ_1, γ_2, and γ_3 are the decay rates for the negative damping, nonlinear damping, and linear damping, respectively, η is the efficiency of the measurement (we set $\eta = 1$ for the case with measurement and $\eta = 0$ for the case without measurement), θ specifies the quadrature angle of the measurement, W represents a Wiener process satisfying $\mathbb{E}[dW] = 0$ and $\mathbb{E}[dW^2] = dt$, Y is the output of the measurement result, and the reduced Planck constant is set as $\hbar = 1$.

We assume that when the measurement is not performed ($\eta = 0$), the oscillator is synchronized with the driving signal and the Wigner distribution, a quasiprobability distribution [81], of the steady-state density matrix ρ_{ss} of Eq. (5.1) is concentrated around a stable phase-locking point along the limit-cycle orbit in the classical limit (see Fig. 5.3(a)).

The feedback control Δ_{fb} is chosen as (see Appendix for details)

$$\Delta_{fb} = -K_{fb}(\theta_{est} - \theta_0), \tag{5.2}$$

where K_{fb} (> 0) represents the feedback gain, $\theta_0 = \arctan\left(\mathrm{Tr}\left[p\rho_{ss}\right]/\mathrm{Tr}\left[x\rho_{ss}\right]\right)$ represents the locking phase in the absence of the measurement, which is calculated as the angle of the expectation values of the position operator $x = (a + a^\dagger)/2$ and the momentum operator $p = -i(a - a^\dagger)/2$ with

respect to the steady state ρ_{ss} of Eq. (5.1) without measurement, and $\theta_{est} = \arctan\left(\mathrm{Tr}\left[p\rho_{est}\right]/\mathrm{Tr}\left[x\rho_{est}\right]\right)$ represents the phase of the system calculated from the instantaneous state ρ_{est} of Eq. (5.1) with measurement, where ρ_{est} is estimated from the measurement record. In the next section, we demonstrate that the above feedback control can actually suppress the fluctuations of the system state around the phase-locking point.

To evaluate the degree of phase coherence of the quantum vdP oscillator, we use the absolute value $|S_1|$ of the quantity [43, 57]

$$S_1 = |S_1|e^{i\phi_1} = \frac{\mathrm{Tr}\left[a\rho\right]}{\sqrt{\mathrm{Tr}\left[a^\dagger a\rho\right]}} \tag{5.3}$$

as the order parameter, which is a quantum analog of the order parameter for a single classical noisy oscillator [2, 4] and takes values in $0 \leq S_1 \leq 1$ with $S_1 = 1$ representing the perfectly phase-coherent state and $S_1 = 0$ when the state is perfectly phase-incoherent.

5.3 Results

In this section, we perform numerical simulations of the model described in the previous section. We set the parameter values in the weak quantum regime, $(\Delta, \gamma_2, \gamma_3, E)/\gamma_1 = (0.05, 0.05, 0.1, \sqrt{0.1})$, in order to clarify the relation between the quantum system and its classical limit [88]. The feedback gain is set at $K_{fb}/\gamma_1 = 1$ when the feedback control is applied. In Secs. 5.3.1 and 5.3.2, we set $\theta = 0$ for the quadrature of measurement and, in Sec. 5.3.3, the effect of varying θ is analyzed. The initial state of the simulation is always taken as the vacuum state, i.e. $\rho = |0\rangle\langle 0|$. We use QuTiP [85] numerical toolbox for the numerical simulations.

5.3.1 Without a feedback control

We first consider the case without the feedback control, i.e. $K_{fb} = 0$. When the measurement is performed, the system trajectories behave stochastically. We therefore calculate averaged values over 300 trajectories obtained by numerical simulations of Eq. (5.1) from the same initial sate ($\rho = |0\rangle\langle 0|$) and use them for comparing the results with the case without measurement. Note that the system trajectory is deterministic when the measurement is not performed.

Figures 5.2(a), 5.2(b), 5.2(c), and 5.2(d) show the trajectories of the absolute values of the order parameter $|S_1|$ characterizing the degree of phase

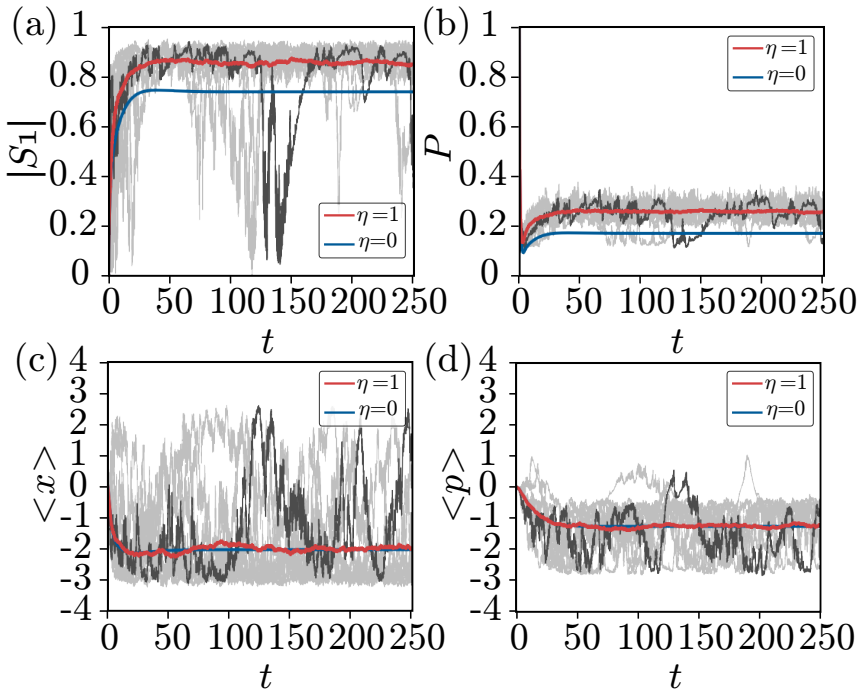

Figure 5.2: Measurement-induced increase in phase coherence without a feedback control. (a): Order parameter $|S_1|$. (b): Purity P. (c): Expectation values of the position operator $\langle x \rangle$. (d): Expectation values of the momentum operator $\langle p \rangle$. For the case with measurement ($\eta = 1$), averaged values of the results calculated from 300 trajectories are shown by the red lines and 10 out of 300 individual trajectories are shown by gray lines (the dark one represents a single realization of the trajectory). For the case without measurement ($\eta = 0$), results of a single trajectory is shown by blue lines.

coherence, the purity $P = \mathrm{Tr}\,[\rho^2]$, the expectation value of the position operator $\langle x \rangle = \mathrm{Tr}\,[x\rho]$, and the expectation value of the momentum operator $\langle p \rangle = \mathrm{Tr}\,[p\rho]$, respectively. Note that these expectation values are fluctuating quantities in the case with measurement.

As seen in Fig. 5.2(a), the average value of the order parameter $|S_1|$ with measurement is larger than the (deterministic) value of $|S_1|$ without measurement, e.g. $|S_1| = 0.847$ with measurement and $|S_1| = 0.737$ without measurement at time $t = 250$, indicating that the phase coherence is

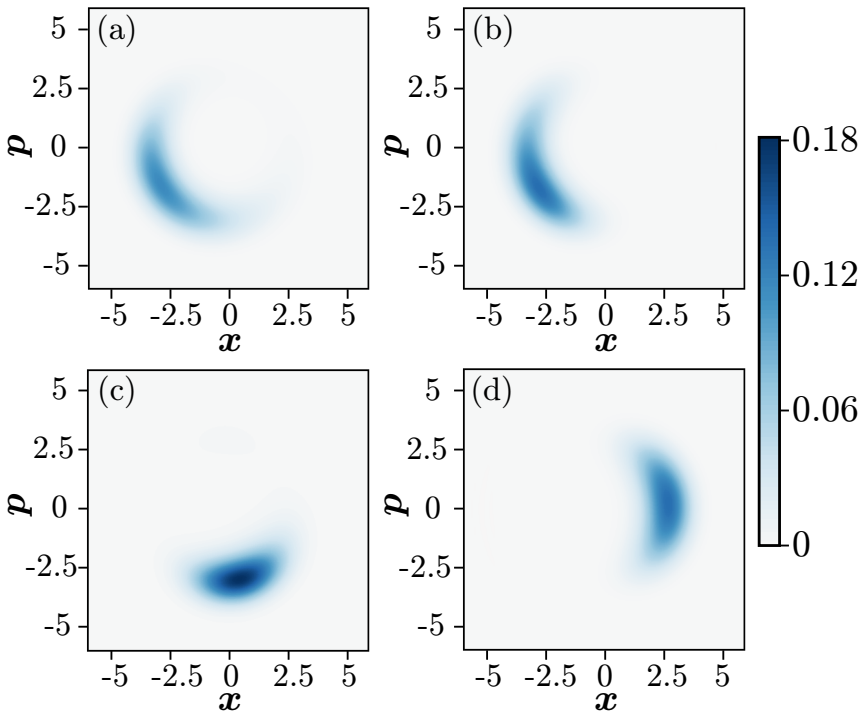

Figure 5.3: Wigner distributions of the system without a feedback control. (a): Wigner distribution of the steady state of Eq. (5.1) without measurement. (b,c,d): Wigner distributions at time $t = 250$ for 3 different trajectories of Eq. (5.1) with measurement.

increased on average by the continuous homodyne measurement. We can also see in Fig. 5.2(b) that the average values of the purity P with measurement are larger than the stationary value of P without measurement, e.g. $P = 0.254$ with measurement and $P = 0.169$ without measurement at time $t = 250$ sufficiently after the initial relaxation.

Here, we note that the observed increase in $|S_1|$ or P is an average effect; the values of these quantities for a single trajectory of Eq. (5.1) with measurement strongly fluctuate and can take smaller values than those without measurement, as shown by the dark-gray lines in Figs. 5.2(a) and 5.2(b). As we show in Appendix, the increase in the purity implies the reduction in the phase diffusion of the oscillator.

As a drawback of the increase in phase coherence by the measurement,

the measurement backaction inevitably induces fluctuations of the system state around the phase-locking point. This can be clearly seen in Figs. 5.2(c) and 5.2(d), where 10 trajectories of $\langle x \rangle$ and $\langle p \rangle$ obtained by simulating Eq. (5.1) with measurement (gray lines) exhibit strong fluctuations depending on the outcomes of the measurement.

The increase in phase coherence can also be observed from the Wigner distribution. Figure 5.3(a) shows the steady-state Wigner distribution obtained from Eq. (5.1) without measurement (note that ρ converges to a steady state in this case), and Figs. 5.3(b), 5.3(c), and 5.3(d) show the instantaneous Wigner distributions at time $t = 250$ of 3 trajectories obtained by simulating Eq. (5.1) with measurement (ρ behaves stochastically in this case). Comparing Figs. 5.3(b), 5.3(c), and 5.3(d) with Fig. 5.3(a), we can observe the increase in phase coherence by the continuous homodyne measurement from the strongly concentrated Wigner distributions. We also observe that the location of the distribution differs from trajectory to trajectory. These fluctuations of the system state are caused by the backaction of the measurement.

5.3.2 With a feedback control

In Sec. 5.3.1, we observed that the measurement increases phase coherence but it induces fluctuations around the phase-locking points at the same time. Here, we study the effect of the feedback control given by Eq. (5.2), which is introduced in order to suppress the fluctuations of the system state.

Figures 5.4(a), 5.4(b), 5.4(c), and 5.4(d) show the trajectories of $|S_1|$, P, $\langle x \rangle$, and $\langle p \rangle$, respectively. The feedback control is applied from $t = 100$. As we see in Fig. 5.4(a), the averaged order parameter $|S_1|$ with measurement takes larger values than $|S_1|$ without measurement, e.g. $|S_1| = 0.888$ with measurement and $|S_1| = 0.737$ without measurement at time $t = 250$. We also see in Fig. 5.2(b) that the averaged values of P with measurement are larger than the values of P without measurement, e.g. $P = 0.274$ with measurement and $P = 0.169$ without measurement at time $t = 250$.

The role of the feedback control can be clearly seen in Fig. 5.4(c) and 5.4(d), where 10 trajectories of $\langle x \rangle$ and $\langle p \rangle$ obtained by simulating Eq. (5.1) with measurement are plotted (gray lines). We see that the fluctuations around the phase-locking point are suppressed after $t = 100$ at which the feedback control is turned on. We note that we used the same sequences of the Wiener increments in the numerical simulations of Eq. (5.1) as the case without the feedback control.

The suppression of fluctuations by the feedback control can also be seen

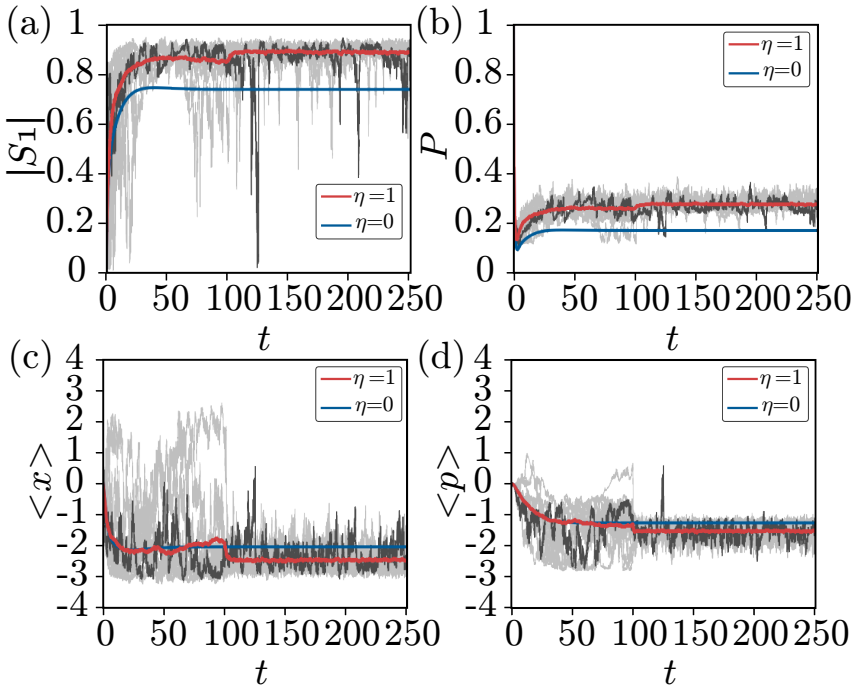

Figure 5.4: Measurement-induced enhancement of quantum synchronization with a feedback control. The feedback control is applied from $t = 100$. (a): Order parameter $|S_1|$. (b): Purity P. (c): Expectation values of the position operator $\langle x \rangle$. (d): Expectation values of the momentum operator $\langle p \rangle$. For the case with measurement ($\eta = 1$), averaged values of the results calculated from 300 trajectories are shown by the red lines and 10 out of 300 individual trajectories are shown by gray lines (the dark one represents a single realization of the trajectory). For the case without measurement ($\eta = 0$), results of a single trajectory is shown by blue lines.

from the Wigner distribution of the system. Figure 5.5(a) shows the steady-state Wigner distribution of Eq. (5.1) without measurement and Figs. 5.5(b), 5.5(c), 5.5(d) show three realizations of the Wigner distributions at $t = 250$ of Eq. (5.1) with measurement. Comparing Figs. 5.5(b), 5.5(c), and 5.5(d) with Figs. 5.3(b), 5.3(c), and 5.3(d), we see that the fluctuations around the phase-locking point are well suppressed by the feedback control.

The above results indicate that the measurement-induced enhancement of synchronization, namely, larger phase coherence and smaller fluctuations

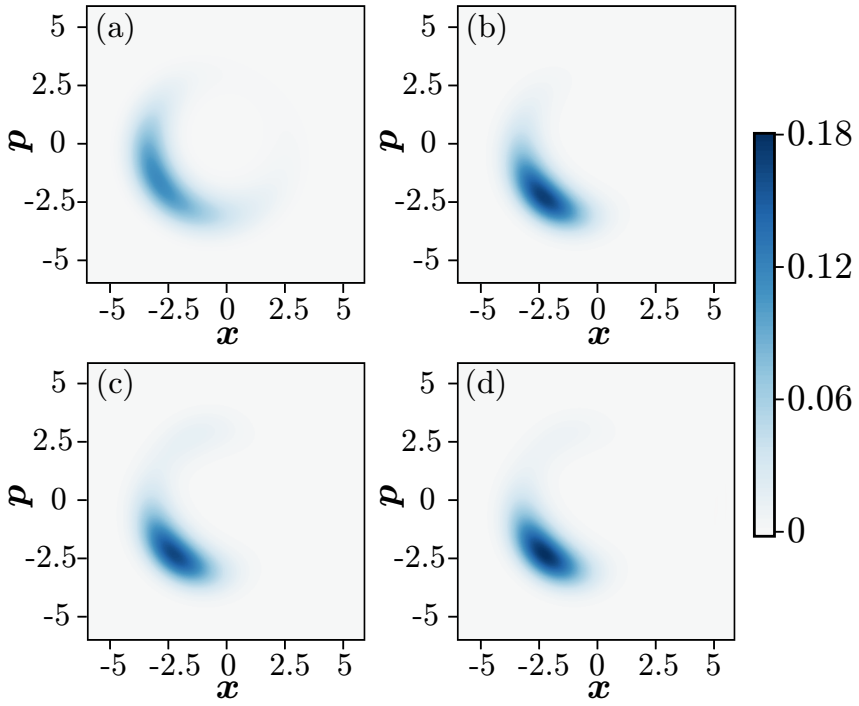

Figure 5.5: Wigner distributions of the system with feedback control. (a): Wigner distribution of the steady state of Eq. (5.1) without measurement. (b,c,d): Wigner distributions at time $t = 250$ for 3 different trajectories of Eq. (5.1) with measurement. The feedback control is performed from time $t = 100$.

around the phase-locking point, can be achieved when the feedback control is introduced.

5.3.3 Dependence on the quadrature of the measurement

We have so far fixed θ, which specifies the quadrature, at 0. We here consider the effect of varying θ on the phase coherence in the case with the feedback control.

Figures 5.6(a) and 5.6(b) show the averaged values of $|S_1|$ and P at time $t = 250$ for $0 \leq \theta \leq 2\pi$, respectively, which are calculated from 300 trajectories of Eq. (5.1) with measurement. For comparison, we also show the values of $|S_1|$ and P for the steady state of Eq. (5.1) without measure-

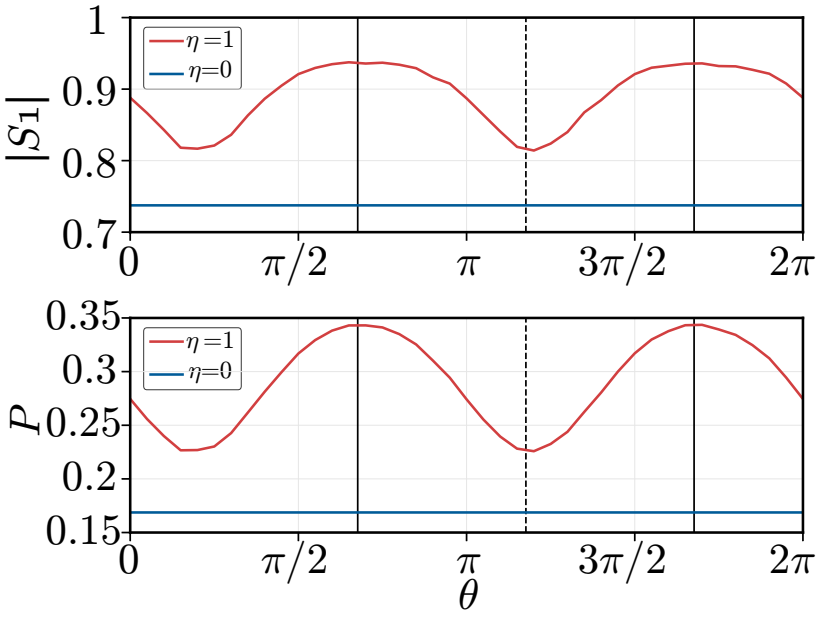

Figure 5.6: Dependence of the phase coherence on the quadrature of the measurement. (a): Order parameter $|S_1|$. (b): Purity P. The order parameter and purity averaged over 300 trajectories with measurement at time $t = 250$ (red lines) are compared with those for a single trajectory without measurement (blue lines). The phase-locking point θ_0 is shown by a black-dotted vertical line, and the points orthogonal to the phase-locking point $\theta_0 + \pi/2$ are shown by black-solid vertical lines.

ment. The maximum values of $|S_1|$ and P are attained at $\theta = 5.341$ and $\theta = 2.042$, respectively, which are approximately orthogonal to the locking phase, $\theta_0 = 3.696$.

This result can be understood as follows. Because the phase diffusion of the oscillator is maximized when θ is orthogonal to θ_0, performing the measurement on the quadrature specified by this θ can extract the maximum information about the phase of the oscillator. As a result, maximal reduction of quantum fluctuations and enhancement of synchronization are realized.

5.4 Conclusion

We considered synchronization of a quantum van der Pol oscillator with a harmonic driving signal. We demonstrated that introducing an additional bath coupled linearly to the system and performing continuous homodyne measurement of the bath can increase phase coherence of the system. We also proposed a simple feedback policy for suppressing the fluctuations of the system state around the phase-locking point by adjusting the frequency detuning of the driving signal from the oscillator, and achieved the measurement-induced enhancement of synchronization. We further showed that the maximum enhancement of synchronization is achieved when we perform measurement on the quadrature angle at which the phase diffusion of the oscillator is maximal and the maximum information about the phase of the oscillator is extracted. In this study, we only considered the case that the system is in the weak quantum regime, and investigation in the strong quantum regime will be our future subject. The quantum measurement, an essential feature in quantum systems, can be helpful for resolving the issue of quantum fluctuations that disturbs strict quantum synchronization. It can thus play an essentially important role for the realization and future applications of quantum synchronization in the growing fields of quantum technologies.

Chapter 6

Conclusions

6.1 Summary

In this thesis, we presented the several theoretical results using phase dynamics for the analysis of quantum synchronization. Brief summaries of the results in each chapter are as follows.

In Chapter 2, we developed a general framework of the phase reduction theory for quantum limit-cycle oscillators under the semiclassical approximation, enabling a systematic analysis of quantum synchronization in a general class of asymmetric limit-cycle oscillators.

In Chapter 3, using the semiclassical phase-reduction theory formulated in the previous chapter, we considered optimal entrainment of a quantum nonlinear oscillator to a periodically modulated weak harmonic drive in the semiclassical regime. We analyzed two types of optimization problems, one for the stability and the other for the phase coherence of the oscillator, and discussed the performance of the optimization schemes and their differences.

In Chapter 4, we proposed a fully quantum-mechanical definition of the asymptotic phase for quantum nonlinear oscillators and used it to reveal the torus-like behavior of the nontrivial multiple phase locking of the oscillator in the strong quantum regime.

In Chapter 5, we applied continuous measurement and feedback control for enhancement of quantum synchronization and showed that the quantum measurement can be helpful for resolving the issue of quantum fluctuations that generally disturbs strict quantum synchronization.

6.2 Outlook

The study on phase dynamics approach to the analysis of quantum synchronization is in its early stage. In what follows, we introduce several future directions of the works presented in the thesis.

First, it is challenging to formulate a fully-quantum mechanical phase-reduction theory for quantum nonlinear oscillators. By using the quantum-mechanical definition of the asymptotic phase introduced in Chapter 4, We would be able to derive an approximated one-dimensional equation for the asymptotic phase variable describing quantum synchronization dynamics beyond the semiclassical regime.

Second, it is interesting to apply other optimization and control methods developed for classical limit-cycle oscillators to quantum limit-cycle oscillators by using the reduced semiclassical phase equation. For example, using the phase distribution control of a population of classical oscillators [11], we would be able to obtain desired phase distribution of a quantum limit-cycle oscillator.

Third, analysis of quantum synchronization in spin triplet systems using the asymptotic phase variable would provide new insight into the novel features of synchronization in quantum spin systems. This direction of research is very important since such small spin systems are suitable for investigation of synchronization in quantum many-body systems [50] and for experimental realization of quantum synchronization [115].

Lastly, it is interesting to investigate the effect of quantum measurement back-action on the two dissipatively coupled quantum limit-cycle oscillators. Continuous measurement and feedback control could also enhance the phase coherence between the two oscillators.

Quantum synchronization is a burgeoning topic at the boundary between quantum physics and nonlinear dynamics and attracting much attention not only in pure and applied physics but also in information science, applied mathematics, and various engineering fields. The phase equation has provided systematic tools for the fundamental analysis of synchronization between classical nonlinear oscillators [1, 2, 7, 3, 8, 9] and has been important for analyzing technical applications of synchronization such as the ring laser gyroscope [22, 23, 24, 25], phase-locked loop [28, 4], and Josephson voltage standard [26, 27, 4]. Therefore, the phase dynamics approach to quantum synchronization that we developed in this thesis will not only provide a framework for systematic analysis of quantum synchronization, but also help us find novel technical applications of quantum synchronization in the growing fields of quantum technologies, such as quantum information,

quantum metrology, and quantum standard.

Appendix A

Explicit form of $\boldsymbol{\beta}(\boldsymbol{\alpha})$

In this section, we derive an explicit expression of $\boldsymbol{\beta}(\boldsymbol{\alpha})$ in Eq. (2.3). The diffusion matrix of the FPE in Eq. (2.2) in the complex representation is given by

$$\boldsymbol{D}(\boldsymbol{\alpha}) = \boldsymbol{\beta}(\boldsymbol{\alpha})\boldsymbol{\beta}(\boldsymbol{\alpha})^T = \begin{pmatrix} D_{11}(\boldsymbol{\alpha}) & D_{12}(\boldsymbol{\alpha}) \\ D_{21}(\boldsymbol{\alpha}) & D_{22}(\boldsymbol{\alpha}) \end{pmatrix} \in \mathbb{C}^{2\times 2}, \tag{A.1}$$

where $D_{22}(\boldsymbol{\alpha}) = D_{11}^*(\boldsymbol{\alpha})$ and $D_{12}(\boldsymbol{\alpha}) = D_{21}(\boldsymbol{\alpha})$. The non-diagonal element $D_{12}(\boldsymbol{\alpha}) = D_{21}(\boldsymbol{\alpha})$ is real and positive, because it is a constant of cross diffusion described by $\partial^2 P(\boldsymbol{\alpha}, t)/\partial\alpha\partial\alpha^*$ and it can be obtained as an absolute value of a complex variable.

We rewrite the FPE in Eq. (2.2) corresponding to the SDE in Eq. (2.4) in the real-valued representation, i.e., for the quasiprobability distribution $P(\boldsymbol{X}, t)$ with $\boldsymbol{X} = (x, p)^T = (\mathrm{Re}\ \alpha, \mathrm{Im}\ \alpha)^T$, as

$$\frac{\partial}{\partial t}P(\boldsymbol{X}, t) = \left[-\frac{\partial}{\partial \boldsymbol{X}}\{\boldsymbol{F}(\boldsymbol{X}) + \epsilon\boldsymbol{q}(\boldsymbol{X}, t)\} + \frac{1}{2}\frac{\partial^2}{\partial \boldsymbol{X}^2}\boldsymbol{D}(\boldsymbol{X})\right] P(\boldsymbol{X}, t), \tag{A.2}$$

where

$$\frac{\partial}{\partial\alpha} = \frac{1}{2}\left(\frac{\partial}{\partial x} - i\frac{\partial}{\partial p}\right), \quad \frac{\partial}{\partial\alpha^*} = \frac{1}{2}\left(\frac{\partial}{\partial x} + i\frac{\partial}{\partial p}\right). \tag{A.3}$$

The real-valued diffusion matrix $\boldsymbol{D}(\boldsymbol{X})$ in the above FPE and the complex-valued diffusion matrix $\boldsymbol{D}(\boldsymbol{\alpha})$ are related as

$$\begin{aligned} \boldsymbol{D}(\boldsymbol{X}) &= \frac{1}{4}\begin{pmatrix} 1 & 1 \\ -i & i \end{pmatrix} \boldsymbol{D}(\boldsymbol{\alpha}) \begin{pmatrix} 1 & -i \\ 1 & i \end{pmatrix} \\ &= \frac{1}{2}\begin{pmatrix} \mathrm{Re}\ D_{11}(\boldsymbol{\alpha}) + D_{12}(\boldsymbol{\alpha}) & \mathrm{Im}\ D_{11}(\boldsymbol{\alpha}) \\ \mathrm{Im}\ D_{11}(\boldsymbol{\alpha}) & -\mathrm{Re}\ D_{11}(\boldsymbol{\alpha}) + D_{12}(\boldsymbol{\alpha}) \end{pmatrix} \in \mathbb{R}^{2\times 2} \end{aligned} \tag{A.4}$$

and

$$\boldsymbol{D}(\boldsymbol{\alpha}) = \begin{pmatrix} 1 & i \\ 1 & -i \end{pmatrix} \boldsymbol{D}(\boldsymbol{X}) \begin{pmatrix} 1 & 1 \\ i & -i \end{pmatrix}. \tag{A.5}$$

By denoting the matrix components of $\boldsymbol{D}(\boldsymbol{\alpha})$ in the polar representation as $D_{11}(\boldsymbol{\alpha}) = R_{11}(\boldsymbol{\alpha})e^{i\chi(\boldsymbol{\alpha})}$ and $D_{12}(\boldsymbol{\alpha}) = R_{12}(\boldsymbol{\alpha})$, where $R_{11}(\boldsymbol{\alpha}), R_{22}(\boldsymbol{\alpha}) \geq 0$ and $\chi(\boldsymbol{\alpha}) \in [0, 2\pi)$, the eigenvalues $\lambda_{\pm}(\boldsymbol{X})$ and eigenvectors $\boldsymbol{v}_{\pm}(\boldsymbol{X})$ of $\boldsymbol{D}(\boldsymbol{X})$ can be expressed as

$$\begin{aligned} \lambda_{\pm}(\boldsymbol{X}) &= \frac{1}{2}\left(R_{12}(\boldsymbol{\alpha}) \pm R_{11}(\boldsymbol{\alpha})\right), \\ \boldsymbol{v}_{+}(\boldsymbol{X}) &= \begin{pmatrix} \cos\frac{\chi(\boldsymbol{\alpha})}{2} \\ \sin\frac{\chi(\boldsymbol{\alpha})}{2} \end{pmatrix}, \quad \boldsymbol{v}_{-}(\boldsymbol{X}) = \begin{pmatrix} \sin\frac{\chi(\boldsymbol{\alpha})}{2} \\ -\cos\frac{\chi(\boldsymbol{\alpha})}{2} \end{pmatrix}, \end{aligned} \tag{A.6}$$

and $\boldsymbol{D}(\boldsymbol{X})$ can be decomposed as

$$\boldsymbol{D}(\boldsymbol{X}) = \begin{pmatrix} \boldsymbol{v}_{+}(\boldsymbol{X}) & \boldsymbol{v}_{-}(\boldsymbol{X}) \end{pmatrix} \begin{pmatrix} \lambda_{+}(\boldsymbol{X}) & 0 \\ 0 & \lambda_{-}(\boldsymbol{X}) \end{pmatrix} \begin{pmatrix} \boldsymbol{v}_{+}(\boldsymbol{X})^T \\ \boldsymbol{v}_{-}(\boldsymbol{X})^T \end{pmatrix}. \tag{A.7}$$

Thus, $\boldsymbol{G}(\boldsymbol{X})$ is given by

$$\begin{aligned} \boldsymbol{G}(\boldsymbol{X}) &= \begin{pmatrix} \boldsymbol{v}_{+}(\boldsymbol{X}) & \boldsymbol{v}_{-}(\boldsymbol{X}) \end{pmatrix} \begin{pmatrix} \sqrt{\lambda_{+}(\boldsymbol{X})} & 0 \\ 0 & \sqrt{\lambda_{-}(\boldsymbol{X})} \end{pmatrix} \\ &= \begin{pmatrix} \sqrt{\frac{(R_{12}(\boldsymbol{\alpha})+R_{11}(\boldsymbol{\alpha}))}{2}}\cos\frac{\chi(\boldsymbol{\alpha})}{2} & \sqrt{\frac{(R_{12}(\boldsymbol{\alpha})-R_{11}(\boldsymbol{\alpha}))}{2}}\sin\frac{\chi(\boldsymbol{\alpha})}{2} \\ \sqrt{\frac{(R_{12}(\boldsymbol{\alpha})+R_{11}(\boldsymbol{\alpha}))}{2}}\sin\frac{\chi(\boldsymbol{\alpha})}{2} & -\sqrt{\frac{(R_{12}(\boldsymbol{\alpha})-R_{11}(\boldsymbol{\alpha}))}{2}}\cos\frac{\chi(\boldsymbol{\alpha})}{2} \end{pmatrix}, \end{aligned} \tag{A.8}$$

and $\boldsymbol{\beta}(\boldsymbol{\alpha})$ is obtained from $\boldsymbol{G}(\boldsymbol{X})$ as

$$\begin{aligned} \boldsymbol{\beta}(\boldsymbol{\alpha}) &= \begin{pmatrix} 1 & i \\ 1 & -i \end{pmatrix}, \\ \boldsymbol{G}(\boldsymbol{X}) &= \begin{pmatrix} \sqrt{\frac{(R_{12}(\boldsymbol{\alpha})+R_{11}(\boldsymbol{\alpha}))}{2}}e^{i\chi(\boldsymbol{\alpha})/2} & -i\sqrt{\frac{(R_{12}(\boldsymbol{\alpha})-R_{11}(\boldsymbol{\alpha}))}{2}}e^{i\chi(\boldsymbol{\alpha})/2} \\ \sqrt{\frac{(R_{12}(\boldsymbol{\alpha})+R_{11}(\boldsymbol{\alpha}))}{2}}e^{-i\chi(\boldsymbol{\alpha})/2} & i\sqrt{\frac{(R_{12}(\boldsymbol{\alpha})-R_{11}(\boldsymbol{\alpha}))}{2}}e^{-i\chi(\boldsymbol{\alpha})/2} \end{pmatrix}. \end{aligned} \tag{A.9}$$

The assumption in the main text that the diffusion matrix is always positive semidefinite along the limit cycle is equivalent to the assumption that $\lambda_{-}(\boldsymbol{X}_0(\phi)) \geq 0$, that is, $R_{12}(\boldsymbol{\alpha}_0(\phi)) \geq R_{11}(\boldsymbol{\alpha}_0(\phi))$ is satisfied for all ϕ, because $\lambda_{+}(\boldsymbol{X})$ is always positive. With this assumption, if the initial state is given in the form of Eq. (2.11), for instance, by a pure coherent state $\rho = |\alpha_0(\phi_0)\rangle\langle\alpha_0(\phi_0)|$ at a given phase point ϕ_0 on the limit cycle, the state always remains in the two-dimensional phase space of the classical variables.

Appendix B

Derivation of the phase equation

In this section, we give a detailed derivation of the phase equation in Eq. (2.5). The asymptotic phase function $\Phi(\boldsymbol{X}) : B \subset \mathbb{R}^{2\times 1} \to [0, 2\pi)$ introduced in the main text satisfies

$$\boldsymbol{F}(\boldsymbol{X}) \cdot \nabla\Phi(\boldsymbol{X}) = \omega \tag{B.1}$$

in the basin B of the limit cycle, where $\nabla\Phi \in \mathbb{R}^{2\times 1}$ indicates the gradient of Φ with respect to $\boldsymbol{X}$. Using this $\Phi(\boldsymbol{X})$, we define the phase ϕ of the oscillator state $\boldsymbol{X}$ as $\phi = \Phi(\boldsymbol{X})$. As long as $\boldsymbol{X}$ evolves in B, $\dot{\phi} = \dot{\Phi}(\boldsymbol{X}) = \dot{\boldsymbol{X}} \cdot \nabla\Phi(\boldsymbol{X}) = \boldsymbol{F}(\boldsymbol{X}) \cdot \nabla\Phi(\boldsymbol{X}) = \omega$ holds. Recently, it has been shown that this phase function is closely related to an eigenfunction of the Koopman operator of the system $\dot{\boldsymbol{X}} = \boldsymbol{F}(\boldsymbol{X})$ associated with the eigenvalue $i\omega$ [116].

When $\boldsymbol{X}$ obeys the Ito SDE in Eq. (2.4), we obtain an Ito SDEs for the phase ϕ as

$$\begin{aligned} d\phi =& \left[(\nabla\Phi(\boldsymbol{X})) \cdot (\boldsymbol{F}(\boldsymbol{X}) + \epsilon\boldsymbol{q}(\boldsymbol{X}, t)) + \tfrac{1}{2}\epsilon \mathrm{Tr}\left\{\boldsymbol{G}(\boldsymbol{X})^T(\nabla^T\nabla\Phi(\boldsymbol{X}))\boldsymbol{G}(\boldsymbol{X})\right\}\right] dt \\ &+ \sqrt{\epsilon}(\nabla\Phi(\boldsymbol{X})) \cdot (\boldsymbol{G}(\boldsymbol{X})d\boldsymbol{W}) \\ =& \left[\omega + \epsilon(\nabla\Phi(\boldsymbol{X})) \cdot \boldsymbol{q}(\boldsymbol{X}, t) + \frac{1}{2}\epsilon \mathrm{Tr}\left\{\boldsymbol{G}(\boldsymbol{X})^T(\nabla^T\nabla\Phi(\boldsymbol{X}))\boldsymbol{G}(\boldsymbol{X})\right\}\right] dt \\ &+ \sqrt{\epsilon}(\boldsymbol{G}(\boldsymbol{X})^T\nabla\Phi(\boldsymbol{X})) \cdot d\boldsymbol{W}, \end{aligned} \tag{B.2}$$

where the third term in the drift part arises from the change of the variables by the Ito formula and $\nabla^T\nabla\Phi \in \mathbb{R}^{2\times 2}$ represents the Hessian matrix of

$\Phi(\boldsymbol{X})$ with respect to $\boldsymbol{X}$. This equation is still not closed in the phase variable ϕ, because each term on the right-hand side depends on $\boldsymbol{X}$.

When the perturbation and quantum noise are weak, the deviation of the system state $\boldsymbol{X}$ from the limit cycle is small and of the order of $\mathcal{O}(\sqrt{\epsilon})$ because the limit cycle is exponentially stable and the system state is subjected to Gaussian-white noise. Thus, in the lowest-order approximation, we can approximate the state $\boldsymbol{X}$ by a state $\boldsymbol{X}_0(\phi)$ on the limit cycle as $\boldsymbol{X}(t) = \boldsymbol{X}_0(\phi(t)) + \mathcal{O}(\sqrt{\epsilon})$. We then obtain an Ito SDE for the phase variable ϕ,

$$d\phi = \{\omega + \epsilon f(\phi, t) + \epsilon g(\phi)\}\, dt + \sqrt{\epsilon}\boldsymbol{h}(\phi) \cdot d\boldsymbol{W}, \tag{B.3}$$

which is correct up to $\mathcal{O}(\epsilon)$ in the drift term and up to $\mathcal{O}(\sqrt{\epsilon})$ in the noise intensity, where

$$f(\phi, t) = \nabla\Phi(\boldsymbol{X})|_{\boldsymbol{X}=\boldsymbol{X}_0(\phi)} \cdot \boldsymbol{q}(\boldsymbol{X}_0(\phi), t) \in \mathbb{R} \tag{B.4}$$

represents the effect of the perturbation on ϕ,

$$\boldsymbol{h}(\phi) = \boldsymbol{G}(\boldsymbol{X}_0(\phi))^T \nabla\Phi(\boldsymbol{X})|_{\boldsymbol{X}=\boldsymbol{X}_0(\phi)} \in \mathbb{R}^{2\times 1} \tag{B.5}$$

represents the effect of the quantum noise on ϕ, and

$$g(\phi) = \frac{1}{2}\mathrm{Tr}\left\{\boldsymbol{G}(\boldsymbol{X}_0(\phi))^T (\nabla^T\nabla\Phi|_{\boldsymbol{X}=\boldsymbol{X}_0(\phi)})\boldsymbol{G}(\boldsymbol{X}_0(\phi))\right\} \tag{B.6}$$

represents a term arising from the change of the variables, respectively.

We denote the gradient vector (PSF) and Hessian matrix of the phase function $\Phi(\boldsymbol{X})$ evaluated at $\boldsymbol{X} = \boldsymbol{X}_0(\phi)$ on the limit cycle as $\boldsymbol{Z}(\phi) = \nabla\Phi|_{\boldsymbol{X}=\boldsymbol{X}_0(\phi)}$ and $\boldsymbol{Y}(\phi) = \nabla^T\nabla\Phi|_{\boldsymbol{X}=\boldsymbol{X}_0(\phi)}$, respectively. The components of the PSF and Hessian matrix $\nabla^T\nabla\Phi|_{\boldsymbol{X}=\boldsymbol{X}_0(\phi)}$ are explicitly given by

$$Z_i(\phi) = \left.\frac{\partial\Phi(\boldsymbol{X})}{\partial X_i}\right|_{\boldsymbol{X}=\boldsymbol{X}_0(\phi)}, \quad (\nabla^T\nabla\Phi|_{\boldsymbol{X}=\boldsymbol{X}_0(\phi)})_{ij} = \left.\frac{\partial^2\Phi(\boldsymbol{X})}{\partial X_i \partial X_j}\right|_{\boldsymbol{X}=\boldsymbol{X}_0(\phi)}, \tag{B.7}$$

for $i, j = 1, 2$, respectively.

It is well known in the classical phase reduction theory [7, 3, 8, 9] that $\boldsymbol{Z}(\phi)$ is given by a 2π-periodic solution to the following adjoint equation and normalization condition:

$$\omega\frac{d}{d\phi}\boldsymbol{Z}(\phi) = -\boldsymbol{J}(\phi)^T\boldsymbol{Z}(\phi), \quad \boldsymbol{Z}(\phi) \cdot \boldsymbol{F}(\boldsymbol{X}_0(\phi)) = \omega. \tag{B.8}$$

It is also known [82, 83] that the Hessian matrix $\boldsymbol{Y}(\phi)$ of the phase function, evaluated at $\boldsymbol{X} = \boldsymbol{X}_0(\phi)$ on the limit cycle, is given by a 2π-periodic solution to a differential equation

$$\omega \frac{d}{d\phi}\boldsymbol{Y}(\phi) = -\boldsymbol{J}(\phi)^T\boldsymbol{Y}(\phi) - \boldsymbol{Y}(\phi)\boldsymbol{J}(\phi) - \boldsymbol{Z}(\phi) \circ \boldsymbol{K}(\phi), \tag{B.9}$$

which satisfies a constraint

$$\boldsymbol{Z}(\phi) \cdot \boldsymbol{J}(\phi)\boldsymbol{F}(\boldsymbol{X}_0(\phi)) + \boldsymbol{F}(\boldsymbol{X}_0(\phi)) \cdot \boldsymbol{Y}(\phi)\boldsymbol{F}(\boldsymbol{X}_0(\phi)) = 0. \tag{B.10}$$

In the above equations, $\boldsymbol{J}(\phi) \in \mathbb{R}^{2\times 2}$ is a Jacobian matrix of $\boldsymbol{F}(\boldsymbol{X})$ at $\boldsymbol{X} = \boldsymbol{X}_0(\phi)$ and $\boldsymbol{K}(\phi) \in \mathbb{R}^{2\times 2\times 2}$ is a third order tensor, respectively, whose components are given by

$$J(\theta)_{ij} = \left.\frac{\partial F_i}{\partial X_j}\right|_{\boldsymbol{X}=\boldsymbol{X}_0(\theta)}, \quad K(\theta)_{ijk} = \left.\frac{\partial^2 F_i}{\partial X_j \partial X_k}\right|_{\boldsymbol{X}=\boldsymbol{X}_0(\theta)}, \tag{B.11}$$

and the matrix components of the product $\boldsymbol{Z}(\phi) \circ \boldsymbol{K}(\phi) \in \mathbb{R}^{2\times 2}$ are given by

$$[\boldsymbol{Z}(\phi) \circ \boldsymbol{K}(\phi)]_{j,k} = \sum_{i=1}^{2} Z_i(\phi) K_{ijk}(\phi) \tag{B.12}$$

for $i, j, k = 1, 2$.

Thus, when the noise and perturbations are sufficiently weak, we obtain an approximate Ito SDE for the phase variable as

$$d\phi = \{\omega + \epsilon f(\phi, t) + \epsilon g(\phi)\}dt + \sqrt{\epsilon}\boldsymbol{h}(\phi) \cdot d\boldsymbol{W} \tag{B.13}$$

at the lowest order, which corresponds to Eq. (2.5) in the main text. It can be shown that the amplitude effect does not enter the phase dynamics at the lowest order [117]. As Eq. (B.13) is an Ito SDE, using the property of the Wiener process, the noise term can be rewritten as

$$\sqrt{\epsilon}\boldsymbol{h}(\phi) \cdot d\boldsymbol{W} = \sqrt{\epsilon}h(\phi)dW, \tag{B.14}$$

where $h(\phi) = \sqrt{\sum_{i=1}^{2}(\boldsymbol{h}(\phi))_i^2}$ and $W(t)$ is a one-dimensional Wiener process.

The errors in the evolution of the phase variable resulting from the lowest-order approximation above are $\mathcal{O}(\epsilon^2)$ in the drift term and $\mathcal{O}(\epsilon)$ in the noise intensity, respectively. Therefore, the error in the mean of ϕ from the true value grows with time as $\mathcal{O}(\epsilon^2 t)$, and the error in the variance of ϕ grows as $\mathcal{O}(\epsilon^2 t)$. Thus, these errors in the phase dynamics remain $\mathcal{O}(\epsilon)$ up to $t = \mathcal{O}(1/\epsilon)$.

Appendix C

Averaged phase equation

In this section, we derive the averaged phase equation, Eq. (2.9), by using the near-identity transform. Although Eq. (2.5) is a correct phase equation for the phase ϕ in the lowest-order approximation, it has an additional function $g(\phi)$ in the drift term, which adds tiny periodic fluctuations to the deterministic part. By further introducing a new phase ψ that is only slightly different from ϕ, we can eliminate this term and obtain a simpler SDE,

$$d\psi = \{\tilde{\omega} + \epsilon f(\psi, t)\}dt + \sqrt{\epsilon}h(\psi)dW, \tag{C.1}$$

where $f(\psi, t) = \boldsymbol{Z}(\psi) \cdot \boldsymbol{q}(\psi, t)$, $W(t)$ is a one-dimensional Wiener process, and $h(\psi)$ is a 2π-periodic function of ψ. Here, the new phase ψ is defined from ϕ by a near-identity transform as $\phi = \psi + \epsilon n(\psi)$, where $n(\psi)$ is a 2π-periodic function with $n(0) = 0$. Using this transformation, the additional term $g(\phi)$ in Eq. (2.5) can be renormalized into the frequency term as

$$\tilde{\omega} = \omega + \frac{\epsilon}{2\pi}\int_0^{2\pi} g(\psi')d\psi', \tag{C.2}$$

where $\tilde{\omega}$ is the effective frequency of the system. As ϵ is assumed to be sufficiently small, the transformation between the two variables ϕ and ψ is invertible. Thus, the qualitative properties of the dynamics predicted by the two-phase equations, such as whether synchronization occurs or not, are invariant. In the classical phase-reduction theory, the $\mathcal{O}(\epsilon)$ difference between the phase variables due to the near-identity transformation or averaging is often neglected and both phases are considered to be the same. Below, we derive the simplified phase equation in Eq. (C.1) from the original phase equation, Eq. (2.5) or (B.13), by using the near-identity transform [118].

In Eq. (B.13), the function $g(\phi)$ contains the Hessian matrix $\boldsymbol{Y}(\phi)$ of $\Phi(\boldsymbol{X})$ on the limit cycle, which is typically not included in the phase equation for classical limit-cycle oscillators and gives a tiny but complex periodic contribution to the phase dynamics. To eliminate this term, we renormalize it into the frequency term. For this purpose, we consider a near-identity transform from the original phase ϕ to a new phase ψ,

$$\phi = \psi + \epsilon n(\psi), \tag{C.3}$$

where the transformation function $n(\psi)$ is a smooth 2π-periodic function of ψ satisfying $n(0) = 0$, and assume that ψ obeys an Ito SDE of the form

$$d\psi = \{\omega + \epsilon\Omega + \epsilon f(\psi, t)\}dt + \sqrt{\epsilon}h(\psi)dW \tag{C.4}$$

in the lowest-order approximation, which does not contain a term corresponding to $g(\phi)$ but has a small shift $\epsilon\Omega$ in the frequency. From this SDE, we obtain an Ito SDE for ϕ by using the Ito formula as

$$\begin{aligned} d\phi &= \left[\frac{\partial\phi}{\partial\psi}\{\omega + \epsilon\Omega + \epsilon f(\psi, t)\} + \frac{1}{2}\epsilon h(\psi)^2\frac{\partial^2\phi}{\partial\psi^2}\right]dt + \sqrt{\epsilon}\frac{\partial\phi}{\partial\psi}h(\psi)dW \\ &= \left[(1 + \epsilon n'(\psi))\{\omega + \epsilon\Omega + \epsilon f(\psi, t)\} + \frac{1}{2}\epsilon h(\psi)^2(\epsilon n''(\psi))\right]dt \\ &+ \sqrt{\epsilon}(1 + \epsilon n'(\psi))h(\psi)dW \\ &\approx \left[\omega + \epsilon f(\psi, t) + \epsilon\Omega + \epsilon\omega n'(\psi)\right]dt + \sqrt{\epsilon}h(\psi)dW, \end{aligned} \tag{C.5}$$

where we omitted the tiny terms of $\mathcal{O}(\epsilon^2)$ in the drift term and $\mathcal{O}(\epsilon^{3/2})$ in the noise intensity. The replacement of ϕ by ψ in the functions f and h also results in errors of $\mathcal{O}(\epsilon^2)$ and $\mathcal{O}(\epsilon^{3/2})$ in the drift term and noise intensity, respectively, which can also be neglected.

The above equation coincides with the original Eq. (B.13) if $n(\psi)$ satisfies

$$\Omega + \omega n'(\psi) = g(\phi). \tag{C.6}$$

As $g(\phi) = g(\psi) + \mathcal{O}(\epsilon)$, the equation for $n(\psi)$ is obtained at the lowest order as

$$\frac{d}{d\psi}n(\psi) = g(\psi) - \Omega, \tag{C.7}$$

which gives

$$n(\psi) = \int_0^\psi d\psi' \left[g(\psi') - \Omega\right], \tag{C.8}$$

where $n(0) = 0$ is used. Moreover, as $n(\psi)$ is 2π-periodic, $n(2\pi) = n(0) = 0$ should hold, which determines the frequency shift Ω as

$$\epsilon\Omega = \frac{\epsilon}{2\pi} \int_0^{2\pi} d\psi' g(\psi'). \tag{C.9}$$

Thus, by introducing the near-identity transform, we obtain an averaged phase equation

$$d\psi = \{\tilde{\omega} + \epsilon f(\psi, t)\}dt + \sqrt{\epsilon} h(\psi) dW, \tag{C.10}$$

where $\tilde{\omega} = \omega + \epsilon\Omega$ is a renormalized, effective frequency. This corresponds to Eq. (C.1). The orders of errors caused by the above near-identity transformation are $\mathcal{O}(\epsilon^2)$ in the drift term and $\mathcal{O}(\epsilon^{3/2})$ in the noise intensity. Therefore, the phase equations in Eq. (B.13) and (C.10) are equally correct in the lowest-order approximation and valid up to $t = \mathcal{O}(1/\epsilon)$.

The frequency shift $\epsilon\Omega$ can be evaluated by numerically calculating the Hessian matrix of $\Phi(\boldsymbol{X})$ in $g(\psi)$ and integrating Eq. (C.9), or alternatively by measuring $\tilde{\omega}$ by numerically evolving the SDE in Eq. (2.3) or Eq. (2.4) without perturbations. In the examples used in the main text, the frequency shift $\epsilon\Omega$ is zero in the case of Eq. (2.18) with the symmetric limit cycle with weak squeezing, and takes a tiny value in the case with strong squeezing. In other applications, for example, in the analysis of coupled identical limit-cycle oscillators without external forcing, the precise value of $\tilde{\omega}$ may not be required (only the frequency difference matters). In such cases, one may simply assume $\tilde{\omega} \approx \omega$ and avoid the calculation of $\epsilon\Omega$.

Appendix D

Phase-space representation of a quantum vdP oscillator with harmonic driving and squeezing

D.1 Weak squeezing

Here, we derive a phase equation for a quantum vdP oscillator with harmonic driving and squeezing. In the case of weak squeezing with $\delta = \epsilon$, the rescaled system Hamiltonian and the perturbation Hamiltonian are given by

$$H = -\Delta' a'^{\dagger} a', \quad \epsilon\tilde{H} = \epsilon\left\{iE'(a' - a'^{\dagger}) + i\eta'(a'^{2}e^{-i\theta} - a'^{\dagger 2}e^{i\theta})\right\}, \tag{D.1}$$

respectively, where the squeezing term is included in the perturbation. The functions $\boldsymbol{A}(\boldsymbol{\alpha'})$, $\epsilon\boldsymbol{A'}(\boldsymbol{\alpha'})$, and $\epsilon\boldsymbol{D}(\boldsymbol{\alpha'})$ in the quantum FPE are calculated as

$$\boldsymbol{A}(\boldsymbol{\alpha'}) = \begin{pmatrix} \left(\frac{1}{2} + i\Delta'\right)\alpha' - \gamma_2'\alpha'^{*}\alpha'^{2} \\ \left(\frac{1}{2} - i\Delta'\right)\alpha'^{*} - \gamma_2'\alpha'\alpha'^{*2} \end{pmatrix}, \quad \epsilon\boldsymbol{A'}(\boldsymbol{\alpha'}) = \epsilon\begin{pmatrix} -E' - 2\eta' e^{i\theta}\alpha'^{*} \\ -E' - 2\eta' e^{-i\theta}\alpha' \end{pmatrix}, \tag{D.2}$$

and

$$\epsilon\boldsymbol{D}(\boldsymbol{\alpha'}) = \epsilon\begin{pmatrix} -\gamma_2'\alpha'^{2} & 1 \\ 1 & -\gamma_2'\alpha'^{*2} \end{pmatrix}, \tag{D.3}$$

where the tiny terms of $\mathcal{O}(\epsilon^2)$ in $\epsilon \boldsymbol{D}(\boldsymbol{\alpha}')$ are dropped. The explicit form of $\boldsymbol{\beta}(\boldsymbol{\alpha}')$ given by Eq. (A.9) can be obtained from Eq. (D.3) as

$$\boldsymbol{\beta}(\boldsymbol{\alpha}') = \begin{pmatrix} i\sqrt{\frac{1+\gamma_2' R'^2}{2}} e^{i\delta'} & \sqrt{\frac{1-\gamma_2' R'^2}{2}} e^{i\delta'} \\ -i\sqrt{\frac{1+\gamma_2' R'^2}{2}} e^{-i\delta'} & \sqrt{\frac{1-\gamma_2' R'^2}{2}} e^{-i\delta'} \end{pmatrix}, \tag{D.4}$$

where the modulus R' and argument δ' of α' is introduced as $\alpha' = R' e^{i\delta'}$. In the real-valued representation with $\boldsymbol{X} = (x', p')^T = (\mathrm{Re}\ \alpha, \mathrm{Im}\ \alpha)^T$, the functions $\boldsymbol{F}(\boldsymbol{X})$, $\epsilon \boldsymbol{q}(\boldsymbol{X})$, and $\sqrt{\epsilon}\boldsymbol{G}(\boldsymbol{X})$ are given by

$$\begin{aligned} \boldsymbol{F}(\boldsymbol{X}) &= \begin{pmatrix} \frac{1}{2}x' - \Delta' p' - \gamma_2' x'(x'^2 + p'^2) \\ \frac{1}{2}p' + \Delta' x' - \gamma_2' p'(x'^2 + p'^2) \end{pmatrix}, \\ \epsilon \boldsymbol{q}(\boldsymbol{X}) &= \epsilon \begin{pmatrix} -E' - 2\eta'(x'\cos\theta + p'\sin\theta) \\ 2\eta'(p'\cos\theta - x'\sin\theta) \end{pmatrix}, \end{aligned} \tag{D.5}$$

and

$$\sqrt{\epsilon}\boldsymbol{G}(\boldsymbol{X}) = \sqrt{\epsilon} \begin{pmatrix} -\sqrt{\frac{1+\gamma_2' R'^2}{2}} \sin\delta' & \sqrt{\frac{1-\gamma_2' R'^2}{2}} \cos\delta' \\ \sqrt{\frac{1+\gamma_2' R'^2}{2}} \cos\delta' & \sqrt{\frac{1-\gamma_2' R'^2}{2}} \sin\delta' \end{pmatrix}, \tag{D.6}$$

respectively.

As discussed in the main text, the deterministic part of this equation, $\dot{\boldsymbol{X}} = \boldsymbol{F}(\boldsymbol{X})$, is a normal form of the supercritical Hopf bifurcation, also known as the Stuart-Landau oscillator, and it is analytically solvable. The limit cycle of this system in the classical limit can be obtained as $\boldsymbol{X}_0(\phi) = \sqrt{\frac{1}{2\gamma_2'}}(\cos\phi, \sin\phi)^T$ with $\phi = \omega t$, or $\boldsymbol{\alpha}_0'(\phi) = \sqrt{\frac{1}{2\gamma_2'}}(e^{i\phi}, e^{-i\phi})^T$ in the complex-valued representation, where the natural frequency is given by $\omega = \Delta'$, and the frequency shift $\epsilon\Omega$ vanishes. From Eq. (D.3), the eigenvalues of matrix $\boldsymbol{D}(\boldsymbol{\alpha})$ can be calculated as

$$\lambda_\pm(\boldsymbol{X}) = \frac{1}{2}\left\{R_{12}(\boldsymbol{\alpha'}) \pm R_{11}(\boldsymbol{\alpha'})\right\} = \frac{1}{2}\left(1 \pm \gamma_2'|\alpha'|^2\right). \tag{D.7}$$

By plugging the limit-cycle solution $\boldsymbol{X}_0(\phi)$ into this equation, it can be seen that $\lambda_-(\boldsymbol{X}_0(\phi)) = \frac{1}{4} > 0$ is satisfied for any ϕ on the limit cycle and the diffusion matrix is always positive semidefinite along the limit cycle, because the magnitudes of the squeezing and nonlinear damping, which can cause negative diffusion, are assumed to be sufficiently small.

D.2 Strong squeezing

In the case of strong squeezing with $\delta = 1$, the rescaled system Hamiltonian and the perturbation Hamiltonian are given by

$$H = -\Delta' a'^{\dagger} a' + i\eta'(a'^2 e^{-i\theta} - a'^{\dagger 2} e^{i\theta}), \quad \epsilon\tilde{H} = i\epsilon E'(a' - a'^{\dagger}), \tag{D.8}$$

respectively, where the squeezing term is included in the system Hamiltonian. The functions $\boldsymbol{A}(\boldsymbol{\alpha'})$, $\boldsymbol{A'}(\boldsymbol{\alpha'})$, and $\boldsymbol{D}(\boldsymbol{\alpha'})$ in the phase-space representation are given by

$$\boldsymbol{A}(\boldsymbol{\alpha'}) = \begin{pmatrix} \left(\frac{1}{2} + i\Delta'\right)\alpha' - \gamma_2'\alpha'^* \alpha'^2 - 2\eta' e^{i\theta}\alpha'^* \\ \left(\frac{1}{2} - i\Delta'\right)\alpha'^* - \gamma_2'\alpha'\alpha'^{*2} - 2\eta' e^{-i\theta}\alpha' \end{pmatrix}, \quad \epsilon\boldsymbol{A'}(\boldsymbol{\alpha'}) = \epsilon \begin{pmatrix} -E' \\ -E' \end{pmatrix}, \tag{D.9}$$

and

$$\epsilon\boldsymbol{D}(\boldsymbol{\alpha'}) = \epsilon \begin{pmatrix} -(\gamma_2'\alpha'^2 + 2\eta' e^{i\theta}) & 1 \\ 1 & -(\gamma_2'\alpha'^{*2} + 2\eta' e^{-i\theta}) \end{pmatrix}. \tag{D.10}$$

The explicit form of $\boldsymbol{\beta}(\boldsymbol{\alpha'})$ in this case is given by

$$\boldsymbol{\beta}(\boldsymbol{\alpha'}) = \begin{pmatrix} \sqrt{\frac{(1+R_2')}{2}} e^{i\chi_2'/2} & -i\sqrt{\frac{(1-R_2')}{2}} e^{i\chi_2'/2} \\ \sqrt{\frac{(1+R_2'))}{2}} e^{-i\chi_2'/2} & i\sqrt{\frac{(1-R_2')}{2}} e^{-i\chi_2'/2} \end{pmatrix}, \tag{D.11}$$

where $R_2' e^{i\chi_2'} = -(\gamma_2'\alpha'^2 + 2\eta' e^{i\theta})$. In the real-valued representation with $\boldsymbol{X} = (x', p')^T = (\mathrm{Re}\ \alpha, \mathrm{Im}\ \alpha)^T$, the functions $\boldsymbol{F}(\boldsymbol{X})$, $\epsilon\boldsymbol{q}(\boldsymbol{X})$, and $\sqrt{\epsilon}\boldsymbol{G}(\boldsymbol{X})$ are given by

$$\begin{aligned} \boldsymbol{F}(\boldsymbol{X}) &= \begin{pmatrix} \frac{1}{2}x' - \Delta' p' - \gamma_2' x'(x'^2 + p'^2) - 2\eta'(x'\cos\theta + p'\sin\theta) \\ \frac{1}{2}p' + \Delta' x' - \gamma_2' p'(x'^2 + p'^2) + 2\eta'(p'\cos\theta - x'\sin\theta) \end{pmatrix}, \\ \epsilon\boldsymbol{q}(\boldsymbol{X}) &= \epsilon \begin{pmatrix} -E' \\ 0 \end{pmatrix}, \end{aligned} \tag{D.12}$$

and

$$\boldsymbol{G}(\boldsymbol{X}) = \begin{pmatrix} \sqrt{\frac{(1+R_2')}{2}} \cos\frac{\chi_2'}{2} & \sqrt{\frac{(1-R_2')}{2}} \sin\frac{\chi_2'}{2} \\ \sqrt{\frac{(1+R_2')}{2}} \sin\frac{\chi_2'}{2} & -\sqrt{\frac{(1-R_2')}{2}} \cos\frac{\chi_2'}{2} \end{pmatrix}, \tag{D.13}$$

respectively.

The deterministic part $\boldsymbol{F}(\boldsymbol{X})$ gives an asymmetric limit cycle when $\eta > 0$, which is difficult to solve analytically. However, we can still obtain the

limit cycle $\boldsymbol{X}_0(\phi)$ numerically and use it to evaluate the PSF $\boldsymbol{Z}(\phi)$, Hessian matrix $\boldsymbol{Y}(\phi)$, and the noise intensity $\boldsymbol{G}(\phi)$, and use these quantities in the phase equation. The PSF $\boldsymbol{Z}(\phi)$ can be numerically calculated by the adjoint method, and the Hessian matrix $\boldsymbol{Y}(\phi)$ can be calculated by using a shooting-type numerical algorithm.

When the squeezing is too strong, the diffusion matrix can generally be negative definite on the limit cycle. We choose parameter settings where the diffusion matrix is always positive semidefinite along the limit cycle in the main text.

Appendix E

Derivation of the optimal waveforms

In this Appendix, we give the derivation of the optimal waveforms. The optimization problems for the improvement of entrainment stability and enhancement of phase coherence are rewritten as

$$\text{maximize } \int_0^{2\pi} \left(-Z_x'(\theta)\right) E(\theta) d\theta, \text{ s.t. } \left\langle E^2(\theta) \right\rangle_\theta = P, \tag{E.1}$$

and

$$\text{maximize } \int_0^{2\pi} \left(- \int_\theta^{\theta+\Delta_\psi} Z_x(\bar{\theta}) d\bar{\theta} \right) E(\theta) d\theta, \text{ s.t. } \left\langle E^2(\theta) \right\rangle_\theta = P, \tag{E.2}$$

respectively, where we assume $\psi^* = 0$ without loss of generality. In order to analyze both problems together, we consider a general form of an optimization problem,

$$\text{maximize } \int_0^{2\pi} g(\theta) E(\theta) d\theta, \text{ s.t. } \left\langle E^2(\theta) \right\rangle_\theta = P, \tag{E.3}$$

where $g(\theta) = -Z_x'(\theta)$ for the entrainment stability and $g(\theta) = -\int_\theta^{\theta+\Delta_\psi} Z_x(\phi) d\phi$ for the phase coherence.

We consider an objective function

$$S\{E, \lambda\} = \langle g(\theta) E(\theta) \rangle_\theta + \lambda \left(\left\langle E(\theta)^2 \right\rangle_\theta - P \right), \tag{E.4}$$

where λ is a Lagrange multiplier. Then the extremum conditions are given by

$$\frac{\delta S}{\delta E} = \frac{1}{2\pi} g(\theta) + \frac{\lambda}{\pi} E(\theta) = 0, \tag{E.5}$$

$$\frac{\partial S}{\partial \lambda} = \left\langle E(\theta)^2 \right\rangle_\theta - P = 0. \tag{E.6}$$

The optimal periodic modulation is given by

$$E(\theta) = -\frac{g(\theta)}{2\lambda} \tag{E.7}$$

and the constraint is

$$\frac{1}{4\lambda^2} \left\langle g(\theta)^2 \right\rangle_\theta = P, \tag{E.8}$$

which yields

$$\lambda = -\sqrt{\frac{1}{4P} \left\langle g(\theta)^2 \right\rangle_\theta}, \tag{E.9}$$

where the negative sign should be taken in order that the maximized objective function becomes positive.

Therefore, the optimal periodic modulation is given by

$$E(\theta) = \sqrt{\frac{P}{\left\langle g(\theta)^2 \right\rangle_\theta}} g(\theta). \tag{E.10}$$

From the above result, the optimal waveform for the entrainment stability is given by

$$E(\theta) = -\sqrt{\frac{P}{\left\langle Z_x'(\theta)^2 \right\rangle_\theta}} Z_x'(\theta) \tag{E.11}$$

and that for the phase coherence is given by

$$E(\theta) = -\sqrt{\frac{P}{\left\langle (\int_\theta^{\theta+\Delta_\psi} Z_x(\phi) d\phi)^2 \right\rangle_\theta}} \int_\theta^{\theta+\Delta_\psi} Z_x(\phi) d\phi. \tag{E.12}$$

When the limit cycle is symmetric and the x component Z_x of the PSF has a sinusoidal form, the optimal waveform is also given by a trivial sinusoidal function, because the differential and integral of a sinusoidal function are also sinusoidal.

Appendix F

Asymptotic phase of classical nonlinear oscillators

F.1 Background

In analyzing synchronization properties of limit-cycle oscillators in the deterministic framework, the *asymptotic phase* [1, 2, 4, 7, 3] of the oscillator plays a central role, which is defined by the vector field of the oscillator and increases with a constant frequency in the basin of the limit-cycle attractor. By defining the asymptotic phase, one can approximately reduce the dynamics of a weakly perturbed limit-cycle oscillator to a simple one-dimensional phase equation, which can be analyzed much more easily than the original multidimensional nonlinear dynamical equation. This method, called the *phase reduction* [1, 2, 4, 7, 3], has been successfully used to analyze a large variety of synchronization phenomena in coupled-oscillator systems, including nonlinear wave propagation in self-oscillatory media and collective synchronization in populations of coupled oscillators. The method can be used for limit-cycle oscillators subjected to sufficiently weak noise, and also for quantum nonlinear oscillators in the semiclassical regime described by a quantum Fokker-Planck equation [88, 98].

However, there also exist strongly stochastic oscillatory systems in which the noise plays essentially important roles in generating the oscillatory dynamics. A representative example is the noise-induced oscillations in excitable systems [119]. In this case, the deterministic vector field of the system does not possess a limit-cycle solution, yet approximately regular oscillations are evoked due to continuous excitation of the system by noise. The conventional phase reduction theory cannot be applied to such strongly

stochastic dynamical systems. In particular, we cannot rely on the deterministic limit cycle in defining the asymptotic phase.

To cope with this problem, Schwabedal and Pikovsky [120] introduced a definition of the phase in terms of the mean first return time, and Thomas and Lindner [99] proposed a definition of the asymptotic phase in terms of the slowest decaying eigenfunction of the backward Kolmogorov (Fokker-Planck) operator describing the mean first passage time, both of which yield phase values that increase with a constant frequency on average for stochastic oscillations, in a similar way to the ordinary asymptotic phase for deterministic oscillators.

F.2 Deterministic case

We first explain the asymptotic phase for classical nonlinear oscillators briefly. We consider a deterministic dynamical system $\dot{\boldsymbol{X}} = \boldsymbol{A}(\boldsymbol{X})$ with a state $\boldsymbol{X} \in \mathbb{R}^N$, which has an exponentially stable limit-cycle solution $\boldsymbol{X}_0(t)$ with a natural period T and frequency $\omega = 2\pi/T$. The asymptotic phase function $\Phi(\boldsymbol{X}) : B \subset \mathbb{R}^N \to [0, 2\pi)$ is then defined such that $\nabla\Phi(\boldsymbol{X}) \cdot \boldsymbol{A}(\boldsymbol{X}) = \omega$ is satisfied for all system states $\boldsymbol{X}$ in the basin B of the limit cycle, where $\nabla = \partial/\partial\boldsymbol{X}$ is the gradient with respect to $\boldsymbol{X}$. It then follows that the phase $\phi = \Phi(\boldsymbol{X})$ of the system obeys $\dot{\phi} = \dot{\Phi}(\boldsymbol{X}) = \boldsymbol{A}(\boldsymbol{X}) \cdot \nabla\Phi(\boldsymbol{X}) = \omega$, i.e., ϕ always increases at a constant frequency ω with the evolution of $\boldsymbol{X}$ in B. When the system is weakly perturbed as $\dot{\boldsymbol{X}} = \boldsymbol{A}(\boldsymbol{X}) + \epsilon\boldsymbol{p}(\boldsymbol{X})$ with $0 < \epsilon \ll 1$, the phase approximately obeys $\dot{\phi} = \omega + \epsilon\boldsymbol{Z}(\phi) \cdot \boldsymbol{p}(t)$, where $\boldsymbol{Z}(\phi) = \nabla\Phi(\boldsymbol{X})|_{\boldsymbol{X}=\boldsymbol{X}_0(\phi/\omega)}$ is the gradient of the phase function $\Phi(\boldsymbol{X})$ evaluated at phase ϕ on the limit cycle. The simplicity of this phase equation has facilitated extensive studies on synchronization of coupled-oscillator systems [1, 2, 4, 7, 3].

Here, we point out that the operator $A = \boldsymbol{A}(\boldsymbol{X}) \cdot \nabla$ can be interpreted as an infinitesimal generator of the *Koopman operator* describing evolution of general observables in nonlinear dynamical systems [116, 121, 117, 122]. The Koopman operator U^τ is defined by $(U^\tau g)(\boldsymbol{X}) = g(S^\tau\boldsymbol{X})$, where g is a smooth observable and S^τ is a flow of the system, i.e., $\boldsymbol{X}(t+\tau) = S^\tau\boldsymbol{X}(t)$. Using $S^\tau\boldsymbol{X} = \boldsymbol{X} + \tau\boldsymbol{A}(\boldsymbol{X}) + O(\tau^2)$ and $g(S^\tau\boldsymbol{X}) = g(\boldsymbol{X}) + \tau\boldsymbol{A}(\boldsymbol{X}) \cdot \nabla g(\boldsymbol{X}) + O(\tau^2)$ for small τ, the infinitesimal generator A of U^τ is obtained as

$$\begin{aligned}\frac{d}{dt}g(\boldsymbol{X}) = Ag(\boldsymbol{X}) &= \lim_{\tau\to 0}\frac{U^\tau g(\boldsymbol{X}) - g(\boldsymbol{X})}{\tau} \\ &= \lim_{\tau\to 0}\frac{g(S^\tau\boldsymbol{X}) - g(\boldsymbol{X})}{\tau} = \boldsymbol{A}(\boldsymbol{X}) \cdot \nabla g(\boldsymbol{X}). \end{aligned} \tag{F.1}$$

It can easily be seen from the definition of the asymptotic phase $\Phi(\boldsymbol{X})$ that the exponential $\Psi(\boldsymbol{X}) = e^{i\Phi(\boldsymbol{X})}$ of the phase function $\Phi(\boldsymbol{X})$ gives an eigenfunction of this linear operator A with an eigenvalue $i\omega$, satisfying $A\Psi(\boldsymbol{X}) = i\omega\Psi(\boldsymbol{X})$. Thus, the asymptotic phase function has a natural operator-theoretic interpretation as an argument

$$\Phi(\boldsymbol{X}) = \arg \Psi(\boldsymbol{X}) \tag{F.2}$$

of the eigenfunction $\Psi(\boldsymbol{X})$ of the Koopman operator A [116, 121, 117, 122].

The above definition of the asymptotic phase for deterministic systems is based on the existence of a limit-cycle solution, which is still applicable if the system is subjected to sufficiently weak noise. However, it is no longer valid for strongly stochastic oscillators where the noise plays essential roles.

F.3 Stochastic case

For strongly stochastic oscillators, Thomas and Lindner [99] proposed a definition of the asymptotic phase in terms of the slowest decaying eigenfunction of the backward Fokker-Planck operator, based on the consideration of the mean first passage time. Consider a stochastic system obeying a Fokker-Planck equation (FPE)

$$\frac{\partial}{\partial t}p(\boldsymbol{X},t) = L_{\boldsymbol{X}}p(\boldsymbol{X},t) = \left[-\frac{\partial}{\partial \boldsymbol{X}}\boldsymbol{A}(\boldsymbol{X}) + \frac{1}{2}\frac{\partial^2}{\partial \boldsymbol{X}^2}\boldsymbol{D}(\boldsymbol{X})\right]p(\boldsymbol{X},t), \tag{F.3}$$

where $\boldsymbol{X} \in \mathbb{R}^N$ is the system state, $p(\boldsymbol{X},t)$ is the probability density function of $\boldsymbol{X}$ at time t, $L_{\boldsymbol{X}}$ is a Fokker-Planck operator representing the time evolution of $p(\boldsymbol{X},t)$, $\boldsymbol{A}(\boldsymbol{X}) \in \mathbb{R}^N$ and $\boldsymbol{D}(\boldsymbol{X}) \in \mathbb{R}^{N\times N}$ represent the drift vector and diffusion matrix of the FPE, respectively. The transition probability density $p(\boldsymbol{X},t|\boldsymbol{Y},s)$ satisfying $p(\boldsymbol{X},t) = p(\boldsymbol{X},t|\boldsymbol{Y},s)p(\boldsymbol{Y},s)$ $(t \geq s)$ obeys the forward FPE

$$\frac{\partial}{\partial t}p(\boldsymbol{X},t|\boldsymbol{Y},s) = L_{\boldsymbol{X}}p(\boldsymbol{X},t|\boldsymbol{Y},s). \tag{F.4}$$

The corresponding backward FPE is given by [123]

$$\begin{aligned}\frac{\partial}{\partial s}p(\boldsymbol{X},t|\boldsymbol{Y},s) &= -L^{+}_{\boldsymbol{Y}}p(\boldsymbol{X},t|\boldsymbol{Y},s) \\ &= -\left[\boldsymbol{A}(\boldsymbol{Y})\frac{\partial}{\partial \boldsymbol{Y}} + \frac{1}{2}\boldsymbol{D}(\boldsymbol{Y})\frac{\partial^2}{\partial \boldsymbol{Y}^2}\right]p(\boldsymbol{X},t|\boldsymbol{Y},s),\end{aligned} \tag{F.5}$$

where

$$L_{\boldsymbol{X}}^{+} = \boldsymbol{A}(\boldsymbol{X})\frac{\partial}{\partial \boldsymbol{X}} + \frac{1}{2}\boldsymbol{D}(\boldsymbol{X})\frac{\partial^2}{\partial \boldsymbol{X}^2} \tag{F.6}$$

is the adjoint linear operator of $L_{\boldsymbol{X}}$ with respect to the L^2 inner product $\langle G(\boldsymbol{X}), H(\boldsymbol{X})\rangle_{\boldsymbol{X}} = \int \overline{G(\boldsymbol{X})} H(\boldsymbol{X}) d\boldsymbol{X}$ of two functions $G(\boldsymbol{X}) \in \mathbb{C}$ and $H(\boldsymbol{X}) \in \mathbb{C}$, i.e., $\langle L_{\boldsymbol{X}}^{+} G(\boldsymbol{X}), H(\boldsymbol{X})\rangle_{\boldsymbol{X}} = \langle G(\boldsymbol{X}), L_{\boldsymbol{X}} H(\boldsymbol{X})\rangle_{\boldsymbol{X}}$, with the overline indicating complex conjugate.

The linear differential operators $L_{\boldsymbol{X}}$ and $L_{\boldsymbol{X}}^{+}$ have the eigensystem $\{\lambda_k, P_k, Q_k\}$ of the eigenvalue λ_k, the right eigenfunction $P_k(\boldsymbol{X})$, and the left eigenfunction $Q_k(\boldsymbol{X})$, satisfying

$$L_{\boldsymbol{X}} P_k(\boldsymbol{X}) = \lambda_k P_k(\boldsymbol{X}),\ L_{\boldsymbol{X}}^{+} Q_k(\boldsymbol{X}) = \overline{\lambda_k} Q_k(\boldsymbol{X}),\ \langle Q_k(\boldsymbol{X}), P_l(\boldsymbol{X})\rangle_{\boldsymbol{X}} = \delta_{kl}, \tag{F.7}$$

where $k, l = 0, 1, 2, \ldots$. One of the eigenvalues is $\lambda_0 = 0$ due to the conservation of probability, and all other eigenvalues have negative real parts. Considering that the system exhibits stochastic oscillations, it is assumed that the eigenvalues with the largest non-negative real part (the slowest decay rate) are given by a complex-conjugate pair. These eigenvalues are denoted as $\lambda_1 = \mu + i\omega$ and $\overline{\lambda_1} = \mu - i\omega$, where $\mu < 0$ represents the decay rate and ω represents the fundamental oscillation frequency of the associated eigenfunction.

Thomas and Lindner defined a *stochastic asymptotic phase function* for stochastic oscillators as the argument of the left eigenfunction $\overline{Q_1(\boldsymbol{X})}$ associated with λ_1, i.e., $L_{\boldsymbol{X}}^{+}\overline{Q_1(\boldsymbol{X})} = \lambda_1\ \overline{Q_1(\boldsymbol{X})}$, as

$$\Phi(\boldsymbol{X}) = \arg \overline{Q_1(\boldsymbol{X})}, \tag{F.8}$$

and showed that this $\Phi(\boldsymbol{X})$ gives a phase value that varies with a constant frequency ω with the evolution of $\boldsymbol{X}$ on average. This definition of the asymptotic phase for stochastic oscillations is consistent with the definition of the asymptotic phase in the noiseless limit when the deterministic system described by the vector field $\dot{\boldsymbol{X}} = \boldsymbol{A}(\boldsymbol{X})$ has a limit-cycle solution [99].

Here we additionally point out that the above definition is also natural from the Koopman operator viewpoint. First, in the limit of vanishing noise, we obtain the forward and backward (classical) Liouville equations instead of FPEs, where the forward Liouville operator is given by

$$L_{\boldsymbol{X}} = -\frac{\partial}{\partial \boldsymbol{X}}\boldsymbol{A}(\boldsymbol{X}). \tag{F.9}$$

The corresponding backward Liouville operator is given by

$$L_{\boldsymbol{X}}^{+} = \boldsymbol{A}(\boldsymbol{X}) \cdot \nabla = \boldsymbol{A}(\boldsymbol{X}) \cdot \frac{\partial}{\partial \boldsymbol{X}}, \tag{F.10}$$

which is nothing but the Koopman operator A in the deterministic case. Thus, the eigenfunction $Q_1(\boldsymbol{X})$ of $L_{\boldsymbol{X}}^{+}$ with eigenvalue $\lambda_1 = i\omega$ (note that $\mu \to 0$ in this limit) coincides with the Koopman eigenfunction $\Psi(\boldsymbol{X})$ of A with eigenvalue $i\omega$, and therefore the definition of the asymptotic phase in Eq. (F.8) is equivalent to the definition of the asymptotic phase Eq. (F.2) in the deterministic case.

In the case with finite noise, the (negative of the) backward Fokker-Planck operator $L_{\boldsymbol{X}}^{+}$ can also be considered a Koopman operator of the stochastic system described by the Fokker-Planck operator $L_{\boldsymbol{X}}$. For a smooth observable f, the stochastic Koopman operator is defined by [124]

$$U^{\tau} f(\boldsymbol{X}) = \mathbb{E}[f(S^{\tau}\boldsymbol{X})] = \int p(\boldsymbol{Y}, s+\tau|\boldsymbol{X}, s) f(\boldsymbol{Y}) d\boldsymbol{Y}, \tag{F.11}$$

where $\mathbb{E}[\cdot]$ represents expectation over realizations of S^t and s is the initial time. The infinitesimal generator A of the stochastic Koopman operator U^{τ} is then calculated as

$$\begin{aligned} Af(\boldsymbol{X}) &= \lim_{\tau \to 0} \frac{U^{\tau} f(\boldsymbol{X}) - f(\boldsymbol{X})}{\tau} \\ &= \int \lim_{\tau \to 0} \frac{p(\boldsymbol{Y}, s+\tau|\boldsymbol{X}, s) - p(\boldsymbol{Y}, s|\boldsymbol{X}, s)}{\tau} f(\boldsymbol{Y}) d\boldsymbol{Y} \\ &= \int \left. \frac{\partial p(\boldsymbol{Y}, s+\tau|\boldsymbol{X}, s)}{\partial \tau} \right|_{\tau=0} f(\boldsymbol{Y}) d\boldsymbol{Y} = \int L_{\boldsymbol{Y}} p(\boldsymbol{Y}, s|\boldsymbol{X}, s) f(\boldsymbol{Y}) d\boldsymbol{Y} \\ &= \int p(\boldsymbol{Y}, s|\boldsymbol{X}, s) L_{\boldsymbol{Y}}^{+} f(\boldsymbol{Y}) d\boldsymbol{Y} = L_{\boldsymbol{X}}^{+} f(\boldsymbol{X}), \end{aligned} \tag{F.12}$$

where $L_{\boldsymbol{X}}^{+}$ is the adjoint operator of $L_{\boldsymbol{X}}$ given in Eq. (F.6), namely, the (negative of the) backward Fokker-Planck operator. Thus, the eigenfunction $\overline{Q_1(\boldsymbol{X})}$ of $L_{\boldsymbol{X}}^{+}$ with eigenvalue λ_1 coincides with the Koopman eigenfunction $\Psi(\boldsymbol{X})$ of A with the eigenvalue λ_1 also in this case, and the definition of the asymptotic phase by Eq. (F.8) is a natural extension of the definition for deterministic systems.

We note that the relation between the evolution of the probability density function and the evolution of the observable discussed above is parallel to the relation between Schrödinger and Heisenberg pictures in the main text. The quantum master equation, the adjoint superoperator $\mathcal{L}^*$ (or the adjoint

linear differential operator L^+ in the P-representation), and the eigenoperator V_1 (or the eigenfunction v_1 in the P-representation) with eigenvalue $\overline{\Lambda_1}$ correspond to the forward Fokker-Planck equation, the backward Fokker-Planck operator $L^+_{\boldsymbol{X}}$ (or the Koopman operator A), and the eigenfunction $\overline{Q_1(\boldsymbol{X})}$ (or the Koopman eigenfunction $\Psi(\boldsymbol{X})$) with eigenvalue λ_1 in the classical stochastic system discussed here, respectively. In the main text, the theory is further generalized to other principal eigenvalues $\{\Lambda_j\}_{j\geq 2}$.

Appendix G

Quantum van der Pol oscillator with Kerr effect in the semiclassical regime

In the semiclassical regime, the linear operator L of the partial differential equation $\partial_t p(\boldsymbol{\alpha}) = Lp(\boldsymbol{\alpha})$ in the main text, which describes the evolution of the quasiprobability distribution in the P-representation of the quantum van der Pol oscillator with Kerr effect, is explicitly given by a quantum Fokker-Planck operator

$$L = \Big[-\sum_{j=1}^{2} \partial_j \{A_j(\boldsymbol{\alpha})\} + \frac{1}{2} \sum_{j=1}^{2} \sum_{k=1}^{2} \partial_j \partial_k \{D_{jk}(\boldsymbol{\alpha})\} \Big], \tag{G.1}$$

where $\partial_1 = \partial/\partial\alpha$, $\partial_2 = \partial/\partial\bar{\alpha}$. The drift vector $\boldsymbol{A}(\boldsymbol{\alpha}) = (A_1(\boldsymbol{\alpha}), A_2(\boldsymbol{\alpha})) \in \mathbb{C}^2$ and the matrix $\boldsymbol{D}(\boldsymbol{\alpha}) = (D_{jk}(\boldsymbol{\alpha})) \in \mathbb{C}^{2\times 2}$ are given by

$$\boldsymbol{A}(\boldsymbol{\alpha}) = \begin{pmatrix} \left(\frac{\gamma_1}{2} - i\omega_0\right)\alpha - (\gamma_2 + 2Ki)\overline{\alpha}\alpha^2 \\ \left(\frac{\gamma_1}{2} + i\omega_0\right)\overline{\alpha} - (\gamma_2 - 2Ki)\alpha\overline{\alpha}^2 \end{pmatrix}, \tag{G.2}$$

$$\boldsymbol{D}(\boldsymbol{\alpha}) = \begin{pmatrix} -(\gamma_2 + 2Ki)\alpha^2 & \gamma_1 \\ \gamma_1 & -(\gamma_2 - 2Ki)\bar{\alpha}^2 \end{pmatrix}. \tag{G.3}$$

The corresponding stochastic differential equation is then given by

$$d\begin{pmatrix} \alpha \\ \overline{\alpha} \end{pmatrix} = \begin{pmatrix} \left(\frac{\gamma_1}{2} - i\omega_0\right)\alpha - (\gamma_2 + 2Ki)\overline{\alpha}\alpha^2 \\ \left(\frac{\gamma_1}{2} + i\omega_0\right)\overline{\alpha} - (\gamma_2 - 2Ki)\alpha\overline{\alpha}^2 \end{pmatrix} dt + \boldsymbol{\beta}(\boldsymbol{\alpha}) \begin{pmatrix} dW_1 \\ dW_2 \end{pmatrix}, \tag{G.4}$$

where W_1 and W_2 are independent Wiener processes and the matrix $\boldsymbol{\beta}(\boldsymbol{\alpha})$ is given by

$$\boldsymbol{\beta}(\boldsymbol{\alpha}) = \begin{pmatrix} \sqrt{\frac{(\gamma_1+R_{11}(\boldsymbol{\alpha}))}{2}}e^{i\chi(\boldsymbol{\alpha})/2} & -i\sqrt{\frac{(\gamma_1-R_{11}(\boldsymbol{\alpha}))}{2}}e^{i\chi(\boldsymbol{\alpha})/2} \\ \sqrt{\frac{(\gamma_1+R_{11}(\boldsymbol{\alpha}))}{2}}e^{-i\chi(\boldsymbol{\alpha})/2} & i\sqrt{\frac{(\gamma_1-R_{11}(\boldsymbol{\alpha}))}{2}}e^{-i\chi(\boldsymbol{\alpha})/2} \end{pmatrix}, \tag{G.5}$$

where $R_{11}(\boldsymbol{\alpha})e^{i\chi(\boldsymbol{\alpha})} = -(\gamma_2 + 2Ki)\alpha^2$.

In the classical limit, the deterministic part of Eq. (G.4) gives the Stuart-Landau equation (normal form of the supercritical Hopf bifurcation) [2] for the complex variable α in the main text, which can also be expressed by using a real vector $\boldsymbol{X} = (x, p) = (\mathrm{Re}\ \alpha, \mathrm{Im}\ \alpha)$ as

$$\begin{pmatrix} \dot{x} \\ \dot{p} \end{pmatrix} = \begin{pmatrix} \frac{\gamma_1}{2}x + \omega_0 p - (x^2+p^2)(\gamma_2 x - 2Kp) \\ -\omega_0 x + \frac{\gamma_1}{2}p - (x^2+p^2)(2Kx + \gamma_2 p) \end{pmatrix}. \tag{G.6}$$

This equation is analytically solvable and the asymptotic phase function $\Phi_C(x, p)$ can be explicitly obtained as given in the main text [7]. From the discussion in Sec. I of this Supplemental Material, this $\Phi_C(x, p)$ can be expressed as the argument of the Koopman operator $\Psi(\boldsymbol{X})$ with the eigenvalue $i\Omega_C$ of this dynamical system.

Appendix H

Classical limit of the Quantum asymptotic phase function

We here explain that the definition of the quantum asymptotic phase given in the main text reproduces the deterministic asymptotic phase in the classical limit in general. The linear operator L of the partial differential equation $\partial_t p(\boldsymbol{\alpha}) = Lp(\boldsymbol{\alpha})$ in the main text, describing the quasiprobability distribution $p(\boldsymbol{\alpha})$ in the P-representation, can be approximated by a Fokker-Planck operator of the form Eq. (G.1) in the semiclassical regime. By introducing a real vector $\boldsymbol{X} = (\mathrm{Re}\ \alpha, \mathrm{Im}\ \alpha)$ and the corresponding distribution function $p(\boldsymbol{X})$, the Fokker-Planck operator L for $p(\boldsymbol{\alpha})$ can be cast into a real Fokker-Planck operator $L_{\boldsymbol{X}}$ for $p(\boldsymbol{X})$ given by Eq. (F.3). From the corresponding backward Fokker-Planck operator $L^+_{\boldsymbol{X}}$ in Eq. (F.6), we obtain the quantum asymptotic phase function as the argument of the eigenfunction of $L^+_{\boldsymbol{X}}$ associated with the eigenvalue $\Lambda_1 = -\mu + i\Omega$ with the slowest decay rate μ and the fundamental frequency Ω. Now, in the classical limit, the diffusion operator in the Fokker-Planck operator $L_{\boldsymbol{X}}$ asymptotically vanishes and $L_{\boldsymbol{X}}$ converges to a classical Liouville operator given by Eq. (F.9). Also, the decay rate μ converges to 0 and the eigenvalue Λ_1 approaches $i\Omega$. Thus, from the corresponding backward Liouville operator (or the deterministic Koopman operator) $L^+_{\boldsymbol{X}}$ given by Eq. (F.10), we obtain the classical asymptotic phase function Φ_1 in the deterministic limit as the argument of the eigenfunction Ψ_1 associated with $\Lambda_1 = i\Omega$. Thus, the quantum asymptotic phase function defined in the main text reproduces the deterministic asymptotic phase function in the classical limit without quantum noise.

Appendix I

Asymptotic phase functions in the strong quantum regime

Figure I.1 shows the asymptotic phase function Φ_j given by the argument of the eigenoperator V_j with the principal eigenvalue Λ_j, $\Phi_j(\boldsymbol{\alpha}) = \arg\langle\alpha|V_j|\alpha\rangle$, for $j = 1, 2, 3$ and 4 on the ($x = \mathrm{Re}\ \alpha, p = \mathrm{Im}\ \alpha$) plane. The parameters are the same as in Fig. 4.1(d)-(f) in the main text. These asymptotic phase functions look similar to each other, but they are associated with different fundamental frequencies and also they are slightly different from each other near the origin. Thus, they capture different oscillation modes of the system as demonstrated in the main text.

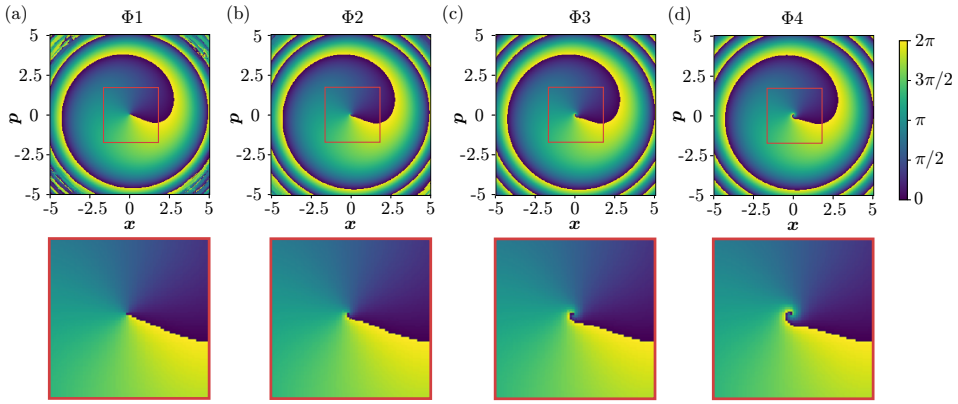

Figure I.1: Asymptotic phase functions of the quantum van der Pol oscillator with Kerr effect in the strong quantum regime. (a): Φ_1, (b): Φ_2, (c): Φ_3, (d): Φ_4. The parameters are $\gamma_1 = 0.1$ and $(\omega_0, \gamma_2, K)/\gamma_1 = (300, 4, 100)$. Figures in the bottom panel show enlargements of the regions near the origin in the corresponding figures in the top panel. In all figures, $(x, p) = (2.5, 0)$ is chosen as the phase origin, $\Phi_j = 0$ $(j = 1, 2, 3, 4)$.

Appendix J

Asymptotic phase function for a damped harmonic oscillator

We here consider a simple damped harmonic oscillator and formally calculate the quantum asymptotic phase. Though this system is completely linear and does not exhibit synchronization phenomena in the classical sense, the eigenoperator V_1 of the adjoint Liouville operator can be analytically obtained and we can gain physical intuition on the definition of the asymptotic phase function. In Ref. [125], Thomas and Lindner considered the stochastic asymptotic phase for a classical linear damped harmonic oscillator described by a multi-dimensional Ornstein-Uhlenbeck process, and the following result can be considered a quantum-mechanical version of their result.

The time evolution of a damped harmonic oscillator is given by a master equation

$$\dot{\rho} = \mathcal{L}\rho = -i[-\omega a^\dagger a, \rho] + \gamma \mathcal{D}[a]\rho, \tag{J.1}$$

where $\omega > 0$ is the natural frequency of the system, γ denotes the decay rate for the linear damping, and $\mathcal{D}$ is the Lindblad form as defined in the main text [80]. The eigenoperator associated with the slowest non-vanishing decay rate of the adjoint Liouville superoperator $\mathcal{L}^*$ of $\mathcal{L}$ is simply given by $V_1 = a$, i.e., $\mathcal{L}^* a = \overline{\Lambda_1} a$, where $\overline{\Lambda_1} = -\gamma/2 + i\omega$ [126, 127]. Therefore, the asymptotic phase function is obtained as

$$\arg\langle\alpha|a|\alpha\rangle = \arg\alpha = \arg\left(re^{i\theta}\right) = \theta, \tag{J.2}$$

where $\alpha = re^{i\theta}$. Thus, the asymptotic phase simply gives the geometric angle on the phase plane of the P representation. For the initial condition $\rho = |\alpha_0\rangle\langle\alpha_0|$ with $\alpha_0 = r_0 e^{i\theta_0}$, it is easy to show that the expectation of a is given by

$$\langle a\rangle(t) = \mathrm{Tr}\,[a\rho(t)] = \langle\alpha_0|a(t)|\alpha_0\rangle = e^{\overline{\Lambda_1}t}\langle\alpha_0|a(0)|\alpha_0\rangle = e^{(-\gamma/2+i\omega)t}\alpha_0. \tag{J.3}$$

If we take the phase origin on the positive x axis, the angle θ is given by

$$\theta = \arg e^{(-\gamma/2+i\omega)t}\alpha_0 = \omega t + \theta_0, \tag{J.4}$$

which increases with a constant frequency ω.

Appendix K

Feedback policy

In this section, we discuss the feedback policy for suppressing the fluctuations around the phase-locking point inevitably caused by the measurement backaction. We consider the system described by Eq. (5.1) without the linear coupling to the bath, i.e. $\gamma_3 = 0$. The phase equation for the oscillator in the classical limit is given by (see also the next section) [54, 88]

$$\frac{d\phi}{dt} = \left(\Delta + \Delta_{fb} + \sqrt{\frac{2\gamma_2}{\gamma_1}} E \sin\phi \right). \tag{K.1}$$

If $|\Delta + \Delta_{fb}| \leq \sqrt{\frac{2\gamma_2}{\gamma_1}} E$, there exists a stable fixed point of Eq. (K.1), which corresponds to the phase-locking point of the system with the driving signal under the feedback control, satisfying $\phi_{fb} = -\arcsin\left(\frac{\Delta + \Delta_{fb}}{E} \sqrt{\frac{\gamma_1}{2\gamma_2}} \right)$. The fixed point in the absence of the feedback control, i.e. $\Delta_{fb} = 0$, is given by $\phi_0 = -\arcsin\left(\frac{\Delta}{E} \sqrt{\frac{\gamma_1}{2\gamma_2}} \right)$.

Figure K.1 shows a schematic diagram of the feedback policy for suppressing the fluctuations around the phase-locking point. As seen in Fig. K.1, when $\theta_{est} > \theta_0$, the feedback control is $\Delta_{fb} = -K_{fb}(\theta_{est} - \theta_0) < 0$ and thus $\phi_{fb} < \phi_0$. Similarly, when $\theta_{est} < \theta_0$, we obtain $\phi_{fb} > \phi_0$. Therefore, the feedback control shifts the locking phase from ϕ_0 to ϕ_{fb}, which is opposite to the direction from θ_0 to θ_{est}. Thus, the feedback control is expected to suppress the fluctuations around the phase-locking point.

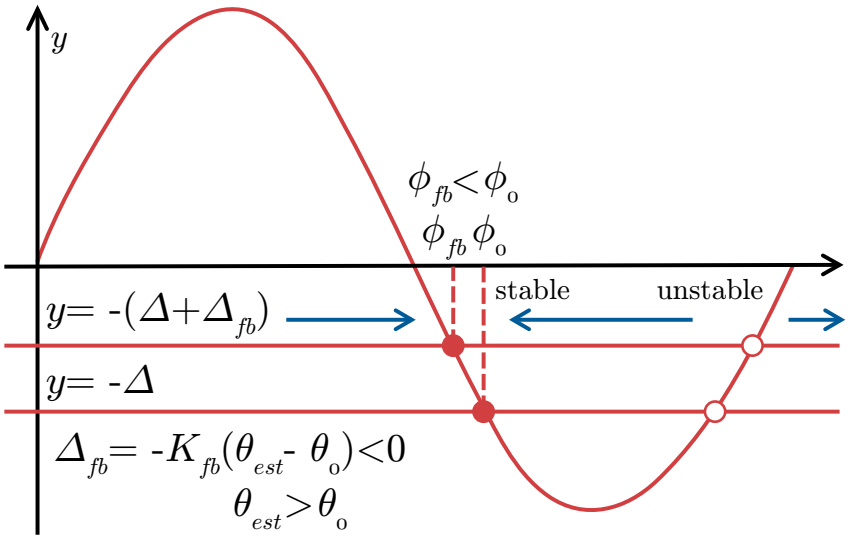

Figure K.1: Schematic diagram of the feedback policy for suppressing the fluctuations around the phase-locking point. Feedback control shifts the phase-locking point from ϕ_0 to ϕ_{fb} that is opposite to the direction from θ_0 to θ_{est}.

Appendix L

Relation between the phase diffusion and purity

In this section, we discuss the relation between the phase diffusion and purity of the quantum vdP oscillator when the measurement is absent. We consider the system described by Eq. (5.1) without the linear coupling to the bath, i.e. $\gamma_3 = 0$.

We assume that the system is in the semiclassical regime and driven by the weak perturbation, and can be approximately described by a stochastic differential equation of the phase variable of the oscillator by using the semiclassical phase reduction theory [88].

We introduce rescaled parameters $\gamma_2 = \sigma\gamma_1{\gamma_2}', \Delta + \Delta_{fb} = \gamma_1(\Delta' + \Delta'_{fb}), E = \epsilon\gamma_1 E'/\sqrt{\sigma}, dt' = \gamma_1 dt, dW' = \sqrt{\gamma_1}dW$ with dimensionless parameters ${\gamma_2}'$, Δ', Δ'_{fb}, and E' of $\mathcal{O}(1)$. We set $0 < \sigma \ll 1$ (the system is in the semiclassical regime) and $0 < \epsilon \ll 1$ (the perturbation is weak). The corresponding semiclassical phase equation for the quantum system in Eq. (5.1) is then obtained as [88] $d\phi = \left(\Delta' + \Delta'_{fb} + \epsilon\sqrt{2\gamma'_2}E'\sin\phi\right)dt' + \sqrt{\sigma D_0}dW'$, with $D_0 = \frac{3\gamma'_2}{2}$.

We first evaluate the phase diffusion of the oscillator. It is given by the effective diffusion constant [128]

$$D_{eff} \propto 1/(\langle\exp(v(\phi)/(\sigma D_0))\rangle_\phi \langle\exp(-v(\phi)/(\sigma D_0))\rangle_\phi),$$

where the potential is given by $v(\phi) = -\int_{\phi_0}^{\phi}(\Delta' + \Delta'_{fb} + \epsilon\sqrt{2\gamma'_2}E'\sin\phi')d\phi'$ with a reference phase point ϕ_0 and $\langle\cdot\rangle_\phi = \frac{1}{2\pi}\int_0^{2\pi}(\cdot)d\phi$. When σ is sufficiently small, using saddle-point approximation, $\langle\exp(v(\phi)/(\sigma D_0))\rangle_\phi \propto \exp(v_{max}/(\sigma D_0))$ and $\langle\exp(-v(\phi)/(\sigma D_0))\rangle_\phi \propto \exp(-v_{min}/(\sigma D_0))$, which

leads to

$$D_{eff} \propto \frac{1}{\exp((v_{max} - v_{min})/(\sigma D_0))}, \tag{L.1}$$

where v_{max} and v_{min} are the maximum and minimum values of the potential $v(\phi)$, respectively (See [18] for details).

Next, we evaluate the purity. In the semiclassical phase reduction theory [88], the density matrix can be approximately reconstructed from the phase equation as $\rho \approx \int_0^{2\pi} d\phi P(\phi) \left|\alpha_0(\phi)\right\rangle \left\langle\alpha_0(\phi)\right|$, where $\alpha_0(\phi) = \sqrt{\frac{1}{2\sigma\gamma_2'}} \exp(i\phi)$ is the system state at ϕ on the classical limit cycle in the phase space of the P representation [81] and $P(\phi)$ is the steady-state probability distribution of the Fokker-Planck equation for the phase variable [4], given by $P(\phi) \propto \int_0^{2\pi} d\phi' \exp\left[\frac{2(v(\phi'+\phi)-v(\phi))}{D_0\sigma}\right]$. Since the size of the limit cycle is $O(1/\sqrt{\sigma})$, i.e. $\alpha_0(\phi) = O(1/\sqrt{\sigma})$, the purity in the weak noise limit can be approximately evaluated as

$$\begin{aligned}
P = \mathrm{Tr}\,(\rho^2) &\approx \int_0^{2\pi}\int_0^{2\pi} d\phi d\phi' P(\phi)P(\phi') \exp(-|\alpha_0(\phi) - \alpha_0(\phi')|^2) \\
&\propto \int_0^{2\pi} d\phi P^2(\phi) \propto \int_0^{2\pi} d\phi \left(\int_0^{2\pi} d\phi' \exp\left[\frac{2(v(\phi'+\phi) - v(\phi))}{D_0\sigma}\right]\right)^2 \\
&\propto \int_0^{2\pi} d\phi \left(\exp\left[\frac{2(v_{max} - v(\phi))}{D_0\sigma}\right]\right)^2 \propto \exp\left[\frac{4(v_{max} - v_{min})}{D_0\sigma}\right].
\end{aligned}$$

Thus, introducing a constant of proportionality C, the effective diffusion constant D_{eff} in the weak noise limit can be approximately represented as

$$D_{eff} \approx \frac{C}{(P)^{1/4}}, \tag{L.2}$$

which indicates that higher purity leads to smaller phase diffusion of the oscillator.

Bibliography

[1] A. T Winfree. *The geometry of biological time*. Springer, New York, 2001.

[2] Y Kuramoto. *Chemical oscillations, waves, and turbulence*. Springer, Berlin, 1984.

[3] G. B Ermentrout and D. H Terman. *Mathematical foundations of neuroscience*. Springer, New York, 2010.

[4] A Pikovsky, M Rosenblum, and J Kurths. *Synchronization: a universal concept in nonlinear sciences*. Cambridge University Press, Cambridge, 2001.

[5] L Glass and M. C Mackey. *From clocks to chaos: the rhythms of life*. Princeton University Press, Princeton, 1988.

[6] S Strogatz. *Nonlinear dynamics and chaos*. Westview Press, 1994.

[7] H Nakao. Phase reduction approach to synchronisation of nonlinear oscillators. *Contemporary Physics*, 57(2):188–214, 2016.

[8] B Ermentrout. Type i membranes, phase resetting curves, and synchrony. *Neural computation*, 8(5):979–1001, 1996.

[9] E Brown, J Moehlis, and P Holmes. On the phase reduction and response dynamics of neural oscillator populations. *Neural computation*, 16(4):673–715, 2004.

[10] S. H Strogatz, D. M Abrams, A McRobie, B Eckhardt, and E Ott. Crowd synchrony on the millennium bridge. *Nature*, 438(7064):43–44, 2005.

[11] B Monga, D Wilson, T Matchen, and J Moehlis. Phase reduction and phase-based optimal control for biological systems: a tutorial. *Biological Cybernetics*, 113(1-2):11–46, 2019.

[12] J Moehlis, E Shea-Brown, and H Rabitz. Optimal inputs for phase models of spiking neurons. *Journal of Computational and Nonlinear Dynamics*, 1(4):358–367, 2006.

[13] A Zlotnik and J.-S Li. Optimal entrainment of neural oscillator ensembles. *Journal of Neural Engineering*, 9(4):046015, 2012.

[14] T Harada, H.-A Tanaka, M. J Hankins, and I. Z Kiss. Optimal waveform for the entrainment of a weakly forced oscillator. *Physical Review Letters*, 105(8):088301, 2010.

[15] A Zlotnik, Y Chen, I. Z Kiss, H.-A Tanaka, and J.-S Li. Optimal waveform for fast entrainment of weakly forced nonlinear oscillators. *Physical Review Letters*, 111(2):024102, 2013.

[16] S Shirasaka, N Watanabe, Y Kawamura, and H Nakao. Optimizing stability of mutual synchronization between a pair of limit-cycle oscillators with weak cross coupling. *Physical Review E*, 96(1):012223, 2017.

[17] N Watanabe, Y Kato, S Shirasaka, and H Nakao. Optimization of linear and nonlinear interaction schemes for stable synchronization of weakly coupled limit-cycle oscillators. *Physical Review E*, 100:042205, Oct 2019.

[18] A Pikovsky. Maximizing coherence of oscillations by external locking. *Physical Review Letters*, 115(7):070602, 2015.

[19] A Zlotnik, R Nagao, I. Z Kiss, and J.-S Li. Phase-selective entrainment of nonlinear oscillator ensembles. *Nature Communications*, 7:10788, 2016.

[20] R Adler. A study of locking phenomena in oscillators. *Proceedings of the IRE*, 34(6):351–357, 1946.

[21] K Kurokawa. Injection locking of microwave solid-state oscillators. *Proceedings of the IEEE*, 61(10):1386–1410, 1973.

[22] W. M Macek and D Davis Jr. Rotation rate sensing with traveling-wave ring lasers. *Applied Physics Letters*, 2(3):67–68, 1963.

[23] J Cresser, W Louisell, P Meystre, W Schleich, and M Scully. Quantum noise in ring-laser gyros. i. theoretical formulation of problem. *Physical Review A*, 25(4):2214, 1982.

[24] J Cresser, D Hammonds, W Louisell, P Meystre, and H Risken. Quantum noise in ring-laser gyros. ii. numerical results. *Physical Review A*, 25(4):2226, 1982.

[25] J Cresser. Quantum noise in ring-laser gyros. iii. approximate analytic results in unlocked region. *Physical Review A*, 26(1):398, 1982.

[26] B. D Josephson. Possible new effects in superconductive tunnelling. *Physics Letters*, 1(7):251–253, 1962.

[27] S Shapiro. Josephson currents in superconducting tunneling: The effect of microwaves and other observations. *Physical Review Letters*, 11(2):80, 1963.

[28] R. E Best. *Phase-locked loops: theory, design, and applications*. McGraw-Hill, New York, 1984.

[29] P. A Tass. Desynchronizing double-pulse phase resetting and application to deep brain stimulation. *Biological Cybernetics*, 85(5):343–354, 2001.

[30] W Eccles and J Vincent. British patent spec. clxiii. 1920.

[31] E. V Appleton. Automatic synchronization of triode oscillators. In *Proc. Cambridge Phil. Soc*, volume 21, page 231, 1922.

[32] B Van Der Pol. Vii. forced oscillations in a circuit with non-linear resistance.(reception with reactive triode). *The London, Edinburgh, and Dublin Philosophical Magazine and Journal of Science*, 3(13):65–80, 1927.

[33] B V. d Pol and J Van Der Mark. Frequency demultiplication. *Nature*, 120(3019):363–364, 1927.

[34] A. T Winfree. Biological rhythms and the behavior of populations of coupled oscillators. *Journal of theoretical biology*, 16(1):15–42, 1967.

[35] Y Kuramoto. Self-entrainment of a population of coupled non-linear oscillators. In *International symposium on mathematical problems in theoretical physics*, pages 420–422. Springer, 1975.

[36] S Shim, M Imboden, and P Mohanty. Synchronized oscillation in coupled nanomechanical oscillators. *Science*, 316(5821):95–99, 2007.

[37] M Zhang, G. S Wiederhecker, S Manipatruni, A Barnard, P McEuen, and M Lipson. Synchronization of micromechanical oscillators using light. *Physical Review Letters*, 109(23):233906, 2012.

[38] M Zhang, S Shah, J Cardenas, and M Lipson. Synchronization and phase noise reduction in micromechanical oscillator arrays coupled through light. *Physical Review Letters*, 115(16):163902, 2015.

[39] M Bagheri, M Poot, L Fan, F Marquardt, and H. X Tang. Photonic cavity synchronization of nanomechanical oscillators. *Physical Review Letters*, 111(21):213902, 2013.

[40] M. H Matheny, M Grau, L. G Villanueva, R. B Karabalin, M Cross, and M. L Roukes. Phase synchronization of two anharmonic nanomechanical oscillators. *Physical Review Letters*, 112(1):014101, 2014.

[41] M. H Matheny, J Emenheiser, W Fon, A Chapman, A Salova, M Rohden, J Li, M. H d Badyn, M Pósfai, L Duenas-Osorio, et al. Exotic states in a simple network of nanoelectromechanical oscillators. *Science*, 363(6431):eaav7932, 2019.

[42] M Ludwig and F Marquardt. Quantum many-body dynamics in optomechanical arrays. *Physical Review Letters*, 111(7):073603, 2013.

[43] T Weiss, A Kronwald, and F Marquardt. Noise-induced transitions in optomechanical synchronization. *New Journal of Physics*, 18(1):013043, 2016.

[44] E Amitai, N Lörch, A Nunnenkamp, S Walter, and C Bruder. Synchronization of an optomechanical system to an external drive. *Physical Review A*, 95(5):053858, 2017.

[45] M Xu, D. A Tieri, E Fine, J. K Thompson, and M. J Holland. Synchronization of two ensembles of atoms. *Physical Review Letters*, 113(15):154101, 2014.

[46] M Xu and M Holland. Conditional ramsey spectroscopy with synchronized atoms. *Physical Review Letters*, 114(10):103601, 2015.

[47] T. E Lee and H Sadeghpour. Quantum synchronization of quantum van der pol oscillators with trapped ions. *Physical Review Letters*, 111(23):234101, 2013.

[48] T. E Lee, C.-K Chan, and S Wang. Entanglement tongue and quantum synchronization of disordered oscillators. *Physical Review E*, 89(2):022913, 2014.

[49] M. R Hush, W Li, S Genway, I Lesanovsky, and A. D Armour. Spin correlations as a probe of quantum synchronization in trapped-ion phonon lasers. *Physical Review A*, 91(6):061401, 2015.

[50] A Roulet and C Bruder. Synchronizing the smallest possible system. *Physical Review Letters*, 121(6):053601, 2018.

[51] A Roulet and C Bruder. Quantum synchronization and entanglement generation. *Physical Review Letters*, 121(6):063601, 2018.

[52] M Koppenhöfer and A Roulet. Optimal synchronization deep in the quantum regime: Resource and fundamental limit. *Physical Review A*, 99(4):043804, 2019.

[53] S. E Nigg. Observing quantum synchronization blockade in circuit quantum electrodynamics. *Physical Review A*, 97(1):013811, 2018.

[54] S Walter, A Nunnenkamp, and C Bruder. Quantum synchronization of a driven self-sustained oscillator. *Physical Review Letters*, 112(9):094102, 2014.

[55] S Sonar, M Hajdušek, M Mukherjee, R Fazio, V Vedral, S Vinjanampathy, and L.-C Kwek. Squeezing enhances quantum synchronization. *Physical Review Letters*, 120(16):163601, 2018.

[56] S Walter, A Nunnenkamp, and C Bruder. Quantum synchronization of two van der pol oscillators. *Annalen der Physik*, 527(1-2):131–138, 2015.

[57] N Lörch, E Amitai, A Nunnenkamp, and C Bruder. Genuine quantum signatures in synchronization of anharmonic self-oscillators. *Physical Review Letters*, 117(7):073601, 2016.

[58] K Ishibashi and R Kanamoto. Oscillation collapse in coupled quantum van der pol oscillators. *Physical Review E*, 96(5):052210, 2017.

[59] E Amitai, M Koppenhöfer, N Lörch, and C Bruder. Quantum effects in amplitude death of coupled anharmonic self-oscillators. *Physical Review E*, 97(5):052203, 2018.

[60] C Navarrete-Benlloch, T Weiss, S Walter, and G. J d Valcárcel. General linearized theory of quantum fluctuations around arbitrary limit cycles. *Physical Review Letters*, 119(13):133601, 2017.

[61] T Weiss, S Walter, and F Marquardt. Quantum-coherent phase oscillations in synchronization. *Physical Review A*, 95(4):041802, 2017.

[62] A Hriscu and Y. V Nazarov. Quantum synchronization of conjugated variables in a superconducting device leads to the fundamental resistance quantization. *Physical Review Letters*, 110(9):097002, 2013.

[63] R Hamerly and H Mabuchi. Optical devices based on limit cycles and amplification in semiconductor optical cavities. *Physical Review Applied*, 4(2):024016, 2015.

[64] T. E Lee and M Cross. Quantum-classical transition of correlations of two coupled cavities. *Physical Review A*, 88(1):013834, 2013.

[65] A Mari, A Farace, N Didier, V Giovannetti, and R Fazio. Measures of quantum synchronization in continuous variable systems. *Physical Review Letters*, 111(10):103605, 2013.

[66] V Ameri, M Eghbali-Arani, A Mari, A Farace, F Kheirandish, V Giovannetti, and R Fazio. Mutual information as an order parameter for quantum synchronization. *Physical Review A*, 91(1):012301, 2015.

[67] D Witthaut, S Wimberger, R Burioni, and M Timme. Classical synchronization indicates persistent entanglement in isolated quantum systems. *Nature Communications*, 8:14829, 2017.

[68] C Davis-Tilley, C Teoh, and A Armour. Dynamics of many-body quantum synchronisation. *New Journal of Physics*, 20(11):113002, 2018.

[69] N Lörch, S. E Nigg, A Nunnenkamp, R. P Tiwari, and C Bruder. Quantum synchronization blockade: Energy quantization hinders synchronization of identical oscillators. *Physical Review Letters*, 118(24):243602, 2017.

[70] I. H d Mendoza, L. A Pachón, J Gómez-Gardenes, and D Zueco. Synchronization in a semiclassical kuramoto model. *Physical Review E*, 90(5):052904, 2014.

[71] K Kotani, I Yamaguchi, Y Ogawa, Y Jimbo, H Nakao, and G. B Ermentrout. Adjoint method provides phase response functions for delay-induced oscillations. *Physical Review Letters*, 109(4):044101, 2012.

[72] V Novičenko and K Pyragas. Phase reduction of weakly perturbed limit cycle oscillations in time-delay systems. *Physica D: Nonlinear Phenomena*, 241(12):1090–1098, 2012.

[73] S Shirasaka, W Kurebayashi, and H Nakao. Phase reduction theory for hybrid nonlinear oscillators. *Physical Review E*, 95(1):012212, 2017.

[74] H Nakao, S Yasui, M Ota, K Arai, and Y Kawamura. Phase reduction and synchronization of a network of coupled dynamical elements exhibiting collective oscillations. *Chaos: An Interdisciplinary Journal of Nonlinear Science*, 28(4):045103, 2018.

[75] Y Kawamura and H Nakao. Collective phase description of oscillatory convection. *Chaos: An Interdisciplinary Journal of Nonlinear Science*, 23(4):043129, 2013.

[76] H Nakao, T Yanagita, and Y Kawamura. Phase-reduction approach to synchronization of spatiotemporal rhythms in reaction-diffusion systems. *Physical Review X*, 4(2):021032, 2014.

[77] S Kaka, M. R Pufall, W. H Rippard, T. J Silva, S. E Russek, and J. A Katine. Mutual phase-locking of microwave spin torque nano-oscillators. *Nature*, 437(7057):389, 2005.

[78] J. M Weiner, K. C Cox, J. G Bohnet, and J. K Thompson. Phase synchronization inside a superradiant laser. *Physical Review A*, 95(3):033808, 2017.

[79] H Heimonen, L. C Kwek, R Kaiser, and G Labeyrie. Synchronization of a self-sustained cold-atom oscillator. *Physical Review A*, 97(4):043406, 2018.

[80] H. J Carmichael. *Statistical Methods in Quantum Optics 1, 2*. Springer, New York, 2007.

[81] C. W Gardiner. *Quantum Noise*. Springer, New York, 1991.

[82] Ö Suvak and A Demir. Quadratic approximations for the isochrons of oscillators: a general theory, advanced numerical methods, and accurate phase computations. *IEEE Transactions on Computer-Aided Design of Integrated Circuits and Systems*, 29(8):1215–1228, 2010.

[83] D Takeshita and R Feres. Higher order approximation of isochrons. *Nonlinearity*, 23(6):1303, 2010.

[84] M. A Nielsen and I. L Chuang. *Quantum Computation and Quantum Information*. Cambridge University Press, 2000.

[85] J Johansson, P Nation, and F Nori. Qutip: An open-source python framework for the dynamics of open quantum systems. *Computer Physics Communications*, 183(8):1760–1772, 2012.

[86] J Johansson, P Nation, and F Nori. Qutip 2: A python framework for the dynamics of open quantum systems. *Computer Physics Communications*, 184:1234–1240, 2013.

[87] B Monga, G Froyland, and J Moehlis. Synchronizing and desynchronizing neural populations through phase distribution control. In *2018 Annual American Control Conference (ACC)*, pages 2808–2813. IEEE, 2018.

[88] Y Kato, N Yamamoto, and H Nakao. Semiclassical phase reduction theory for quantum synchronization. *Phys. Rev. Research*, 1:033012, Oct 2019.

[89] S Strogatz. *Sync: The emerging science of spontaneous order*. Penguin UK, 2004.

[90] G. B Ermentrout and J Rinzel. Beyond a pacemaker's entrainment limit: phase walk-through. *American Journal of Physiology-Regulatory, Integrative and Comparative Physiology*, 246(1):R102–R106, 1984.

[91] A. E Motter, S. A Myers, M Anghel, and T Nishikawa. Spontaneous synchrony in power-grid networks. *Nature Physics*, 9(3):191, 2013.

[92] F Dörfler, M Chertkov, and F Bullo. Synchronization in complex oscillator networks and smart grids. *Proceedings of the National Academy of Sciences*, 110(6):2005–2010, 2013.

[93] D Bures. An extension of kakutani's theorem on infinite product measures to the tensor product of semifinite w*-algebras. *Transactions of the American Mathematical Society*, 135:199–212, 1969.

[94] K. J Åström and T Hägglund. *PID controllers: theory, design, and tuning*, volume 2. Instrument society of America Research Triangle Park, NC, 1995.

[95] S Kreinberg, X Porte, D Schicke, B Lingnau, C Schneider, S Höfling, I Kanter, K Lüdge, and S Reitzenstein. Mutual coupling and synchronization of optically coupled quantum-dot micropillar lasers at ultra-low light levels. *Nature communications*, 10(1):1539, 2019.

[96] H Singh, S Bhuktare, A Bose, A Fukushima, K Yakushiji, S Yuasa, H Kubota, and A. A Tulapurkar. Mutual synchronization of spin-torque nano-oscillators via oersted magnetic fields created by waveguides. *Physical Review Applied*, 11(5):054028, 2019.

[97] M Colombano, G Arregui, N Capuj, A Pitanti, J Maire, A Griol, B Garrido, A Martinez, C Sotomayor-Torres, and D Navarro-Urrios. Synchronization of optomechanical nanobeams by mechanical interaction. *Physical Review Letters*, 123(1):017402, 2019.

[98] Y Kato and H Nakao. Semiclassical optimization of entrainment stability and phase coherence in weakly forced quantum limit-cycle oscillators. *Physical Review E*, 101(1):012210, 2020.

[99] P. J Thomas and B Lindner. Asymptotic phase for stochastic oscillators. *Physical Review Letters*, 113(25):254101, 2014.

[100] A. C Li, F Petruccione, and J Koch. Perturbative approach to markovian open quantum systems. *Scientific reports*, 4:4887, 2014.

[101] K. E Cahill and R. J Glauber. Density operators and quasiprobability distributions. *Physical Review*, 177(5):1882, 1969.

[102] P Grindrod and E. L Patel. Phase locking to the n-torus. *IMA Journal of Applied Mathematics*, 81(1):152–164, 2016.

[103] J v Neumann. *Mathematical Foundations of Quantum Mechanics*. Springer, 1932.

[104] V. P Belavkin. Quantum stochastic calculus and quantum nonlinear filtering. *Journal of Multivariate analysis*, 42(2):171–201, 1992.

[105] H. M Wiseman and G. J Milburn. *Quantum measurement and control*. Cambridge University Press, 2009.

[106] K Jacobs. Feedback control using only quantum back-action. *New Journal of Physics*, 12(4):043005, 2010.

[107] Y Kato and N Yamamoto. Structure identification and state initialization of spin networks with limited access. *New Journal of Physics*, 16(2):023024, 2014.

[108] M Gu, A Parkins, and H Carmichael. Entangled-state cycles from conditional quantum evolution. *Physical Review A*, 73(4):043813, 2006.

[109] T Bhattacharya, S Habib, and K Jacobs. Continuous quantum measurement and the emergence of classical chaos. *Physical Review Letters*, 85(23):4852, 2000.

[110] A Scott and G. J Milburn. Quantum nonlinear dynamics of continuously measured systems. *Physical Review A*, 63(4):042101, 2001.

[111] J. K Eastman, S. S Szigeti, J. J Hope, and A. R Carvalho. Controlling chaos in the quantum regime using adaptive measurements. *Physical Review A*, 99(1):012111, 2019.

[112] M Hatridge, S Shankar, M Mirrahimi, F Schackert, K Geerlings, T Brecht, K Sliwa, B Abdo, L Frunzio, S. M Girvin, et al. Quantum back-action of an individual variable-strength measurement. *Science*, 339(6116):178–181, 2013.

[113] Z Minev, S Mundhada, S Shankar, P Reinhold, R Gutiérrez-Jáuregui, R Schoelkopf, M Mirrahimi, H Carmichael, and M Devoret. To catch and reverse a quantum jump mid-flight. *Nature*, 570(7760):200–204, 2019.

[114] M Koppenhöfer, C Bruder, and N Lörch. Unraveling nonclassicality in the optomechanical instability. *Physical Review A*, 97(6):063812, 2018.

[115] A. W Laskar, P Adhikary, S Mondal, P Katiyar, S Vinjanampathy, and S Ghosh. Observation of quantum phase synchronization in spin-1 atoms. *arXiv preprint arXiv:1910.11832*, 2019.

[116] A Mauroy, I Mezić, and J Moehlis. Isostables, isochrons, and koopman spectrum for the action–angle representation of stable fixed point dynamics. *Physica D: Nonlinear Phenomena*, 261:19–30, 2013.

[117] S Shirasaka, W Kurebayashi, and H Nakao. Phase-amplitude reduction of transient dynamics far from attractors for limit-cycling systems. *Chaos*, 27(2):023119, 2017.

[118] J. A Sanders and F Verhulst. *Averaging methods in nonlinear dynamical systems*. Springer Verlag., 1985.

[119] B Lindner, J Garcıa-Ojalvo, A Neiman, and L Schimansky-Geier. Effects of noise in excitable systems. *Physics Reports*, 392(6):321–424, 2004.

[120] J. T Schwabedal and A Pikovsky. Phase description of stochastic oscillations. *Physical Review Letters*, 110(20):204102, 2013.

[121] Y. S Mauroy and I Mezic. The koopman operator in systems and control, 2020.

[122] Y Kuramoto and H Nakao. On the concept of dynamical reduction: the case of coupled oscillators. *Philosophical Transactions of the Royal Society A*, 377(2160):20190041, 2019.

[123] C Gardiner. *Stochastic methods*, volume 4. Springer Berlin, 2009.

[124] I Mezić. Spectral properties of dynamical systems, model reduction and decompositions. *Nonlinear Dynamics*, 41(1-3):309–325, 2005.

[125] P. J Thomas and B Lindner. Phase descriptions of a multidimensional ornstein-uhlenbeck process. *Physical Review E*, 99(6):062221, 2019.

[126] S. M Barnett and S Stenholm. Spectral decomposition of the lindblad operator. *Journal of Modern Optics*, 47(14-15):2869–2882, 2000.

[127] H.-J Briegel and B.-G Englert. Quantum optical master equations: The use of damping bases. *Physical Review A*, 47(4):3311, 1993.

[128] S Lifson and J. L Jackson. On the self-diffusion of ions in a polyelectrolyte solution. *The Journal of Chemical Physics*, 36(9):2410–2414, 1962.